Semiconducting Polymer Design and Interface Engineering for Efficient Charge Transport

by

Da Seul Yang

A dissertation submitted in partial fulfillment
of the requirements for the degree of
Doctor of Philosophy
(Macromolecular Science and Engineering)
in The University of Michigan
2020

Doctoral Committee:

Professor Jinsang Kim, Chair
Professor L. Jay Guo
Professor Anne J. McNeil
Professor Kevin P. Pipe

Da Seul Yang

dasyang@umich.edu

ORCID iD: 0000-0002-6028-9681

Dedication

This dissertation is dedicated to my parents, my brother, and my husband, who believed in me and made me believe in myself.

Acknowledgements

It would never have been possible for me to complete this dissertation without the incredible support from many professors, collaborators, colleagues, friends, and my family.

First, I would like to thank my advisor, Prof. Jinsang Kim, for his guidance, enthusiasm, and motivation from the beginning to the end of this process. He has always encouraged me, not only to explore creative pathways and ideas to solve research problems but also to be curious and cautious about the research data in every respect so I would be able to draw solid and meaningful conclusions as an independent researcher. Whenever I encountered difficulties during my Ph.D. study, he was always available to provide feedback and resources, never hesitating to share his knowledge and experience with me. I cannot thank him enough for all he has done for me. I also wish to express my sincere gratitude to my committee members, Prof. L. Jay Guo, Prof. Anne J. McNeil, and Prof. Kevin P. Pipe for their keen insights and constructive suggestions. They were delightful to work with and their professionalism was noteworthy. I also want to express my appreciation to Prof. Dong Hoon Choi for instilling in me the intellectual curiosity about science that led me in starting my journey in the first place. In addition, I would like to take this opportunity to thank Prof. Richard Robertson and Prof. Shuichi Takayama for giving me helpful advice and furthering my thinking about learning. I also thank my graduate program coordinators Adam Mael and Julie Pollak for all their support.

I am grateful to others for their collaborations with me on the many projects that I was confronted with; Prof. Mohammed Al-Hashimi and Dr. Maciej Barłóg for their valuable

contribution to polymer design projects, Dr. Bo Hyun Kim, Woo-Hwan Sul, and Prof. Soo-Young Park for their help with polymer film characterizations, Dr. Chen Li and Aman Kumar Jha for being a source of motivation and inspiration to the thermal conductivity project, and Dr. Jill K. Wenderott for helping me in the work function modification project and always bringing positive energy to work. It has been a great pleasure working with a person like you. I also appreciate Dukhan and Emily for their collaboration and constant support. All my collaborators' assistance and contribution have made my journey so much easier and more enjoyable.

I would like to express my sincere thanks to my lab mates, Dr. David Bilby, Dr. Kyeongwoon Chung, Dr. Joonkoo Kang, Dr. Min Sang Kwon, Dr. Apoorv Shanker, Dr. Byeongseop Song, and Dr. Seong-Jun Yoon for all the stimulating discussions and invaluable advice. I am also grateful to Deokwon, Dr. Jaehun Jung, and Dr. Youngchang Yu who helped me a great deal with adjusting to the Kim Group. I also thank Jonathan, Jiwon, and Te. The camaraderie that we all developed with each other through the thermal conductivity project was really a great emotional support for me in the lab. I extend my gratitude to all past and present lab members of the Kim Group including Yingying, Dr. Jihan Kim, Wenhao, Mira, Dr. Do Hyun Kang, Ramin, Jonathan Rubio Arias, Dr. Ricardo Vázquez, Dr. Mounggon Kim, Dr. Jongho Kim, Maiko, Mark, Cameron, Dr. Ji Eon Kwon, Jiayin, David, Andrew, Erik, Srivatsan, Lihua, and Shuo for their caring and helpfulness, which made my experience in the Kim Group and graduate school exciting.

I must thank all my friends (too many to name, but I truly appreciate all of you) for their friendship and encouragement. My heartfelt thanks also go to my aunt, uncle, and cousins for helping me get through tough times and always welcoming me warmly to Boston.

I would like to express my deep love and gratitude to my parents, Soon Rye Kim and Jae Won Yang, for their dedication to my aspirations and believing in me as I make decisions in life. Also, I want to thank my brother, Hyun, for his unwavering support. I am so blessed to have such a caring person like you as my brother.

Lastly, special thanks to my husband, Jongsik, who always makes me feel cared for and valued. Your intellectual and personal support has been irreplaceable. Thank you for always understanding, never judging me, and making me want to be a better person.

Table of Contents

List of Tables

List of Figures

Abstract

A major challenge to achieve macroscopic conjugated polymer (CP) alignment leading to efficient charge transport stems from the intrinsic disordered and entangled nature of CP chains. Liquid crystalline (LC) CP design principles for directed alignment and their application to build a better understanding of charge transport in plastic electronics are discussed in this dissertation. First, molecular design parameters affecting the CP alignment are thoroughly investigated. The identified parameters, correlating with alignment characteristics via LC properties, are (a) the planarity of polymer chains; (b) intramolecular interaction moieties for induced chain planarity; (c) the effective bulkiness of side chains; and (d) surface energy of CPs. Second, cleavable side chains were introduced to the LC CPs as another design factor to achieve solvent-resistant highly aligned polymer films. The alignment behavior of the resulting new LC CP was examined in detail by adopting the floating film transfer method (FTM). In this method, an optimum amount of a high boiling point solvent was found to be vital to provide enough time for CPs to align. A high mobility anisotropy of ~14 was obtained through well-aligned CPs under the optimized condition. The subsequent side chain removal led to the formation of solvent-resistant highly aligned CP films. Overall, the outcomes provide insights into the realization of anisotropic properties of CPs in the solid thin films and offer an opportunity to enable a wide range of applications in organic electronics.

FTM was employed as an interface engineering tool to investigate the charge transport of CPs in organic field effect transistors (OFETs). Although the transistor performance has been

known to be critically affected by the polymer film-dielectric interface, it has been very difficult to isolate the contribution of CP alignment near the interface from that of the bulk film to the device performance. FTM has the capability of modulating CP alignment directions discretely in multilayered films, providing an opportunity to solve the daunting task. The resulting CP films prepared by FTM consisted of a bottom layer close to the polymer-dielectric interface and a top layer in contact with the source-drain electrodes. When the bottom layer had a parallel CP orientation and the CPs in the top layer were oriented perpendicular to the source-drain direction, the average hole mobility was larger by a factor of 3.3 than that of the opposite case. Moreover, OFET devices with combinations of the various bottom and top layer CP orientation directions revealed that the CP orientation direction of the bottom layer governed the overall device performance with a much smaller contribution from that of the top layer. These findings support that the CP alignment near the polymer-dielectric interface is a decisive factor for the charge transport in OFETs. Possible device performance enhancement through interface engineering is also demonstrated by investigating how the work function of electrodes can be modulated. Changes in the work function were demonstrated by means of electrophoretic deposition of ionic polyelectrolytes, electrospraying of a neutral polymer, and even after inserting an insulating spacer layer between a work function modifying layer and an electrode. The results consistently show that the work function can be controlled via a combination of the surface interaction and the charge-based through-space interaction, which can lead to the precise work function modification of electrodes for effective charge injection and extraction in organic electronics.

Chapter 1

Introduction

1.1 Conjugated Polymers and their Semiconducting Properties

Conjugated polymers have drawn scientific attention, specifically with respect to their tunable material properties by careful molecular design. The readily tunable properties depending on purposes make the conjugated polymers suitable for various applications, for example, high planarity for efficient charge transport as in organic field effect transistors (OFETs),[1,2] narrow bandgap for broad light absorption in the near-infrared range as in organic photovoltaic cells,[3,4] high sensitivity for certain substances as in sensors,[5–7] and high conductivity as in energy storage systems.[8] Conjugated polymers also have several other advantages over their inorganic analogues, such as lightweight, low cost, flexibility, and solution processability.[9–14] These advantages along with the tunable material properties make conjugated polymers important as emerging semiconducting materials for electronic device applications.

The semiconducting properties of conjugated polymers originate from the delocalized π-electrons through alternating saturated and unsaturated carbon-carbon bonds along the backbone of the polymers.[14,15] This electronic delocalization in a conjugated π-bond system via one unpaired π-electron per carbon provides an efficient pathway for charge transport. However, this conjugated system is often twisted and kinked and forms randomly oriented multiple domains, making the charge transport process slow down significantly.[16,17] The intrinsically disordered nature of polymers is originated from the strong tendency of polymer chains to be intertwined

and entangled with one another. In order to overcome this rather limited charge transport properties of conjugated polymers as semiconductors, a tremendous amount of effort has been made as discussed in the following section.

1.2 Approaches to Improve the Efficiency of Charge Transport in Conjugated Polymers

1.2.1 Molecular Structural Approaches

Charge transport along the polymer backbone (intrachain charge transport) in semiconducting polymer films is known to be much faster than interchain charge transport.[16,17] While this is critical, it is also important to notice that charges essentially move to multiple directions on the plane of the films, not just within a one-dimensional single chain. To be more specific, chains are intertwined and entangled with one another, so a number of chains participate in the charge transport process of the polymer films in any given case. Typical CP films of entangled polymer chains are composed of partially ordered (semi-crystalline) regions embedded in disordered (amorphous) regions, having complex microstructures (Figure 1.1). In order to build a deep understanding of charge transport with the complexity in these films, the formation of favorable microstructures associated with the polymer structure has been widely studied.[18–23]

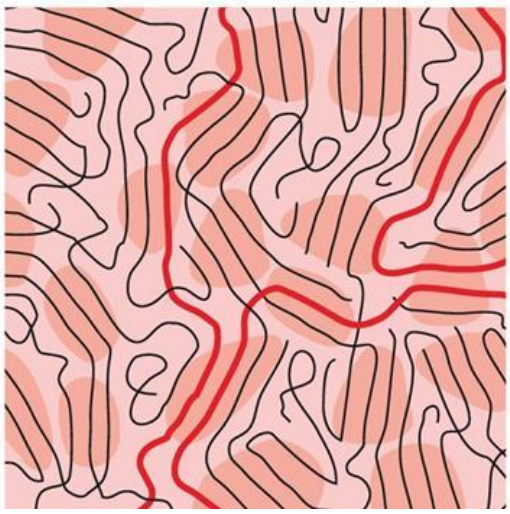

Figure 1.1 Schematic illustration of the microstructure showing the coexistence of ordered (darker shadowed areas) and amorphous regions of a polymer film with disordered aggregates. If the molecular weight and the density of ordered chains are large enough, long polymer chains (highlighted in red) can connect the ordered regions, greatly improving charge transport.[16] (Reprinted by permission from Macmillan Publishers Ltd.: Nature Materials (Ref. 16), Copyright 2013)

For example, the highly ordered microcrystalline domains in poly(3-hexylthiophene) (P3HT) films were found to be critical to achieving high mobilities, which were largely dependent on the regioregularity of P3HT (i.e. the percentage of stereoregular head-to-tail attachments of the hexyl side chains to the 3-position of the thiophene rings in P3HT).[18] The influence of the regioregularity on the conformation of P3HT chain at the single-molecule level was investigated through molecular dynamics simulations in another prior study.[24] The simulation results clearly showed the ability of the polymer to form well-aligned structures in P3HT with high regioregularity (regioregular). In contrast, the P3HT chain with low regioregularity (regiorandom) was calculated to have a twisted structure because of the steric hindrance between the adjacent hexyl side chains of the polymer. In an experimental study with the same polymer, the charge transport pathways in the regioregular and regiorandom P3HT films were investigated by conductive atomic force microscopy (C-AFM) mapping.[25] The

conductivity map showed homogeneous fiber bundle-like structures with excellent electrical conductivity along the fiber bundles in the regioregular P3HT, while a much less ordered and inhomogeneous feature was found in the regiorandom P3HT. The highly ordered microstructure in the regioregular P3HT film led to an outstanding device performance of 2.9 $cm^2 V^{-1} s^{-1}$, which is more than an order of magnitude higher than that in the case of regiorandom P3HT. As discussed above, both the computational and experimental data corroborate the pivotal role of regioregularity in efficient charge transport of P3HT. Along the same line, research efforts have also been directed toward understanding how the regioregularity of other semiconducting conjugated polymers influences their charge transport properties.[23] The Bazan group synthesized regioregular and regiorandom conjugated polymers containing pyridal[2,1,3]thiadiazole units and found that the regioregular polymer has two orders of magnitude higher mobility compared to the regiorandom counterpart, from 0.005 to 0.6 $cm^2 V^{-1} s^{-1}$.[26] This result was explained through the morphological and structural analysis showing a higher degree of structural order in the regioregular polymer films.

Besides the regioregularity control, significant attention has also been placed on the rigidity and planarity of the conjugated polymers to achieve efficient charge transport.[2,27–29] This approach of making rigid and planar polymer chains is beneficial to a close interchain packing and an extended effective conjugation length, which can facilitate interchain and intrachain charge transport, respectively. As expected, reasonably high charge transport properties have been obtained from conjugated polymers with rigid and planar main chains.[2,22,27–31] Interestingly, the reported efficient charge transport is often further improved by applying techniques to induce the alignment of polymer chains. For example, poly(diketopyrrolopyrrole-terthiophene) (PDPP3T), which was first reported by the Janssen group with an average hole mobility of 0.04

cm^2 V^{-1} s^{-1} in the spin-coated films,[30] exhibited a more than an order of magnitude higher mobility when the films were prepared by solution shearing.[32] Poly(2,5-bis(2-octyldodecyl)-3,6-di(thiophen-2-yl)diketopyrrolo[3,4-*c*]pyrrole-1,4-dione-*alt*-thieno[3,2-*b*]thiophene (DPPT-TT) also showed a significantly increased mobility from 0.72 to 1.64 cm^2 V^{-1} s^{-1} when the polymer chains were aligned by bar coating in comparison to the case of conventional spin-coating.[31] Taken together, the contribution of the processing techniques to the polymer chain alignment is absolutely not trivial. In this perspective, various film processing techniques to induce polymer alignment are reviewed in the following section.

1.2.2 Development of Processing Strategies for Anisotropic Alignment of Polymer Chains

A wide variety of powerful film fabrication techniques to align polymer chains have been extensively studied. Among the various methods for the alignment, meniscus-guided coating techniques, such as dip coating,[33–35] zone casting,[36,37] and solution shearing,[13,32,38–42] have shown great potential for high performance and large-area solution-processable organic electronics. "Meniscus-guided" refers to a key feature of these techniques that is the evolution of a meniscus in solution, guiding the polymer solution and consequently controlling film formation triggered by solvent evaporation at the meniscus.[43,44] For instance, in the process of the dip coating, a meniscus is formed where a substrate and a polymer solution meet. Within the meniscus, a concentration gradient is established by solvent evaporation, which induces fluid flow that produces the aligned polymer chains in the dip coating direction.[43] Along this direction, the improved charge carrier mobility, which is about twice as high as along the perpendicular to the coating direction, was reported in polymer films of cyclopentadithiophene-benzothiadiazole copolymer (CDT-BTZ) by the Müllen group.[33] By the dip coating method with different

substrate pulling speeds, the same research group articulated precisely controlled microstructures of polymer films resulting in a significantly large anisotropy of their charge transport properties.[34] Another well-studied meniscus-guided technique is the solution shearing, which was first reported using small molecules in 2008 by researchers led by Dr. Zhenan Bao and later successfully applied to conjugated polymers.[45] This technique requires a small volume of a polymer solution sandwiched between an angled blade on the top and a temperature-controlled substrate at the bottom. As the blade drags a polymer solution across the bottom substrate, solution evaporation-driven fluid flow occurs along the shearing direction.[44] Compared to polymer films processed by other methods, such as spin-coating or drop-casting, largely enhanced charge transport properties have been reported with this shearing process in multiple studies.[39–42] The efficient charge transport in the sheared polymer films was attributed to the aligned chains providing favorable charge transport pathways together with more close packing between polymer chains. Interestingly, the impact of the shearing process on molecular packing of polymers was found to be largely dependent on the structure of the polymers.[38] To be specific, two polymers, poly(2,5-bis(3-hexadecylthiophene-2-yl)thieno[3,2-*b*]thiophene) (PBTTT-C16) and poly(2,5-bis(thiophene-2-yl)-(3,7-dihepta-decanyltetrathienoacene) (P2TDC17FT4) having interdigitated side chains, exhibited change in lamellar spacing as a function of shearing speed, whereas a non-interdigitated P3HT showed no such change in its molecular packing under similar shearing conditions. This result suggests that even if an applicable polymer chain alignment technique exists, it needs to be accompanied by a systematic understanding of molecular structural properties in order to take full advantage of the technique.

In addition to the meniscus-guided coating techniques, several other methods to induce polymer chain alignment have also been developed, such as mechanical force-assisted coating

techniques (e.g. mechanical rubbing, stretching),[46–48] off-center spin coating,[49–51] and the floating film transfer method (FTM).[52–58] Among them, FTM deserves attention, as it specifically focuses on but is not limited to utilizing liquid crystalline (LC) conjugated polymers. Figure 1.2

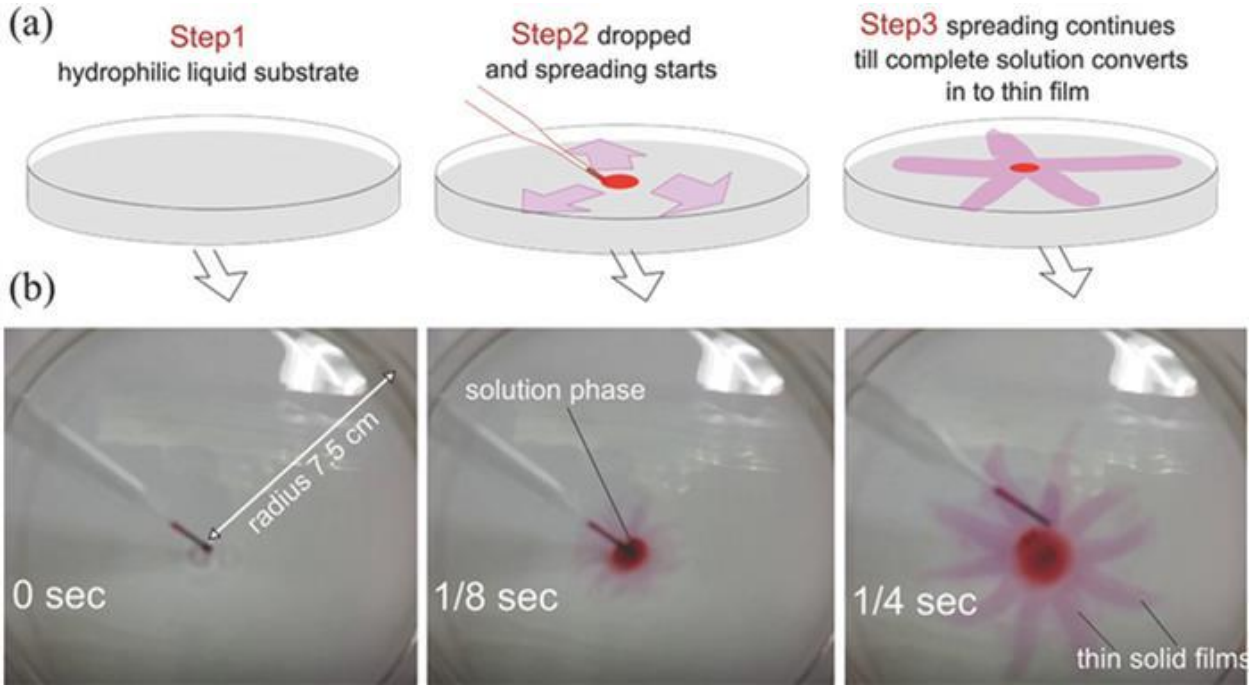

Figure 1.2 (a) Schematic illustrations and (b) the corresponding photographs of the film fabrication process by the floating film transfer method (FTM).[54] (Reprinted by permission from John Wiley & Sons, Inc.: Advanced Materials Interfaces (Ref. 54), Copyright 2018)

illustrates the detailed polymer film formation process.[54] First, a hydrophilic liquid is prepared as a substrate, and a small amount of hydrophobic polymer solution (~15 μL) is dropped on the hydrophilic subphase liquid. This liquid is not miscible with the solvent of the polymer solution and assists in spreading the solution. While the solution spreads, the solvent evaporates, resulting in a highly concentrated region where the LC properties render a well-aligned polymer film on the liquid substrate. The plausible mechanism for the LC phase-assisted polymer chain alignment

is shown in Figure 1.3. The aligned film floating on the liquid is then transferred onto a desired

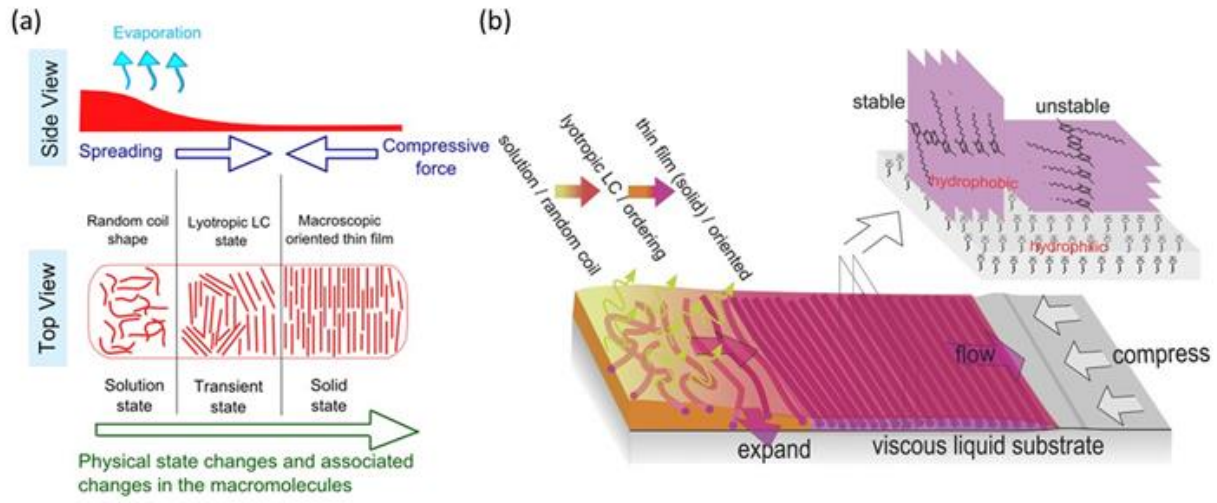

Figure 1.3 Schematic illustrations of (a) the LC state-assisted macroscopic polymer chain orientation by FTM[58] (Reprinted by permission from Elsevier B.V.: Organic Electronics (Ref. 58), Copyright 2017) and (b) the possible mechanism for polymer orientation during PB14TTT film formation on a liquid substrate.[54] (Reprinted with permission from John Wiley & Sons, Inc.: Advanced Materials Interfaces (Ref. 54), Copyright 2018)

substrate by stamping, followed by rinsing and drying at 80 °C. In this film formation process, several parameters play a decisive role in the alignment of the polymer chains. Starting with the pioneering study of FTM by Morita et al,[52] systematic investigations of the detailed parameters, such as viscosity of the hydrophilic liquid, solvent evaporation rate, processing temperature, and polymer backbone structure, have been conducted.[58–60] To illustrate, it was found that the viscosity of the hydrophilic liquid substrate largely affects the spreading speed of the polymer solution (Figure1.4a).[59] Given that the film solidification occurs almost instantaneously while the solution spreads, the viscosity can be considered as a key factor to obtain well-aligned polymer chains in floating films. In another example, a certain polymer backbone structure turned out to be vital for obtaining a high degree of polymer chain alignment.[60] This result was rationalized in terms of the intermolecular packing of polymer chains since FTM utilizes lyotropic LC phase transitions that are closely related to the intermolecular interaction among the chains. To be

specific, when polymer chains have strong intermolecular interactions leading to closely packed structures, the sliding motion between the polymer chains is limited, hampering the LC phase transition and lowering the effectiveness of the chain orientation compared to the case where polymer chains have enough freedom to respond to FTM (Figure 1.4b). This intermolecular interaction dependent LC properties affecting the degree of polymer chain alignment is in well agreement with an earlier study by our group that was designed to explore molecular design parameters with LC conjugated polymers.[61] Clearly, thorough understanding of molecular structural features and their effect on polymer chain interactions is essential to properly exploit the polymer chain alignment technique, as also discussed with respect to the meniscus-guided coating techniques.

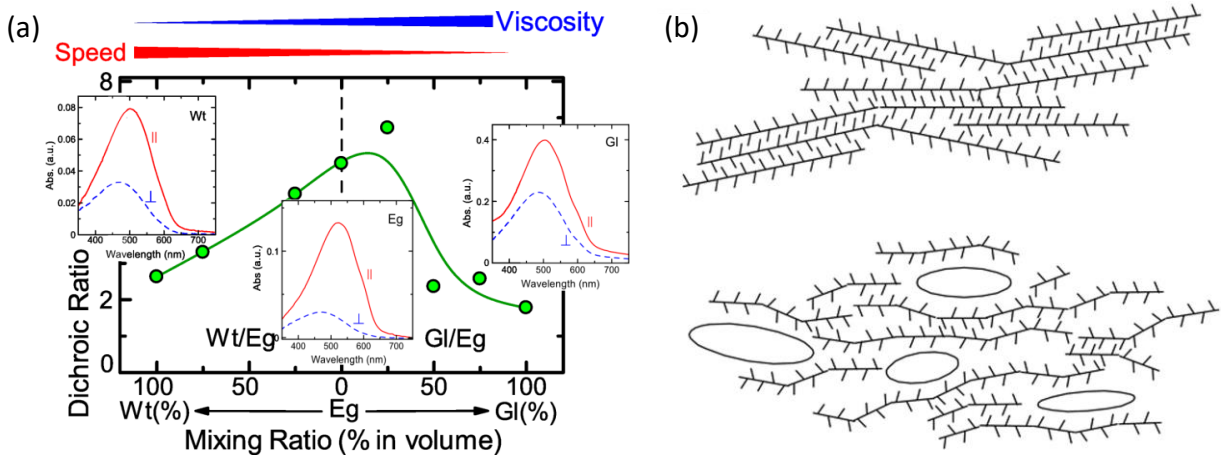

Figure 1.4 (a) Dichroic ratio as a function of mixing ratio in various liquid substrates. The insets show the polarized absorption spectra of the polymer films at water (wt), ethylene glycol (Eg), and glycerol (Gl), respectively.[59] (Reprinted by permission from IOP Publishing Ltd.: Journal of Physics: Conference Series (Ref. 59), Copyright 2016) (b) Schematic illustrations of possible intermolecular packing structures for regioregular (top) and regiorandom (bottom) P3HT.[60] (Reprinted with permission from Elsevier B.V.: Thin Solid Films (Ref. 60), Copyright 2016)

1.2.3 Liquid Crystalline Properties for Facilitating the Alignment of Conjugated Polymers

There is no doubt that macroscopic alignment of polymer chains facilitates efficient charge transport through improved p-orbital overlaps along the conjugated polymer backbone.[62,63] However, it is still unclear what molecular design factors need to be in place to achieve the macroscopic alignment and induce a long-range ordering of CPs.

LC properties of conjugated polymers have been appreciated as effective contributing factors to the molecular assembly of polymer chains leading to long-range ordering for efficient charge transport in organic electronics.[64] This is because polymer chains in LC states have a strong tendency to align parallel to one another with extended chain conformation to relieve steric hindrance between adjacent chains. It has been generally accepted that conjugated polymers with high aspect ratios (i.e. ratio of the long axis to the short axis) can exhibit LC phases under certain conditions (e.g. temperature and/or concentration of the polymer solution). Also, various other factors like amphiphilic character, intermolecular interactions, and the persistence length of polymers come into play in determining the formation of the LC phase and the consequent polymer chain alignment.[64–66] In most instances, the aforementioned factors can be controlled by the careful design of molecular structures. However, the complexity, originating from having many variables and the interrelationships among them, makes it difficult to clearly identify the required molecular design factors to encompass LC properties in conjugated polymers. Because of the lack of universally applicable design principles, LC phase-assisted polymer alignment leading to high efficiency in charge transport of the electronic devices has been limited mostly to polyfluorene copolymers,[53,67,68] and polythiophenes and their derivatives,[36,47,48,53–56,58,69–71] as summarized in Table 1.1; the structures of the polymers are shown in Figure 1.5. Nevertheless, the effect of LC phase-assisted alignment on the charge

transport is clearly demonstrated by the mobility anisotropies (i.e. the ratio between the mobilities measured parallel and perpendicular to the polymer chain alignment direction). In some cases, the anisotropic ratio of charge mobility depending on conjugated polymer alignment direction was found to be larger than 10.[47,58,61,67,68] These high anisotropies reflect the successful polymer chain alignment through the LC phase, which can consequently lead to a significant increase in the charge transport efficiency. At this point, it should be noted that some of the polymers showing this efficient LC phase-assisted chain alignment were designed and often reported with a conventional spin-coating method.[72,73] Therefore, an LC polymer structure combined with a suitable processing method will have a synergic effect in reaching significantly high anisotropies if the chain alignment through the LC phase is taken into consideration from the polymer design stage.

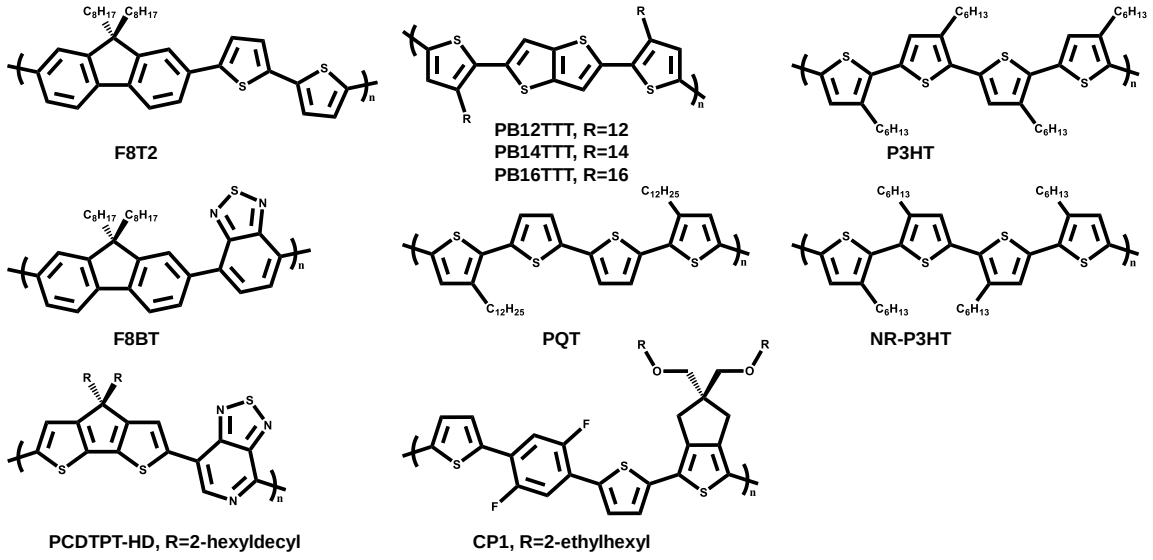

Figure 1.5 Chemical structures of several LC conjugated polymers.

Table 1.1 Anisotropic optical and electrical properties of LC conjugated polymers by LC phase-assisted alignment methods[a]

Liquid Crystalline Conjugate Polymers		Dichroic Ratios	Mobility Anisotropies	$\mu_{//}$ ($cm^2 V^{-1} s^{-1}$)	μ_{iso} ($cm^2 V^{-1} s^{-1}$)	Methods[b]	References
Polyfluorene copolymers	F8T2	8-10	5-8	9×10^{-3} -2×10^{-2}	$3\text{-}5\times10^{-3}$	Spin coating on a rubbed polyimide alignment layer	74
		5.5	40	2×10^{-2}	-	Photoalignment	67
		2.5	2.9	1.05×10^{-3}	2.0×10^{-4}	A modified FTM	53
	F8BT	7	10-15	$8\text{-}12\times10^{-4}$	-	Nanoimprinting	68
Polythiophene derivatives	PB12TTT	6	72	1.8×10^{-2}	$\mu_{//} < \mu_{iso}$	High temperature rubbing	47
	PB14TTT	6.6	3-5	4×10^{-1}	-	Zone casting	36
		6.5	12.8	1.1×10^{-1}	2.3×10^{-2}	FTM	58
		2.2	1.5	7.5×10^{-3}	5.2×10^{-3}	A modified FTM	53
		4.8	4-5	1.52	$8\text{-}9\times10^{-1}$	Stretching	48
		13	10	4×10^{-1}	$7\text{-}9\times10^{-2}$	FTM	54
	PB16TTT	15.6	-	6.2×10^{-1}	0.1	A film formation on an ionic liquid	70
Polythiophenes	PQT	22	~10	2.6×10^{-2}	-	A modified FTM	55
		5.1	7.1	5.0×10^{-2}	6.7×10^{-4}	A modified FTM	53
		-	~8	1.7×10^{-1}	-	Roll-transfer printing	71
	P3HT	-	-	1.07×10^{-4}	2.11×10^{-4}	FTM	56
	NR-P3HT	2.4	3.5	4.2×10^{-3}	1.0×10^{-5}	A modified FTM	53
PCDTPT-HD		~1.3	-	5.52×10^{-3}	1.97×10^{-3}	Solution shearing	69
CP1		9.8	~1600	8.6×10^{-1}	$10^{-3} < \mu_{iso} < 10^{-2}$	Blade coating	61

[a]$\mu_{//}$ is the carrier mobility of the device when the source-drain electrodes are deposited parallel to the polymer chain alignment direction, and μ_{iso} is the carrier mobility of the isotropic device. [b]FTM is the floating film transfer method.

1.3 Applications of Semiconducting Conjugated Polymers in Electronic Devices

1.3.1 Device Structure of OFETs

OFETs are three-terminal devices that use an electric field to control the flow of current. These devices consist of the organic semiconductor layer, the gate dielectric layer, and the three terminals (source, drain and gate electrodes). Depending on the position of the source and drain electrodes relative to the gate electrode, the OFET device configurations can be classified as coplanar and staggered. Also, each of the two device configurations (coplanar and staggered) can be further classified as either top gate or bottom gate configurations, depending on the position of the gate electrode. Accordingly, there are four different OFET device configurations: coplanar bottom gate, coplanar top gate, staggered bottom gate, and staggered top gate, as illustrated in Figure 1.6. Each device configuration possesses both advantages and limitations. For example, the charge injection area of the staggered configurations is larger than that of the coplanar configurations. This difference leads to a tendency of the staggered configurations to have a smaller contact resistance between the source and drain electrodes and the semiconductor layer.[75,76] Regarding the top gate and bottom gate device geometries, the top gate structures are preferable especially when oxygen and/or moisture sensitive materials are used for the semiconductor layer. Since the semiconductor layer is covered with the gate dielectric layer in the top gate structures, the exposure to oxygen and/or moisture can be prohibited, thus protecting the sensitive materials.[77] However, it is worth mentioning that the bottom gate type is relatively easier to fabricate compared to its top gate analogue. In the top gate structure, there is possibility of causing damage to an underlying semiconductor during the deposition of the gate dielectric layer on the semiconductor layer, which makes the process more difficult.[78]

A bottom gate staggered structure is used in this dissertation given the ease of fabrication and low contact resistance between the source and drain electrodes and the semiconductor layer.[75,76]

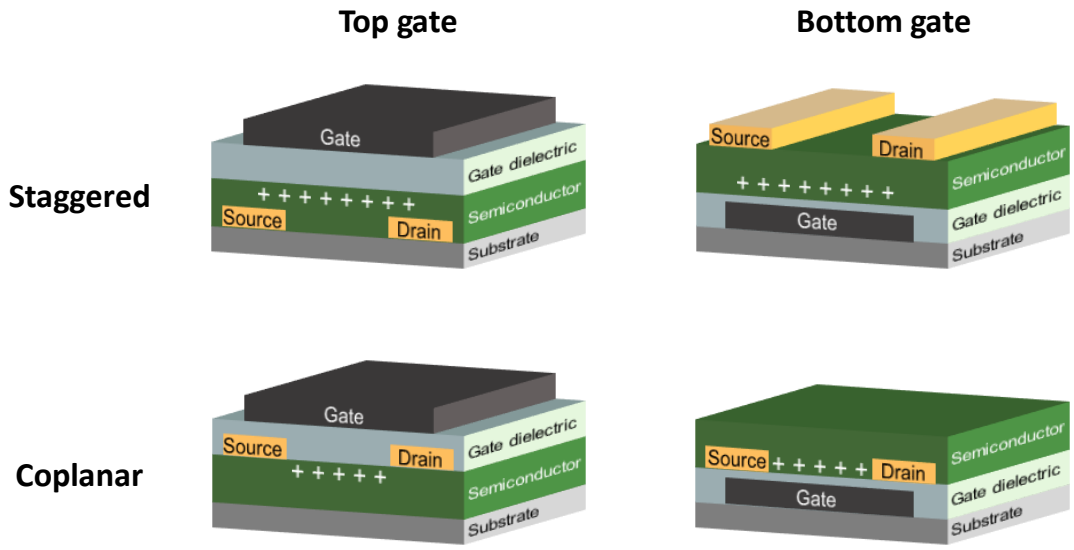

Figure 1.6 OFET device configurations.

1.3.2 Device Operation and Characterization of OFETs

When a voltage (V_G) is applied to the gate electrode, charges are accumulated at the gate dielectric/semiconductor interface (Figure 1.6, indicated by positive charges (+) as an example of a p-type OFET). The accumulated charges that form a conducting channel between source and drain generate a current (I_{DS}) when a voltage (V_{DS}) is applied to the drain electrode where the source is connected to ground. The output characteristics in Figure 1.7a show two operation regimes of transistors: linear and saturation. At a small V_{DS} region, the FET works in the linear regime where the source-drain current (I_{DS}) linearly increases with V_{DS}, which can be written as Eq. (1):

$$I_{DS} = \frac{WC_i}{L}\mu[(V_G - V_{th})V_{DS} - \frac{1}{2}{V_{DS}}^2] \quad (1)$$

where μ is the field effect carrier mobility, V_{th} is the threshold voltage, which is the minimum voltage that is required to create a conducting channel between the source and drain electrodes, W and L are, respectively, the channel width and length, and C_i is the capacitance per unit area of the gate dielectric. Note that compared to the threshold voltage, a higher voltage has to be applied to the gate. When V_{DS} equals V_G-V_{th}, the transistor enters into the saturation regime. In this regime, the difference between V_G and V_{DS} is now below the threshold voltage, leading to the formation of a depletion region next to the drain electrode. This means that further increasing V_{DS} has no effect on I_{DS} and the current in this saturation regime can be derived from Eq. (2) by replacing V_{DS} with V_G-V_{th}.

$${I_{DS}}^{sat} = \frac{WC_i}{2L}\mu_{sat}(V_G - V_{th})^2 \quad (2)$$

In the saturation regime, the mobility that describes how quickly a charge moves through semiconductor when pulled by an electric field can be extracted by the slope of the plot of $I_{DS}^{1/2}$ as a function of V_G at a fixed V_{DS}, as shown in Figure 1.7b. When V_G becomes larger than V_{th}, the transistor switches on and a thin conducting channel is formed. The ratio between the maximum and the minimum I_{DS} (I_{on}/I_{off}) is defined as the signal when the device is on over the signal when the device is off. For an effective switching OFET device, a high I_{on}/I_{off} is desirable.

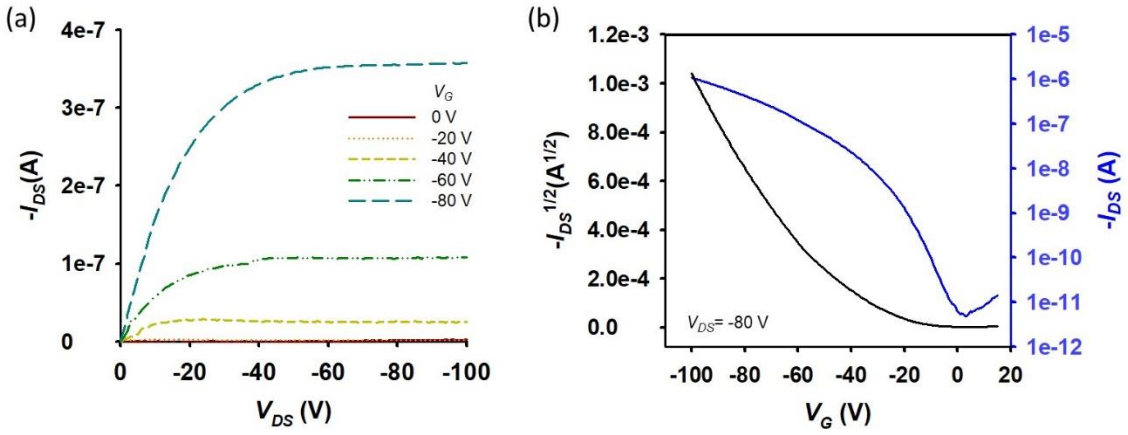

Figure 1.7 Output (left) and transfer (right) curves of a p-type OFET.

1.3.3 Charge Injection and Work Function of Electrodes in OFETs

In order to achieve high performance in OFET devices, efficient injection of charges (holes or electrons) from a metal electrode into a semiconductor layer, followed by charge transport through the semiconductor, is critically important. The injection efficiency is affected by charge injection barriers at the interface between the source/drain metal electrodes and an organic semiconductor layer. The injection barriers are determined by taking the difference between the energy level of the Fermi level (E_F) of the source/drain metal electrodes, based on their work function, and the Highest Occupied Molecular Orbital (HOMO) or the Lowest Unoccupied Molecular Orbital (LUMO) energy level of the semiconductor layers for either holes (p-type) and electrons (n-type), respectively.[79] In the case of efficient hole injection, the HOMO energy level is close to the E_F of the source/drain electrodes, leading to a small charge injection barrier.[80,81] Gold is commonly used for the source/drain electrodes due to its high work function (~5 eV), which, in the majority of cases, matches well with the HOMO energy levels of p-type (hole-transporting) semiconductors.[82] The energy level diagram of the source/drain electrodes-

semiconductor shown in Figure 1.8 depicts how holes are injected in OFET devices when applying voltages to the electrodes.

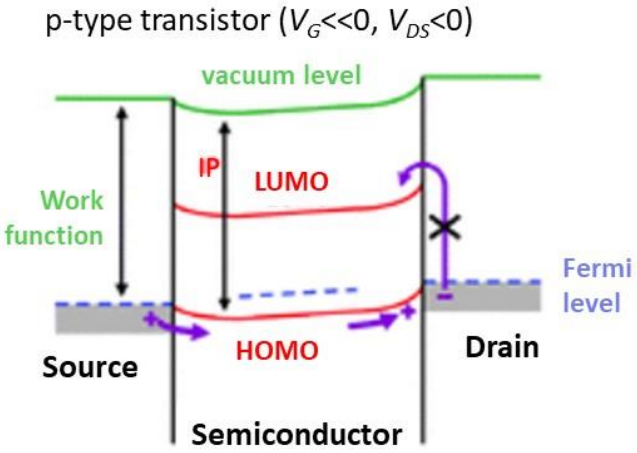

Figure 1.8 Energy level diagram of a p-type organic transistor, showing the transport of positive carriers from the source through the semiconductor to the drain in the case of a p-channel transistor. The transfer of negative charges into the semiconductor is blocked because of the large energy difference between the Fermi level of the contact and the LUMO energy level of the semiconductor.[80] (Reprinted with permission from Royal Society of Chemistry: Chemical Society Reviews (Ref. 80), Copyright 2010)

1.4 Summary and Dissertation Outline

This chapter provides introductory background information about conjugated polymers as semiconductors followed by a concise explanation regarding the intrinsic limitations of semiconducting conjugated polymers in charge transport in organic electronics (**Chapter 1**, section 1.1). The discussion in the following section (section 1.2) provides essential information about prior research to overcome the limitations. Specifically, the literature review in this section shows that past efforts have leaned heavily toward the development of processing strategies for anisotropic alignment of polymer chains using known CPs rather than designing novel CPs for the sake of aligning the chains in the first place. In this context, the polymer design for their LC

phase-assisted alignment is described as a strategy towards the inherently favorable chain alignment characteristics. Based on this strategy, **Chapter 2** details the design parameters of LC conjugated polymers. The parameters identified through a systematic investigation with eight new polymers in this chapter are: (a) the planarity of polymer chains, (b) intramolecular interaction moieties for chain planarity, (c) the effective bulkiness of side chains, and (d) surface energy of the polymers. **Chapter 3** introduces cleavable side chains to the aforementioned design requirements to enable the synthesis of an LC polymer to form solvent-resistant highly aligned films after the cleavage of the solubilizing yet cleavable side chains. The detailed chain alignment and solvent resistance of the polymer having cleavable side chains are investigated by means of FTM as an LC phase-assisted film fabrication method. With an optimum amount of high boiling point solvent during the film formation process, successful alignment was achieved, which was confirmed by a high anisotropy in optical absorption (~4.8) and charge mobility (~14) of the resulting films. The subsequent side chain removal allowed the films to acquire solvent resistance without sacrificing their aligned feature.

This introduction chapter also provides fundamentals of organic transistors (section 1.3) as essential information for the discussion topics of **Chapters 4 and 5**, which are related to the importance of interface engineering for efficient charge transport in organic electronic devices. It has been widely accepted that the overall charge transport in OFETs is known to be governed by a thin effective charge accumulation layer near the polymer film/gate dielectric layer interface.[2,83,84] Thus, the contribution of the semiconducting polymer films near the interface to the charge transport properties is critically important. Studies of this contribution have been conducted by controlling the thickness of the films.[85–90] However, when the film thickness is changed, it is difficult to exclude the contribution of other factors. For example, controlling

thickness can affect the charge transport path and homogeneity as well as the thickness itself. As an effective approach to tackle the problem, **Chapter 4** focuses on a unique feature of the previously adopted film fabrication method, FTM, which enables a discrete modulation of the polymer chain alignment direction for each layer in multilayered films. To be specific, the polymer films for OFETs discussed in this chapter were fabricated by FTM in a bi-layered structure where the bottom layer is close to the polymer/dielectric interface and the top layer is in contact with the source-drain electrodes. When the bottom layer had a parallel chain orientation and the chains in the top layer were oriented perpendicular to the source-drain direction, much higher mobility was observed as compared to the opposite case. OFET devices were also fabricated varying the polymer chain orientation directions of bottom and top layers. The performance of the devices was found to be determined dominantly by the orientation direction of the bottom layer. This is presumably because of the effective charge accumulation at the bottom layer/dielectric interface. These results point to that the alignment near the polymer/dielectric interface has a significant impact on the charge transport in OFETs.

Chapter 5 also discusses the importance of interface engineering in high performance organic electronics. This chapter illustrates how we should understand the work function modification mechanism of electrodes in organic electronic devices. The experimental results from (1) electrophoretic deposition of ionic polyelectrolytes, (2) electrospraying of a neutral polymer, and (3) placing an insulating spacer between a work function modifying layer and an electrode consistently suggest that the work function can be controlled via a combination of the surface interaction and the charge-based through-space interaction. This comprehensive understanding provides a platform for the design and selection of the materials for work function modifying layers leading to effective charge injection and extraction in organic electronics.

1.5 References

1. Holliday, S.; Donaghey, J. E.; McCulloch, I. Advances in Charge Carrier Mobilities of Semiconducting Polymers Used in Organic Transistors. *Chem. Mater.* **2014**, *26*, 647–663.
2. Khim, D.; Luzio, A.; Bonacchini, G. E.; Pace, G.; Lee, M.-J.; Noh, Y.-Y.; Caironi, M. Uniaxial Alignment of Conjugated Polymer Films for High-Performance Organic Field-Effect Transistors. *Adv. Mater.* **2018**, *30*, 1705463.
3. Xu, T.; Yu, L. How to Design Low Bandgap Polymers for Highly Efficient Organic Solar Cells. *Mater. Today* **2014**, *17*, 11–15.
4. Li, Y.; Yang, Y.; Bao, X.; Qiu, M.; Liu, Z.; Wang, N.; Zhang, G.; Yang, R.; Zhang, D. New π-Conjugated Polymers as Acceptors Designed for All Polymer Solar Cells Based on Imide/Amide-Derivatives. *J. Mater. Chem. C* **2016**, *4*, 185–192.
5. Sun, X.; Wang, Y.; Lei, Y. Fluorescence Based Explosive Detection: From Mechanisms to Sensory Materials. *Chem. Soc. Rev.* **2015**, *44*, 8019–8061.
6. Rochat, S.; Swager, T. M. Conjugated Amplifying Polymers for Optical Sensing Applications. *ACS Appl. Mater. Interfaces* **2013**, *5*, 4488–4502.
7. McQuade, D. T.; Pullen, A. E.; Swager, T. M. Conjugated Polymer-Based Chemical Sensors. *Chem. Rev.* **2000**, *100*, 2537–2574.
8. Kim, J.; Lee, J.; You, J.; Park, M.-S.; Al Hossain, M. S.; Yamauchi, Y.; Kim, J. H. Conductive Polymers for Next-Generation Energy Storage Systems: Recent Progress and New Functions. *Mater. Horiz.* **2016**, *3*, 517–535.
9. Forrest, S. R. The Path to Ubiquitous and Low-Cost Organic Electronic Appliances on Plastic. *Nature* **2004**, *428*, 911–918.
10. Nielsen, C. B.; Turbiez, M.; McCulloch, I. Recent Advances in the Development of

Semiconducting DPP-Containing Polymers for Transistor Applications. *Adv. Mater.* **2013**, *25*, 1859–1880.

11. Luo, H.; Yu, C.; Liu, Z.; Zhang, G.; Geng, H.; Yi, Y.; Broch, K.; Hu, Y.; Sadhanala, A.; Jiang, L.; Qi, P.; Cai, Z.; Sirringhaus, H.; Zhang, D. Remarkable Enhancement of Charge Carrier Mobility of Conjugated Polymer Field-Effect Transistors upon Incorporating an Ionic Additive. *Sci. Adv.* **2016**, *2*, e1600076.
12. Reese, C.; Roberts, M.; Ling, M.; Bao, Z. Organic Thin Film Transistors. *Mater. Today* **2004**, *7*, 20–27.
13. Molina-Lopez, F.; Wu, H.-C.; Wang, G.-J. N.; Yan, H.; Shaw, L.; Xu, J.; Toney, M. F.; Bao, Z. Enhancing Molecular Alignment and Charge Transport of Solution-Sheared Semiconducting Polymer Films by the Electrical-Blade Effect. *Adv. Electron. Mater.* **2018**, *4*, 1800110.
14. Zhao, X.; Zhan, X. Electron Transporting Semiconducting Polymers in Organic Electronics. *Chem. Soc. Rev*. **2011**, *40*, 3728–3743.
15. Heeger, A. J. Semiconducting Polymers: The Third Generation. *Chem. Soc. Rev*. **2010**, *39*, 2354–2371.
16. Noriega, R.; Rivnay, J.; Vandewal, K.; Koch, F. P. V.; Stingelin, N.; Smith, P.; Toney, M. F.; Salleo, A. A General Relationship between Disorder, Aggregation and Charge Transport in Conjugated Polymers. *Nat. Mater.* **2013**, *12*, 1038–1044.
17. Olivier, Y.; Niedzialek, D.; Lemaur, V.; Pisula, W.; Müllen, K.; Koldemir, U.; Reynolds, J. R.; Lazzaroni, R.; Cornil, J.; Beljonne, D. 25th Anniversary Article: High-Mobility Hole and Electron Transport Conjugated Polymers: How Structure Defines Function. *Adv. Mater.* **2014**, *26*, 2119–2136.

18. Sirringhaus, H.; Brown, P. J.; Friend, R. H.; Nielsen, M. M.; Bechgaard, K.; Langeveld-Voss, B. M. W.; Spiering, A. J. H.; Janssen, R. A. J.; Meijer, E. W.; Herwig, P.; de Leeuw, D. M. Two-Dimensional Charge Transport in Self-Organized, High-Mobility Conjugated Polymers. *Nature* **1999**, *401*, 685–688.

19. Liu, J.; Arif, M.; Zou, J.; Khondaker, S. I.; Zhai, L. Controlling Poly(3-hexylthiophene) Crystal Dimension: Nanowhiskers and Nanoribbons. *Macromolecules* **2009**, *42*, 9390–9393.

20. Kline, R. J.; McGehee, M. D.; Kadnikova, E. N.; Liu, J.; Fréchet, J. M. J.; Toney, M. F. Dependence of Regioregular Poly(3-hexylthiophene) Film Morphology and Field-Effect Mobility on Molecular Weight. *Macromolecules* **2005**, *38*, 3312–3319.

21. Wang, S.; Kappl, M.; Liebewirth, I.; Müller, M.; Kirchhoff, K.; Pisula, W.; Müllen, K. Organic Field-Effect Transistors Based on Highly Ordered Single Polymer Fibers. **2012**, *24*, 417–420.

22. Zhai, L.; Khondaker, S. I.; Thomas, J.; Shen, C.; McInnis, M. Ordered Conjugated Polymer Nano- and Microstructures: Structure Control for Improved Performance of Organic Electronics. *Nano Today* **2014**, *9*, 705–721.

23. Ying, L.; Huang, F.; Bazan, G. C. Regioregular Narrow-Bandgap-Conjugated Polymers for Plastic Electronics. *Nat. Commun*. **2017**, *9*, 14047.

24. Adachi, T.; Brazard, J.; Ono, R. J.; Hanson, B.; Traub, M. C.; Wu, Z.-Q.; Li, Z.; Bolinger, J. C.; Ganesan, V.; Bielawski, C. W.; Bout, D. A. V.; Barbara, P. F. Regioregularity and Single Polythiophene Chain Conformation. *J. Phys. Chem. Lett.* **2011**, *2*, 1400–1404.

25. Qu, S.; Ming, C.; Yao, Q.; Lu, W.; Zeng, K.; Shi, W.; Shi, X.; Uher, C.; Chen, L. Understanding the Intrinsic Carrier Transport in Highly Oriented Poly(3-hexylthiophene):

Effect of Side Chain Regioregularity. *Polymers* **2018**, *10*, 815.

26. Ying, L.; Hsu, B. B. Y.; Zhan, H.; Welch, G. C.; Zalar, P.; Perez, L. A.; Kramer, E. J.; Nguyen, T.-Q.; Heeger, A. J.; Wong, W.-Y.; Bazan, G. C. Regioregular Pyridal[2,1,3]Thiadiazole π-Conjugated Copolymers. *J. Am. Chem. Soc.* **2011**, *133*, 18538–18541.

27. Park, K. S.; Kwok, J. J.; Dilmurat, R.; Qu, G.; Kafle, P.; Luo, X.; Jung, S.-H.; Olivier, Y.; Lee, J.-K.; Mei, J.; Beljonne, D.; Diao, Y. Tuning Conformation, Assembly, and Charge Transport Properties of Conjugated Polymers by Printing Flow. *Sci. Adv.* **2019**, *5*, eaaw7757.

28. Zhang, X.; Bronstein, H.; Kronemeijer, A. J.; Smith, J.; Kim, Y.; Kline, R. J.; Richter, L. J.; Anthopoulos, T. D.; Sirringhaus, H.; Song, K.; Heeney, M.; Zhang, W.; McCulloch, I.; DeLongchamp, D. M. Molecular Origin of High Field-Effect Mobility in an Indacenodithiophene–Benzothiadiazole Copolymer. *Nat. Commun.* **2013**, *4*, 2238.

29. Hwang, H.; Kim, Y.; Kang, M.; Lee, M.-H.; Heo, Y.-J.; Kim, D.-Y. A Conjugated Polymer with High Planarity and Extended π-Electron Delocalization: via a Quinoid Structure Prepared by Short Synthetic Steps. *Polym. Chem.* **2017**, *8*, 361–365.

30. Bijleveld, J. C.; Zoombelt, A. P.; Mathijssen, S. G. J.; Wienk, M. M.; Turbiez, M.; de Leeuw, D. M.; Janssen, R. A. J. Poly(diketopyrrolopyrrole−terthiophene) for Ambipolar Logic and Photovoltaics. *J. Am. Chem. Soc.* **2009**, *131*, 16616–16617.

31. Khim, D.; Han, H.; Baeg, K.-J.; Kim, J.; Kwak, S.-W.; Kim, D.-Y.; Noh, Y.-Y. Simple Bar-Coating Process for Large-Area, High-Performance Organic Field-Effect Transistors and Ambipolar Complementary Integrated Circuits. *Adv. Mater.* **2013**, *25*, 4302–4308.

32. Shaw, L.; Hayoz, P.; Diao, Y.; Reinspach, J. A.; To, J. W. F.; Toney, M. F.; Weitz, R. T.;

Bao, Z. Direct Uniaxial Alignment of a Donor-Acceptor Semiconducting Polymer Using Single-Step Solution Shearing. *ACS Appl. Mater. Interfaces* **2016**, *8*, 9285–9296.

33. Tsao, H. B.; Cho, D.; Andreasen, J. W.; Rouhanipour, A.; Breiby, D. W.; Pisula, W.; Müllen, K. The Influence of Morphology on High-Performance Polymer Field-Effect Transistors. *Adv. Mater.* **2009**, *21*, 209–212.

34. Wang, S.; Kiersnowski, A.; Pisula, W.; Müllen, K. Microstructure Evolution and Device Performance in Solution-Processed Polymeric Field-Effect Transistors: The Key Role of the First Monolayer. *J. Am. Chem. Soc.* **2012**, *134*, 4015–4018.

35. Li, M.; An, C.; Marszalek, T.; Baumgarten, M.; Müllen, K.; Pisula, W. Impact of Interfacial Microstructure on Charge Carrier Transport in Solution-Processed Conjugated Polymer Field-Effect Transistors. *Adv. Mater.* **2016**, *28*, 2245–2252.

36. Lee, M. J.; Gupta, D.; Zhao, N.; Heeney, M.; McCulloch, I.; Sirringhaus, H. Anisotropy of Charge Transport in a Uniaxially Aligned and Chain-Extended, High-Mobility, Conjugated Polymer Semiconductor. **2011**, *21*, 932–940.

37. Schuettfort, T.; Watts, B.; Thomsen, L.; Lee, M.; Sirringhaus, H.; McNeill, C. R. Microstructure of Polycrystalline PBTTT Films: Domain Mapping and Structure Formation. *ACS Nano* **2012**, *6*, 1849–1864.

38. Giri, G.; DeLongchamp, D. M.; Reinspach, J.; Fischer, D. A.; Richter, L. J.; Xu, J.; Benight, S.; Ayzner, A.; He, M.; Fang, L.; Xue, G.; Toney, M. F.; Bao, Z. Effect of Solution Shearing Method on Packing and Disorder of Organic Semiconductor Polymers. *Chem. Mater.* **2015**, *27*, 2350–2359.

39. Schott, S.; Gann, E.; Thomsen, L.; Jung, S.-H.; Lee, J.-K.; McNeill, C. R.; Sirringhaus, H. Charge-Transport Anisotropy in a Uniaxially Aligned Diketopyrrolopyrrole-Based

Copolymer. *Adv. Mater.* **2015**, *27*, 7356–7364.

40. Lee, J.; Han, A.-R.; Hong, J.; Seo, J. H.; Oh, J. H.; Yang, C. Inversion of Dominant Polarity in Ambipolar Polydiketopyrrolopyrrole with Thermally Removable Groups. *Adv. Funct. Mater.* **2012**, *22*, 4128–4138.

41. Lee, J.; Han, A.-R.; Kim, J.; Kim, Y.; Oh, J. H.; Yang, C. Solution-Processable Ambipolar Diketopyrrolopyrrole–Selenophene Polymer with Unprecedentedly High Hole and Electron Mobilities. *J. Am. Chem. Soc.* **2012**, *134*, 20713–20721.

42. Lee, W.-Y.; Giri, G.; Diao, Y.; Tassone, C. J.; Matthews, J. R.; Sorensen, M. L.; Mannsfeld, S. C. B.; Chen, W.-C.; Fong, H. H.; Tok, J. B.-H.; Toney, M. F.; He, M.; Bao, Z. Effect of Non-Chlorinated Mixed Solvents on Charge Transport and Morphology of Solution-Processed Polymer Field-Effect Transistors. *Adv. Funct. Mater.* **2014**, *24*, 3524–3534.

43. Diao, Y.; Shaw, L.; Bao, Z.; Mannsfeld, S. C. B. Morphology Control Strategies for Solution-Processed Organic Semiconductor Thin Films. *Energy Environ. Sci.* **2014**, *7*, 2145–2159.

44. Gu, X.; Shaw, L.; Gu, K.; Toney, M. F.; Bao, Z. The Meniscus-Guided Deposition of Semiconducting Polymers. *Nat. Commun.* **2018**, *9*, 534.

45. Becerril, H. A.; Roberts, M. E.; Liu, Z.; Locklin, J.; Bao, Z. High-Performance Organic Thin-Film Transistors through Solution-Sheared Deposition of Small-Molecule Organic Semiconductors . *Adv. Mater.* **2008**, *20*, 2588–2594.

46. Chang, M.; Lim, G. T.; Park, B.; Reichmanis, E. Control of Molecular Ordering, Alignment, and Charge Transport in Solution-Processed Conjugated Polymer Thin Films. *Polymers* **2017**, *9*, 212

47. Biniek, L.; Leclerc, N.; Heiser, T.; Bechara, R.; Brinkmann, M. Large Scale Alignment and Charge Transport Anisotropy of pBTTT Films Oriented by High Temperature Rubbing. *Macromolecules* **2013**, *46*, 4014–4023.

48. Xue, X.; Chandler, G.; Zhang, X.; Kline, R. J.; Fei, Z.; Heeney, M.; Diemer, P. J.; Jurchescu, O. D.; O'Connor, B. T. Oriented Liquid Crystalline Polymer Semiconductor Films with Large Ordered Domains. *ACS Appl. Mater. Interfaces* **2015**, *7*, 26726–26734.

49. Shin, E.-S.; Ha, Y. H.; Gann, E.; Lee, Y.-J.; Kwon, S.-K.; McNeill, C. R.; Noh, Y.-Y.; Kim, Y.-H. Design of New Isoindigo-Based Copolymer for Ambipolar Organic Field-Effect Transistors. *ACS Appl. Mater. Interfaces* **2018**, *10*, 13774–13782.

50. Kim, N.-K.; Jang, S.-Y.; Pace, G.; Caironi, M.; Park, W.-T.; Khim, D.; Kim, J.; Kim, D.-Y.; Noh, Y.-Y. High-Performance Organic Field-Effect Transistors with Directionally Aligned Conjugated Polymer Film Deposited from Pre-Aggregated Solution. *Chem. Mater.* **2015**, *27*, 8345–8353.

51. Kim, N.-K.; Shin, E.-S.; Noh, Y.-Y.; Kim, D.-Y. A Selection Rule of Solvent for Highly Aligned Diketopyrrolopyrrole-Based Conjugated Polymer Film for High Performance Organic Field-Effect Transistors. *Org. Electron.* **2018**, *55*, 6–14.

52. Morita, T.; Singh, V.; Nagamatsu, S.; Oku, S.; Takashima, W.; Kaneto, K. Enhancement of Transport Characteristics in Poly(3-hexylthiophene) Films Deposited with Floating Film Transfer Method. *Appl. Phys. Express* **2009**, *2*, 111502.

53. Tripathi, A. S. M.; Kumari, N.; Nagamatsu, S.; Hayase, S.; Pandey, S. S. Facile Fabrication of Large Area Oriented Conjugated Polymer Films by Ribbon-Shaped FTM and Its Implication on Anisotropic Charge Transport. *Org. Electron.* **2019**, *65*, 1–7.

54. Pandey, M.; Gowda, A.; Nagamatsu, S.; Kumar, S.; Takashima, W.; Hayase, S.; Pandey,

S. S. Rapid Formation and Macroscopic Self-Assembly of Liquid-Crystalline, High-Mobility, Semiconducting Thienothiophene. *Adv. Mater. Interfaces* **2018**, *5*, 1700875.

55. Tripathi, A. S. M.; Pandey, M.; Sadakata, S.; Nagamatsu, S.; Takashima, W.; Hayase, S.; Pandey, S. S. Anisotropic Charge Transport in Highly Oriented Films of Semiconducting Polymer Prepared by Ribbon-Shaped Floating Film. *Appl. Phys. Lett.* **2018**, *112*, 123301.
56. Tiwari, S.; Takashima, W.; Nagamatsu, S.; Balasubramanian, S. K.; Prakash, R. A Comparative Study of Spin Coated and Floating Film Transfer Method Coated Poly (3-hexylthiophene)/Poly (3-hexylthiophene)-Nanofibers Based Field Effect Transistors. *J. Appl. Phys.* **2014**, *116*, 094306.
57. Nawaz, A.; Kumar, A.; Hümmelgen, I. A. Ultra-High Mobility in Defect-Free Poly(3-hexylthiophene-2,5-diyl) Field-Effect Transistors through Supra-Molecular Alignment. *Org. Electron.* **2017**, *51*, 94–102.
58. Pandey, M.; Pandey, S. S.; Nagamatsu, S.; Hayase, S.; Takashima, W. Solvent Driven Performance in Thin Floating-Films of PBTTT for Organic Field Effect Transistor: Role of Macroscopic Orientation. *Org. Electron.* **2017**, *43*, 240–246.
59. Pandey, M.; Nagamatsu, S.; Pandey, S. S.; Hayase, S.; Takashima, W. Orientation Characteristics of Non-Regiocontrolled Poly (3-hexyl-thiophene) Film by FTM on Various Liquid Substrates. *J. Phys. Conf. Ser.* **2016**, *704*, 012005.
60. Pandey, M.; Pandey, S. S.; Nagamatsu, S.; Hayase, S.; Takashima, W. Influence of Backbone Structure on Orientation of Conjugated Polymers in the Dynamic Casting of Thin Floating-Films. *Thin Solid Films* **2016**, *619*, 125–130.
61. Kim, B.-G.; Jeong, E. J.; Chung, J. W.; Seo, S.; Koo, B.; Kim, J. A Molecular Design Principle of Lyotropic Liquid-Crystalline Conjugated Polymers with Directed Alignment

Capability for Plastic Electronics. *Nat. Mater.* **2013**, *12*, 659–664.

62. Chung, K.; Yu, Y.; Kwon, M. S.; Swets, J.; Kim, J.; Youk, J. H. Assembly and Alignment of Conjugated Polymers: Materials Design, Processing, and Applications. *MRS Commun.* **2015**, *5*, 169–189.

63. Shao, W.; Dong, H.; Jiang, L.; Hu, W. Morphology Control for High Performance Organic Thin Film Transistors. *Chem. Sci*. **2011**, *2*, 590–600.

64. Zhang, L.; Zhao, K.; Li, H.; Zhang, T.; Liu, D.; Han, Y. Liquid Crystal Ordering on Conjugated Polymers Film Morphology for High Performance. *J. Polym. Sci. Part B Polym. Phys.* **2019**, *57*, 1572–1591.

65. Collyer, A. A. Lyotropic Liquid Crystal Polymers for Engineering Applications. *Mater. Sci. Technol.* **1990**, *6*, 981–992.

66. Bridges, C. R.; Ford, M. J.; Popere, B. C.; Bazan, G. C.; Segalman, R. A. Formation and Structure of Lyotropic Liquid Crystalline Mesophases in Donor−Acceptor Semiconducting Polymers. *Macromolecules* **2016**, *49*, 7220–7229.

67. Fujiwara, T.; Locklin, J.; Bao, Z. Solution Deposited Liquid Crystalline Semiconductors on a Photoalignment Layer for Organic Thin-Film Transistors. *Appl. Phys. Lett.* **2007**, *90*, 232108.

68. Zheng, Z.; Yim, K.-H.; Saifullah, M. S. M.; Welland, M. E.; Friend, R. H.; Kim, J.-S.; Huck, W. T. S. Uniaxial Alignment of Liquid-Crystalline Conjugated Polymers by Nanoconfinement. *Nano Lett.* **2007**, *7*, 987–992.

69. Bridges, C. R.; Ford, M. J.; Bazan, G. C.; Segalman, R. A. Molecular Considerations for Mesophase Interaction and Alignment of Lyotropic Liquid Crystalline Semiconducting Polymers. *ACS Macro Lett.* **2017**, *6*, 619–624.

70. Soeda, J.; Matsui, H.; Okamoto, T.; Osaka, I.; Takimiya, K.; Takeya, J. Highly Oriented Polymer Semiconductor Films Compressed at the Surface of Ionic Liquids for High-Performance Polymeric Organic Field-Effect Transistors. *Adv. Mater.* **2014**, *26*, 6430–6435.

71. Kushida, T.; Nagase, T.; Naito, H. Mobility Enhancement in Solution-Processable Organic Transistors through Polymer Chain Alignment by Roll-Transfer Printing. *Org. Electron.* **2011**, *12*, 2140–2143.

72. Ong, B. S.; Wu, Y.; Liu, P.; Gardner, S. High-Performance Semiconducting Polythiophenes for Organic Thin-Film Transistors. *J. Am. Chem. Soc.* **2004**, *126*, 3378–3379.

73. McCulloch, I.; Heeney, M.; Bailey, C.; Genevicius, K.; MacDonald, I.; Shkunov, M.; Sparrowe, D.; Tierney, S.; Wagner, R.; Zhang, W.; Chabinyc, M. L.; Kline, J.; McGehee, M. D.; Toney, M. F. Liquid-Crystalline Semiconducting Polymers with High Charge-Carrier Mobility. *Nat. Mater.* **2006**, *5*, 328–333.

74. Sirringhaus, H.; Wilson, R. J.; Friend, R. H.; Inbasekaran, M.; Wu, W.; Woo , E. P.; Grell, M.; Bradley, D. D. C. Mobility Enhancement in Conjugated Polymer Field-Effect Transistors through Chain Alignment in a Liquid-Crystalline Phase. *Appl. Phys. Lett.* **2000**, *77*, 406–408.

75. Liu, C.; Xu, Y.; Noh, Y.-Y. Contact Engineering in Organic Field-Effect Transistors. *Mater. Today* **2015**, *18*, 79–96.

76. Mariucci, L.; Rapisarda, M.; Valletta, A.; Fortunato, G. Contact Effects in Organic Thin-Film Transistors: Device Physics and Modeling. In Chen, J.; Cranto, W.; Fihn, M. (eds.) *Handbook of Visual Display Technology*, Springer, Cham **2016**, pp 945–969.

77. Klug, A.; Denk, M.; Bauer, T.; Sandholzer, M.; Scherf, U.; Slugovc, C.; List, E. J. W. Organic Field-Effect Transistor Based Sensors with Sensitive Gate Dielectrics Used for Low-Concentration Ammonia Detection. *Org. Electron.* **2013**, *14*, 500–504.

78. Noh, Y.-Y.; Sirringhaus, H. Ultra-Thin Polymer Gate Dielectrics for Top-Gate Polymer Field-Effect Transistors. *Org. Electron.* **2009**, *10*, 174–180.

79. Kumatani, A.; Li, Y.; Darmawan, P.; Minari, T.; Tsukagoshi, K. On Practical Charge Injection at the Metal/Organic Semiconductor Interface. *Sci. Rep.* **2013**, *3*, 1026.

80. Klauk, H. Organic Thin-Film Transistors. *Chem. Soc. Rev*. **2010**, *39*, 2643–2666.

81. Baeg, K.-J.; Khim, D.; Kim, D.-Y.; Koo, J. B.; You, I.-K.; Choi, W. S.; Noh, Y.-Y. High Mobility Top-Gated Poly(3-hexylthiophene) Field-Effect Transistors with High Work-Function Pt Electrodes. *Thin Solid Films* **2010**, *518*, 4024–4029.

82. Kumar, B.; Kaushik, B. K.; Negi, Y. S. Organic Thin Film Transistors: Structures, Models, Materials, Fabrication, and Applications: A Review. *Polym. Rev.* **2014**, *54*, 33–111.

83. Menšík, M.; Toman, P.; Bielecka, U.; Bartkowiak, W.; Pflegera, J.; Paruzel, B. On the Methodology of the Determination of Charge Concentration Dependent Mobility from Organic Field-Effect Transistor Characteristics. *Phys. Chem. Chem. Phys.* **2018**, *20*, 2308–2319.

84. Park, Y. D.; Lim, J. A.; Lee, H. S.; Cho, K. W. Interface Engineering in Organic Transistors. *Mater. Today* **2007**, *10*, 46–54.

85. Reséndiz, L.; Estrada, M.; Cerdeira, A.; Iñiguez, B.; Deen, M. J. Effect of Active Layer Thickness on the Electrical Characteristics of Polymer Thin Film Transistors. *Org. Electron.* **2010**, *11*, 1920–1927.

86. Lee, J.; Kim, K.; Kim, J. H.; Im, S.; Jung, D.-Y. Optimum Channel Thickness in Pentacene-Based Thin-Film Transistors. *Appl. Phys. Lett.* **2003**, *82*, 4169–4171.

87. Gupta, D.; Hong, Y. Understanding the Effect of Semiconductor Thickness on Device Characteristics in Organic Thin Film Transistors by Way of Two-Dimensional Simulations. *Org. Electron.* **2010**, *11*, 127–136.

88. Ribierre, J. C.; Watanabe, S.; Matsumoto, M.; Muto, T.; Hashizume, D.; Aoyama, T. Thickness Dependence of the Ambipolar Charge Transport Properties in Organic Field-Effect Transistors Based on a Quinoidal Oligothiophene Derivative. *J. Phys. Chem. C* **2011**, *115*, 20703–20709.

89. Janasz, L.; Gradzka, M.; Chlebosz, D.; Zajaczkowski, W.; Marszalek, T.; Kiersnowski, A.; Ulanski, J.; Pisula, W. Microstructure-Dependent Charge Carrier Transport of Poly(3-hexylthiophene) Ultrathin Films with Different Thicknesses. *Langmuir* **2017**, *33*, 4189–4197.

90. Mannebach, E. M.; Spalenka, J. W.; Johnson, P. S.; Cai, Z.; Himpsel, F. J.; Evans, P. G. High Hole Mobility and Thickness-Dependent Crystal Structure in *α,ω*-Dihexylsexithiophene Single-Monolayer Field-Effect Transistors. *Adv. Funct. Mater.* **2013**, *23*, 554–564.

Chapter 2

Molecular Design Approach for Directed Alignment of Conjugated Polymers

Macromolecules **2019**, *52*, 6485–6494; published by American Chemical Society

2.1 Introduction

Conjugated polymers (CPs) are emerging materials of interest for various optical and electronic applications, including sensors,[1–5] security inks,[6–9] and electronic devices.[10–12] Generally, CPs have a rigid conjugated backbone and flexible solubilizing side chains. Because of the one-dimensional (1-D) π-orbital overlap along their long rigid rodlike backbone, CPs exhibit anisotropic characteristics such as absorption, emission, and charge mobility. Therefore, the macroscopic alignment of CPs in solid thin films is essential in utilizing their interesting 1-D properties in applications. To quantify the degree of CP alignment, the dichroic ratio has been expressed as $I_{//}/I_{\perp}$, where $I_{//}$ and $I_{\perp}$ are the absorption or emission intensity parallel and perpendicular to the alignment direction, respectively. In the case of an isotropic (randomly oriented) CP film, the dichroic ratio is 1, which means no directional difference in absorption and/or emission intensity.

To fully utilize CP's anisotropic optoelectronic properties in the solid state, a great deal of efforts has been devoted to devising various CP-processing methods including Langmuir-Blodgett (LB) technique,[13,14] mechanical rubbing,[15–17] nanoimprinting,[18–20] directional solidification,[21–24] electrospinning,[25–27] and prepatterned substrate[28–31] or matrix[32–38] induced CP

alignment.[39] For example, fairly well-oriented films of poly(*p*-phenylene)[13] and poly(phenylene ethynylene)s[14] were obtained by the LB technique. CP chains are aligned in a monolayer at the air-water interface by repeated compression and expansion of the two barriers, and the aligned CP film was transferred to a substrate. The generated flow field when the substrate moves up and down through the air-water interface further induces CP alignment. Wittmann et al. reported oriented poly(3-hexylthiophene) (P3HT) films by directional crystallization on 1,3,5-trichlorobenzene.[22] Tensile drawing and electrospinning of CPs were also explored. CPs such as poly(2-methoxy-5-(2'-ethyl-hexyloxy)-1,4-phenylenevinylene) (MEH-PPV)[36] and poly(2,5-dialkoxy-p-phenyleneethynylene)s (PPEs)[37] were dissolved with an ultra-high molecular weight polyethylene in a common solvent and cast to form a self-standing film followed by a uniaxial drawing of the film for an embedded CP alignment. The polymer blend showed anisotropic optical properties. For the CP alignment by electrospinning, poly(methyl methacrylate) (PMMA) and poly(ethylene oxide) (PEO) have been widely utilized as a matrix. Electrospun nanofibers of polyfluorene/PMMA[25] and MEH-PPV/PEO[26] composites showed dichroic ratios of 4 and 13, respectively. On the other hand, the mechanical rubbing of the CP film has also been applied to achieve alignment, for instance, mechanically rubbed polydiacetylene films using a silicon cloth[15] and P3HT films using velvet[16] exhibited successful CP alignment. Nanoimprinting[18] and mechanically rubbed polyimide substrate[28] have been used to align liquid crystalline (LC) CPs. To be specific, the alignment of thermotropic LC CP chains to the rubbing direction of the polyimide film was observed with dichroic ratios ranging from 5 to 12, depending on the sample preparation conditions.[28] Most recently, Segalman and coworkers have described macroscopically aligned CPs[40] using a modified blade-coating method previously introduced by

Bao et al.[41] They achieved the alignment of lyotropic LC CPs by controlling the steric repulsion between side chains and attractive interactions between aromatic backbones.

While these processing methods combined with specific types of CPs have achieved decent CP alignments, molecular structural design approaches to enable CP alignment have not been fully established. Our research group previously reported three design requirements to make lyotropic LC CPs having a directed alignment capability, and realized anisotropic optoelectronic properties from aligned CP films.[42] The identified design requirements are (1) concentration-induced planarization unit (S-F interaction), (2) bulky side chains linked to (3) a tetrahedral carbon linker.[42] A CP that satisfies these three design parameters forms lyotropic LC, and is readily aligned to the direction of an applied shear field. The aligned CP1 film exhibited a high dichroic ratio of ca. 16, and the hole mobility of the aligned CP1 film was more than 2 orders of magnitude larger than that of a randomly oriented spin-cast CP1 film. These preliminary results demonstrated the potential of CP alignment in manifesting the inherent optoelectronic property of CPs in various applications.

In this chapter, we further thoroughly investigate molecular structural parameters critically affecting the CP alignment characteristics beyond the previously defined design parameters: out-of-plane side chain linker, main chain planarity, bulky side chains, induced chain planarization unit and surface energy of CPs. We first verify the previously identified structural parameters for directed LC CP alignment. NCP1 is built with a new CP building block and satisfies all three design parameters while NCP2 has the bulky side chains connected to a nitrogen linker instead of a tetrahedral carbon linker. The other six CPs are newly designed to investigate the effects of the main chain planarity (NCP3, NCP4, and NCP5), the role of the branching point of side chains (NCP6), alternative concentration-induced planarization units and

the role of the surface energy of CPs (NCP7 and NCP8). As an application of the unique optoelectronic property of macroscopically aligned CP films, an organic thin film transistor (OTFT) was fabricated with an aligned CP1 film to demonstrate a multimode optical switching. Under polarized light illumination, decent photocurrent gain was observed depending on the alignment of the polarized light to the CP alignment direction, and the on-to-off switching ratio (I_{on}/I_{off}) was large enough for this OTFT to operate in a multimode fashion, allowing both electrical and optical switching. The demonstrated multimode switching suggests a potential application of the directed CP alignment based on its anisotropic response to an anisotropic input signal.

2.2 Results and Discussion

Generally, CPs tend to aggregate due to strong π-π interactions between hydrophobic and rodlike conjugated backbones. Accordingly, to realize the directed macroscopic alignment of CPs in the solid state by exploiting their rodlike structure and large aspect ratio, individual CP chain should be mobile so as to be responsive to an applied external force field. The three design requirements, (1) concentration-induced planarization unit, and (2) bulky side chains linked to (3) a tetrahedral carbon, endow the CPs in a concentrated solution with certain interchain interactions as well as mobility, characteristic properties of a lyotropic LC so that the CPs can be effectively aligned under an applied shear flow.[42] In a diluted solution, the twisted CP conformation together with bulky side chains prevents massive aggregation of CP chains. As the solvent evaporates, the built-in intramolecular S-F interaction induces the conjugated backbone to be planarized,[43,44] which promotes interpolymer π-π interactions. Still, the large side chains on the out-of-plain tetrahedral carbon linker prevent strong aggregation and interdigitation. As a

consequence, mobile CP chains can be aligned with the direction of an applied force field. Indeed, the previously reported CP1 showed a birefringent texture and lyotropic LC characteristics only at a high concentration.[42]

To systematically explore the proper molecular design parameters for directed alignment of CPs, eight new polymers (NCP 1–8) were designed and synthesized using Stille or Suzuki coupling polymerization. Synthetic details are described in the Experimental Section. The polymer purification and contact coating procedures for directed CP alignment have been reported previously.[42] NCP1 has a cyclopenta[2,1-*b*:3,4-*b*′]dithiophene building block, substituting the cyclopenta[*c*]thiophene of CP1 (Figure 2.1a), but still satisfying the three previously identified design requirements by having the concentration-induced planarization unit via S-F interaction as well as the bulky 2-ethylhexyl side chains on a tetrahedral carbon linker. On the other hand, NCP2 has a nitrogen atom replacing the tetrahedral carbon of NCP1 as a linker to connect the bulky side chains, failing the efficient prevention of π-aggregation due to the lack of the out-of-plane side chain linker, tetrahedral carbon. These two new polymers are designed to verify that the design requirement of bulky side chains on a tetrahedral carbon linker to prevent massive π-aggregation is valid.

To provide improved insight on the molecular design for directed CP alignment, we studied the effect of newly defined additional structural factors; main chain planarity and the branching point in bulky side chains (Figure 2.1b,c). NCP3 is built to have less-effective concentration-induced planarization because its fluorene unit, instead of the cyclopenta[2,1-*b*:3,4-*b*′]dithiophene, has a relatively larger thienyl–phenyl dihedral angle due to the repulsion between the hydrogen atoms. In contrast, NCP4 and NCP5 have an intrinsically planar polythiophene backbone, and are used to examine whether an intrinsically more planar unit can

replace the 2,2'-(2,5-difluoro-1,4-phenylene)dithiophene having S-F interactions for the concentration-induced planarization. Three and two thienyl groups were placed between the cyclopenta[*c*]thiophene units in NCP4 and NCP5, respectively. This variation affects the spatial location of the side chains relative to the polymer backbone. While all of the side chains of NCP4 are located on the same side of the conjugated backbone, NCP5 with the bithiophene unit has its side chains alternating on the opposite sides of the main chain. On the other hand, NCP6 is designed to understand the effect of the branching point of bulky side chains by substituting 2-ethylhexyl side chains of NCP1 with 5-methylhexyl side chains (Figure 2.1c).

An alternative intramolecular interaction (S-O interaction) is implemented in CP analogues and examined to extend the design window. We directly replace the S-F interaction unit with the S-O interaction unit in NCP7 to investigate its capability as for the concentration-induced planarization function and its effect on the CP alignment (Figure 2.1d).[43,45–47] An important role of fluorine atoms in CP analogue effecting on the CP alignment characteristic by modifying the surface energy of CPs is perceived from the comparison between CP1 and NCP7 and further explored with NCP8, which has S-O interaction unit with additional two fluorine atoms.

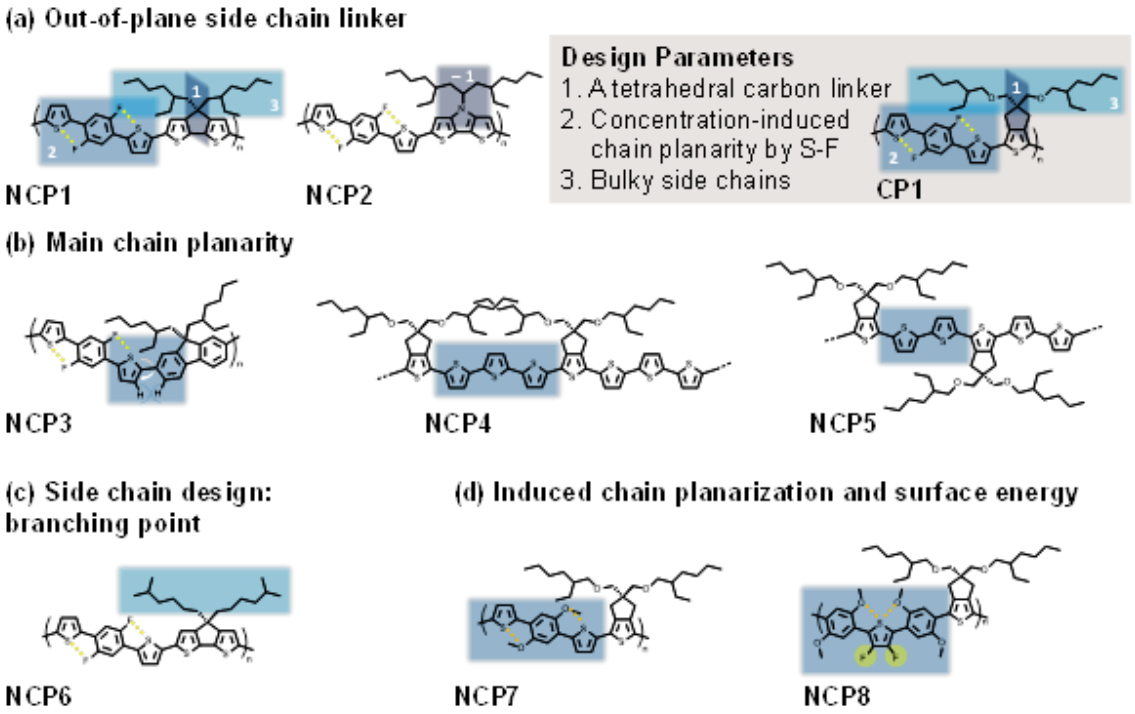

Figure 2.1 Conjugated polymer design and defined molecular design parameters in this study. (a) Out-of-plane side chain linker. (b) Main chain planarity. (c) Side chain design: branching point of the side chain. (d) Concentration-induced main chain planarization and surface energy of CPs.

It is worth to note that CPs, which are capable of directed alignment, have a distinct UV-vis absorption trait: no aggregation band even in a highly concentrated solution (~100 mg mL^{-1}) but largely red-shifted λ_{max} in the solid state due to the concentration-induced planarization and intermolecular packing.[42] Therefore, the simple UV-vis absorption analysis in the solution and the solid state can single out certain CPs for more systematic LC analysis and alignment test.

Figure 2.2 presents the absorption spectra of the solutions and thin films of NCP1–NCP8. NCP1 shows a featureless absorption spectrum in solution, which can be attributed to the conformational disorders in the polymer backbone.[48–50] The disordered and nonplanar polymer chains resulting in no discernable aggregation bands in the absorption spectrum of NCP1 were

presumably caused by the twisted phenyl group and bulky side chains on the tetrahedral carbon linker. A similar behavior was observed in the absorption trait of the CP1 as effective prevention of the interaction between polymer chains.[42] However, in the solid state, NCP1 shows red-shifted λ_{max} (~22 nm, Table 2.1) and an additional aggregation shoulder band due to the concentration-induced chain planarization and interchain packing. Different from NCP1, NCP2 exhibits only a slight change between the absorption spectra of the solution and film. This spectral characteristic of NCP2 can be possibly associated with some pre-aggregates formed in the solution because of the strong interchain interactions.[51] One plausible explanation for the preaggregated solution is the absence of the out-of-plane linker to prevent massive aggregation.[42]

As shown in Figure 2.3a, NCP1, which satisfies the three previously identified design requirements, clearly shows a lyotropic LC phase in a highly concentrated solution (over 200 mg mL^{-1}) and is aligned along the flow field direction with a dichroic ratio of 4.67 (Figure 2.3d, by contact coating, blade speed of 25 μm sec^{-1}). The lyotropic LC formation and alignment behavior of NCP1 support that the previously suggested CP design parameters are applicable to different types of building blocks for the directed alignment of CPs as far as the molecular design features are satisfied. On the other hand, NCP2 which lacks the out-of-plane side chain linker does not show birefringence patterns under crossed polarizers (Figure 2.3b), confirming no lyotropic LC phase formation. As a result, NCP2 exhibits very minor alignment under shear flow (Figure 2.3d and Table 2.1). We conclude that bulky side chains on an out-of-plane side chain linker, tetrahedral carbon linker, are required to accomplish effective CP alignment.

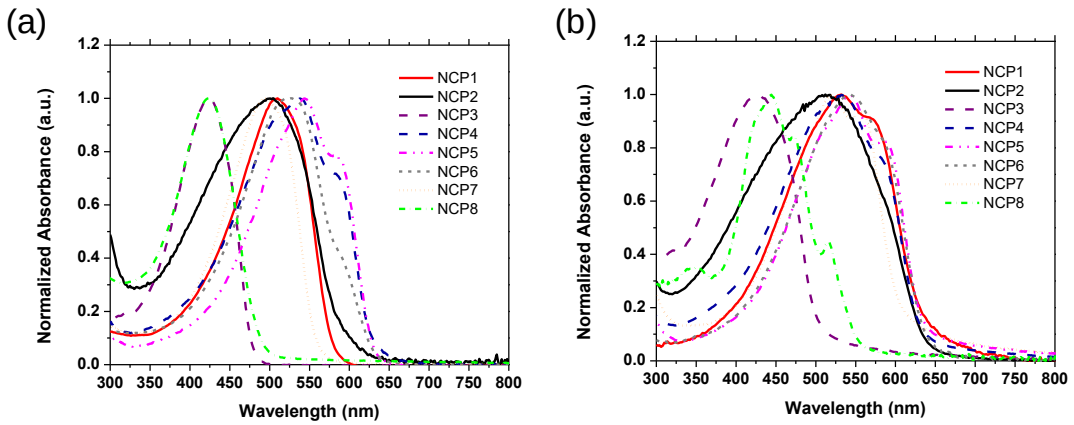

Figure 2.2 UV-vis absorption spectra of NCP1– NCP8 of (a) chloroform solutions and (b) films.

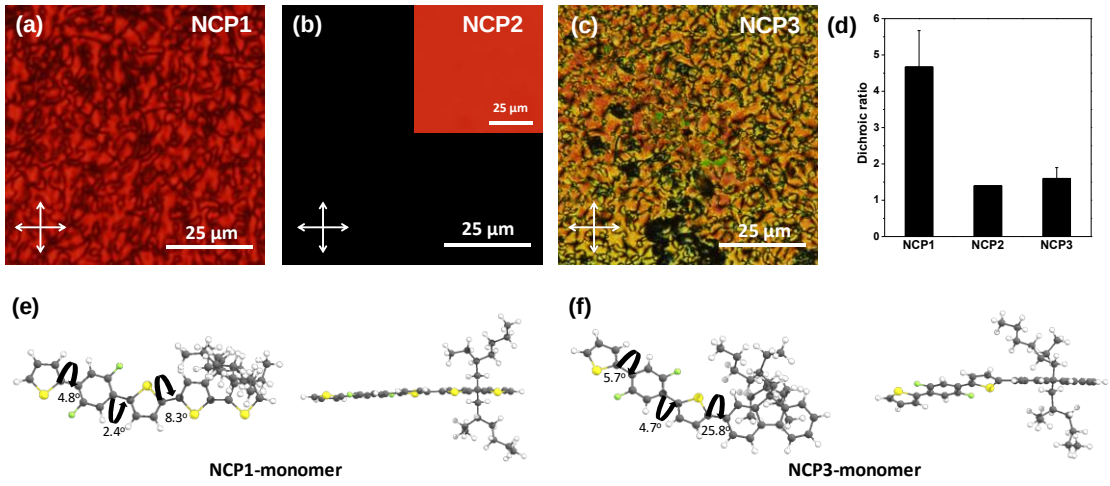

Figure 2.3 Optical microscope images of concentrated CP solutions (over 200 mg mL^{-1}) under crossed polarizers: (a) NCP1, (b) NCP2, and (c) NCP3. Highly concentrated NCP1 and NCP3 solutions exhibit birefringence under crossed polarizers. (the inset of (b): the corresponding bright field micrograph). (d) Dichroic ratio of the aligned CP films. Gaussian-predicted (B3LYP/6-31G (d) basis set) conformations of (e) NCP1 and (f) NCP3 in front view (left) and side view (right).

Table 2.1 Molecular weights, optical properties, and alignment characteristics of NCP1–NCP8

	M_n[a] (g/mol)	M_w[a] (g/mol)	PDI[a]	λ_{max} (nm)		DR
				solution	film	
NCP1	6,800	8,800	1.3	510	532	4.67
NCP2	7,300	9,700	1.3	504	510	1.4
NCP3	2,500	4,200	1.7	424	428	1.6
NCP4	8,100	16,700	2.1	538	536	1.11
NCP5	8,200	10,500	1.3	544	542	1.25
NCP6	7,000	10,400	1.5	526	544	1.2
NCP7	20,200	38,100	1.89	495	518	0.98
NCP8	2,600	3,100	1.2	423	444	1.51

[a] Determined by gel permeation chromatography (GPC) using chloroform as the eluent.

Even though NCP3 has the same concentration-induced planarization unit (S-F interaction) and bulky side chains on a tetrahedral carbon linker, NCP3 films exhibit only a small red shift in the absorption λ_{max} (~4 nm) compared to NCP3 in solution (Table 2.1 and Figure 2.2), indicating inefficient chain planarization and intermolecular packing in the solid state. This observation can be explained by the relatively large thienyl-phenyl dihedral angle (25.8°, Figure 2.3e,f) that restricts chain planarization, yielding small dichroic ratio (Figure 2.3d and Table 2.1), even though NCP3 forms a lyotropic LC phase in a highly concentrated solution (over 200 mg mL^{-1}, Figure 2.3c). The relatively small molecular weight of NCP3 is also believed to be partially responsible for the small dichroic ratio (Table 2.1) because a larger aspect ratio would respond more efficiently to the applied shear field and consequently render a better alignment along the shear direction.[52]

The intrinsically planar NCP4 and NCP5 show a strong aggregation band at ca. 580 nm even in dilute solution (Figure 2.2a). No additional red-shift in the absorption λ_{max} is observed in their thin films because both CPs retain a planar conformation and strong interchain aggregation in the solution (Table 2.1). Consequently, these two CPs exhibit almost no directional alignment under shear flow, which supports that concentration-induced planarization unit is an important design factor to prevent premature massive aggregation in dilute solution and provide the alignment capability to CPs.

Interestingly, even though NCP6 is designed with the concentration-induced planarization unit and the 5-methylhexyl side chains on a tetrahedral carbon linker, it shows a distinct aggregation band at ca. 590 nm in its UV-vis absorption spectrum even in a dilute solution (Figure 2.2), indicating non-efficient prevention of aggregation. Consequently, NCP6 is not capable to form effective CP alignment under applied shear flow (Table 2.1). The distinct difference in aggregation and CP alignment behavior between NCP1 and NCP6 is attributed to the different branching point of the side chains. If the branch junction is close to the conjugated backbone like the 2-ethylhexyl of NCP1, the side chains provide effective steric hindrance between CP main chains so as to efficiently prevent π-π stacking. In contrast, 5-methylhexyl side chains of NCP6, which have the branching points away from the conjugated backbone, are less effective in preventing π-π interaction between CP backbones. Therefore, the chemical structure of the branched bulky side chains in the CP design turns out to be a crucial factor to accomplish the alignment of CP chains.

To investigate S-O interaction as an alternative intramolecular interaction to substitute S-F interaction, we replaced the fluorine atom of CP1 with two methoxy groups in NCP7. In solution, NCP7 shows the absorption maximum (λ_{max}) at 495 nm and no aggregation, while in a

solid film, NCP7 exhibits a bathochromic shift of the peak from 495 nm to 518 nm with a distinct additional aggregation peak at 556 nm (Figure 2.2 and Table 2.1), which indicates an increased effective conjugation length caused by chain planarization and is very similar to how CP1 and NCP1 behave.[53,54] NCP7 also shows a birefringence texture under crossed polarizers implying LC formation (Figure 2.4a).

However, the NCP7 film deposited by contact coating shows no alignment (dichroic ratio ~1, Figure 2.4b and Table 2.1). This discrepancy likely stems from the wettability (surface energy) difference between the two polymers. The two fluorine atoms of CP1 and NCP1 lower the surface energy of the CPs, different from NCP7 bearing two methoxy groups. This surface energy difference might have a significant impact on the wettability and arrangement of the polymer chains on a substrate and makes NCP7 respond differently under the same contact coating condition. Indeed, an interesting result has been published showing that the CP arrangement on a substrate is distinctly differentiated as the incorporated functional groups on the CP analogue differ. Cho *et al.* reported that the substituting methoxy groups with fluorine functional groups converted the CP arrangement from face-on to edge-on on a substrate.[43]

To investigate the role of fluorine in the CP alignment beyond the concentration-induced chain planarization by intramolecular S-F interaction, we designed and synthesized NCP8 in such a way that we kept the same S-O interaction for concentration-induced chain planarization but added two fluorine atoms on the thiophene moiety to lower the surface energy of NCP8. The absorption behaviors of NCP8 are very similar to those of NCP7 even though NCP8 exhibited the shortest absorption λ_{max} among the eight polymers, presumably due to its very low molecular weight (Table 2.1). We tried to improve the polymerization method but were unable to increase the molecular weight of NCP8. Interestingly, NCP8 exhibits birefringence texture under crossed

polarizers implying LC formation (Figure 2.4a) and is somewhat aligned along the contact coating direction with the maximum dichroic ratio of 2.37 and an average dichroic ratio of 1.51 (Figure 2.4b and Table 2.1). We believe that the relatively small dichroic ratio of NCP8 was attributed to its small molecular weight and less planar geometry of its polymer chain similar to the case of NCP3. Taken together, these results imply that the fluorine atoms on the CP backbone affect the effective alignment of CPs along the applied shear field by providing suitable wettability and arrangement relative to the substrate.

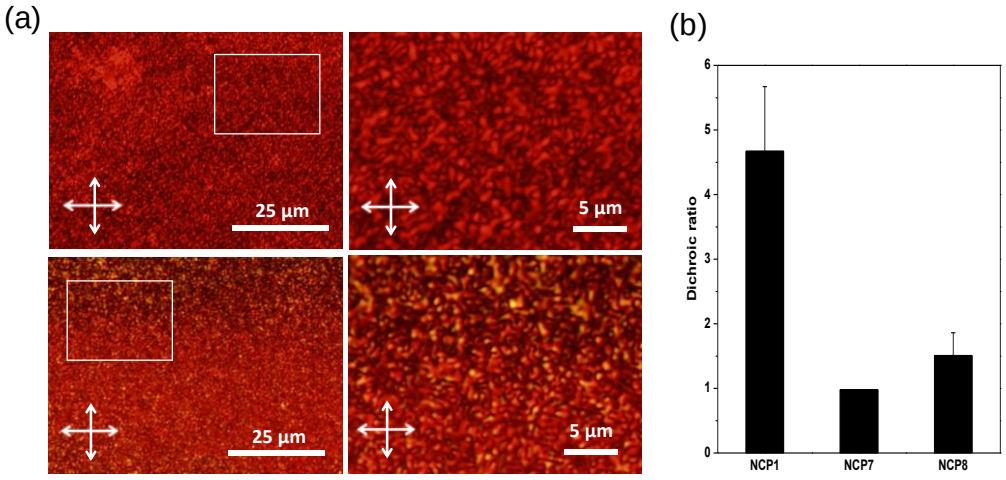

Figure 2.4 Optical microscope images of concentrated CP solutions (over 200 mg mL^{-1}) under crossed polarizers: (a) NCP7 (top) and NCP8 (bottom). The boxed areas are enlarged in the right panels. (b) Dichroic ratio of the aligned CP films.

To further understand how the chemical structure affects the backbone planarity, conformational preferences of the subunits of NCP1, NCP7, and NCP8 were studied. The initial geometries of the molecules were optimized using density functional theory (DFT) with B3LYP/6-31G (d) in Gaussian 09. After the optimization, the potential energy of each subunit at different dihedral angles was calculated while all other degrees of freedom were allowed to relax to an energy minimum. The dihedral angles were varied from 0 degree in 36 steps by 10 degrees.

For simplicity, side chains were replaced with methyl groups in the calculation. The potential energy surface (PES) scans of the thiophene (T)–cyclopentadithiophene (CPDT) for NCP1 and the T-cyclopenta[*c*]thiophene (CPT) for NCP7 showed the minimum energy at around 200° with a very small energy barrier (less than 0.5 kJ/mol) for the completely planar geometry (180°) (Figure 2.5a,b). For NCP8, the energy minima were obtained at dihedral angles of 230° and 130°, which correspond to twisted structures. More importantly, the steep and large energy barrier of 18.0 kJ/mol for the planar conformation suggests that NCP8 likely maintains the twisted conformation. On the other hand, the PES scans around dihedral angles of 2,5-difluorophenyl (FP)-T for NCP1, DMP-P for NCP7, and 3,4-difluorothiophene (FT)-DMP for NCP8 indicate that weak intramolecular interactions such as S-F and S-O can improve the backbone planarity (Figure 2.5c,d). Interestingly, two different conformations of NCP1 at dihedral angles of 0° (360°) and 180°, which correspond to the S-F interaction and H-F interaction, respectively, have almost the same energy. The negligible preference between these two interactions has been reported in the literature.[55] The role of H-F interaction in our molecular alignment system is unclear and needs to be addressed in future work, but this result implies that not only S-F or S-O interaction but also H-F interaction may have a potential for the weak intramolecular interaction design.

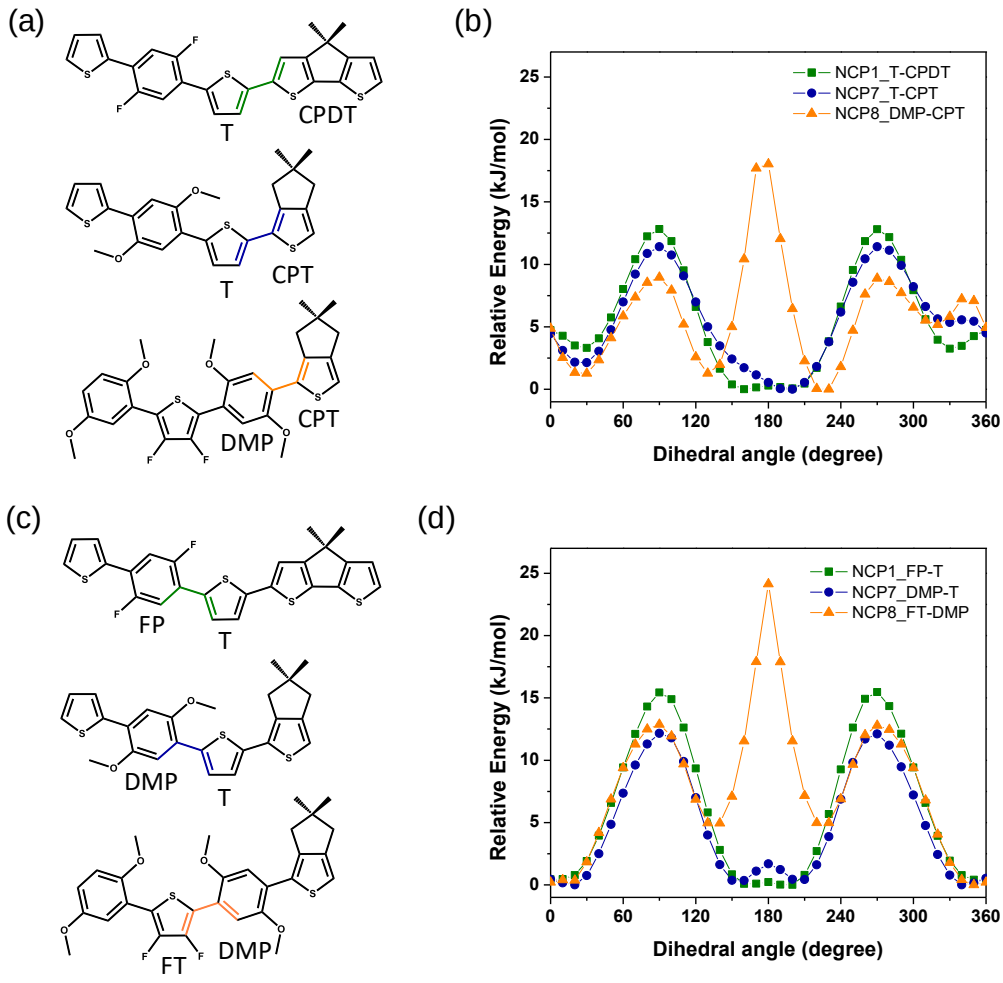

Figure 2.5 Conformational geometry calculation of NCP1, NCP7, and NCP8. (a), (c) Chemical structures of the subunits for NCP1 (top), NCP7 (middle), and NCP8 (bottom). The shown dihedral angles of each structure are (a) 180° for thiophene (T)-cyclopentadithiophene (CPDT) and T-cyclopenta[*c*]thiophene (CPT), 0° for 2,5-dimethoxylphenyl (DMP)-CPT, and (C) 0° for all three structures. (b), (d) Potential energy surface scans of dihedral angles. FP, 2,5-difluorophenyl, FT, 3,4-difluorothiophene.

Grazing Incidence X-ray Diffraction (GIXRD) measurements on NCP1, NCP7, and NCP8 films provide further evidence of the effect of fluorine atoms in CP analogues on the chain arrangement on a substrate. Figure 2.6 presents the GIXRD patterns of NCP1, NCP7, and NCP8 films when the X-ray beam is parallel and perpendicular to the blading direction, and their line profiles along the in-plane and out-of-plane directions. All GIXRD patterns show several

reflections with good orientation. These reflections can be indexed with a monoclinic symmetry, and their observed *d*-spacings are well matched with the calculated *d*-spacings as shown in Tables 2.2 and 2.3. The (100) reflections of NCP1 and NCP8 (at d_{100} = 12.97 and 28.17 Å, respectively) are located along the normal to the substrate (vertical direction), in both parallel and perpendicular patterns, indicating that the crystals of NCP1 and NCP8 have structures with their edges on the substrate, i.e., edge-on structures. However, in the case of NCP7, both (100) and (010) reflections (*d*-spacings are 21.03 and 4.18 Å, respectively) are located along the normal of the substrate in both parallel and perpendicular patterns, while the (010) reflection is broader than the (100) reflection at the azimuthal direction (Figure 2.6b). The difference of width in the azimuthal direction may indicate that the origins of these reflections are different from each other. The *d*-spacing value of the (100) reflection (21.03 Å) indicates that the edge-on structure exists. The *d*-spacing value of the (010) reflection (4.18 Å) is correlated to the spacing between the benzene rings. The orientation (location) and *d*-spacing value of the (010) reflection are also indicative of the face-on structure. A plausible explanation for the coexistence of the edge-on and face-on orientations could be due to the various competing factors, such as the size of the polymer repeating unit, chemical modifications, etc. To be specific, it has been reported that when the size of the repeating unit becomes larger, the polymer tends to have an edge-on dominant orientation.[56] However, when it comes to the structure of the repeating unit, the methoxy-modified polymer is known to have face-on crystallites, whereas primarily edge-on crystallites are produced from its fluorine-substituted analogue.[43] Therefore, the bimodal character (the mixture of edge-on and face-on orientations) of NCP7 can be understood by considering its methoxy-modified large repeating unit. Again, the results imply that the addition

of fluorine atoms on the CP analogue affects the arrangement of CP chains relative to the substrate, which results in the different behavior of CP alignment upon the applied shear field.

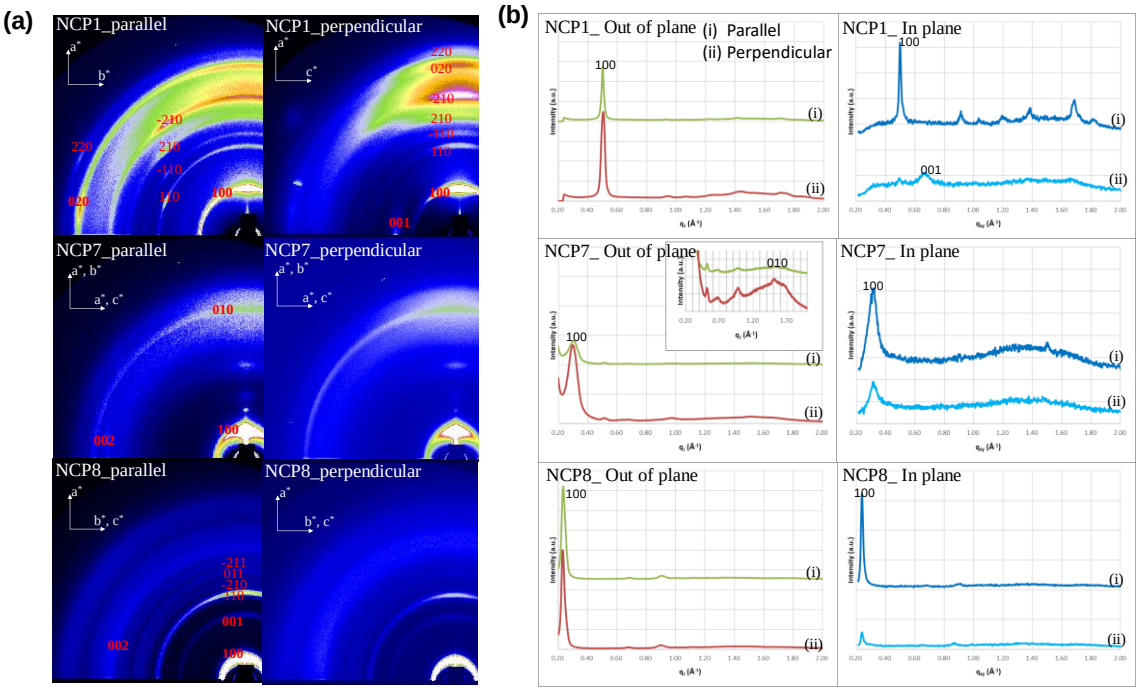

Figure 2.6 (a) Grazing incidence X-Ray Diffraction (GIXRD) patterns of blade-coated NCP1 (top), NCP7 (middle), and NCP8 (bottom) films when X-ray beam are parallel (left) and perpendicular (right) to the blade-coating directions. (b) Line profiles along the out-of-plane (left) and in-plane (right) directions of GIXRD patterns of blade-coated NCP1 (top), NCP7 (middle), and NCP8 (bottom) films when X-ray beam are (i) parallel and (ii) perpendicular to the blade coating directions. The inset in the line profiles of NCP7 out-of-plane is for magnification of (010) plane.

Table 2.2 Miller indices of NCP1, NCP7, and NCP8

No.	NCP1			NCP7			NCP8		
	hkl	d_o (Å)	d_c (Å)	*hkl*	d_o (Å)	d_c (Å)	*hkl*	d_o (Å)	d_c (Å)
1	100	12.97	12.97	100	21.03	21.03	100	28.17	28.17
2	001	9.60	9.60	-	11.92	-	001	9.44	9.44
3	110	6.96	6.96	-	9.23	-	110	7.13	7.13
4	-110	6.14	6.13	-	6.43	-	-210	6.22	6.23
5	210	5.23	5.31	002	4.49	4.49	011	5.76	5.73
6	-210	4.59	4.59	010	4.18	4.18	-211	5.15	5.20
7	020	3.76	3.76				002	4.68	4.72
8	220	3.47	3.48				020	3.61	3.61

Table 2.3 Unit cell structures of NCP1, NCP7, and NCP8

	a (Å)	b (Å)	c (Å)	α	β	γ	Crystal structure
NCP1	13.0	7.5	9.6	90	90	81.6	Monoclinic
NCP7	21.0	4.2	9.0	-	-	-	-
NCP8	28.2	7.2	9.4	90	90	85.5	Monoclinic

Directed alignment of CPs can expand the utility of CPs in various optoelectronic applications. Here, we demonstrate a multimode switching of OTFT devices by fabricating the devices with an aligned CP1 film and achieving an optical gating effect under polarized light illumination. The OTFT devices were fabricated using a top-contact/bottom-gate configuration.[42] A heavily doped n-type Si/SiO_2 wafer was used as a gate electrode and gate dielectric, and CP1

was aligned by contact coating on the phenyl trichlorosilane-treated Si/SiO_2 wafer (Figure 2.7a, red arrow). Subsequently, the source and drain electrodes (Au) were deposited. From the drain current (I_{DS}) - drain voltage (V_{DS}) characteristics of the device, largely different photocurrent gains were observed depending on the relative orientation of the polarized light illumination (7.1 mW cm^{-2}) to the aligned CP1 chains (Figures 2.7b and 2.8). Especially, compared to the output current under no light illumination, the output current at a gate voltage (V_G) of – 40 V was increased by ca. 4-fold when the device was measured under the illumination of polarized light in parallel to the CP1 alignment direction. On the other hand, almost no increase in the output current was observed when the polarized light illuminated in the perpendicular direction of the CP1 alignment. This anisotropic photocurrent gain demonstrates the realization of highly anisotropic optoelectronic properties of CP via directed alignment. Furthermore, it implies that the incident light can substitute the electrical gating as an independent input signal to generate charge carriers in the transistor. The on-to-off switching ratio (I_{on}/I_{off}) under the light illumination was about 7.2×10^4 (Figure 2.7c), which is large enough for an OTFT to operate by an optical trigger.

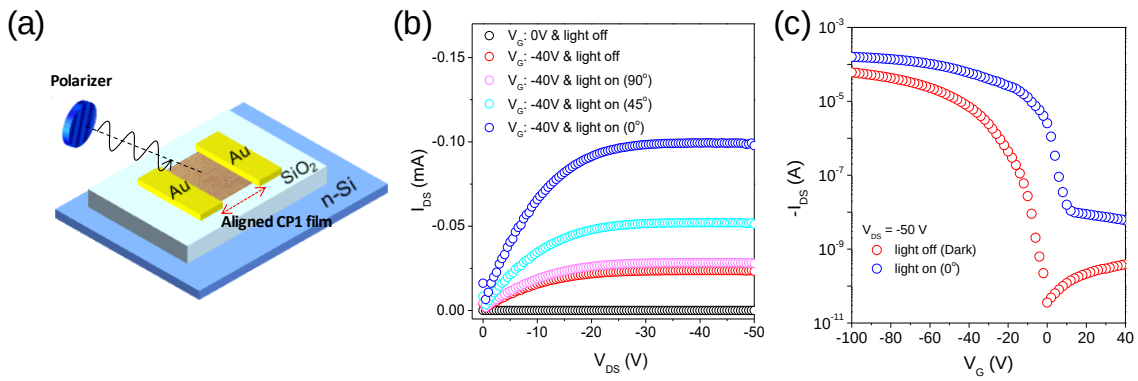

Figure 2.7 Multimode switching of the aligned CP1 OTFT device. (a) Schematic illustration of the optical switching setup of the aligned CP1 OTFT device. CP1 chains are aligned in the direction of the red arrow. (b) Drain current-drain voltage (I_{DS}-V_{DS}) curves of an aligned CP1 OTFT device. The angle in the figure legend (0º, 45º, 90º) is the angle between the polarized incident light and the CP alignment direction. (c) Transfer characteristics of the aligned CP1 OTFT device under dark and polarized light illuminations.

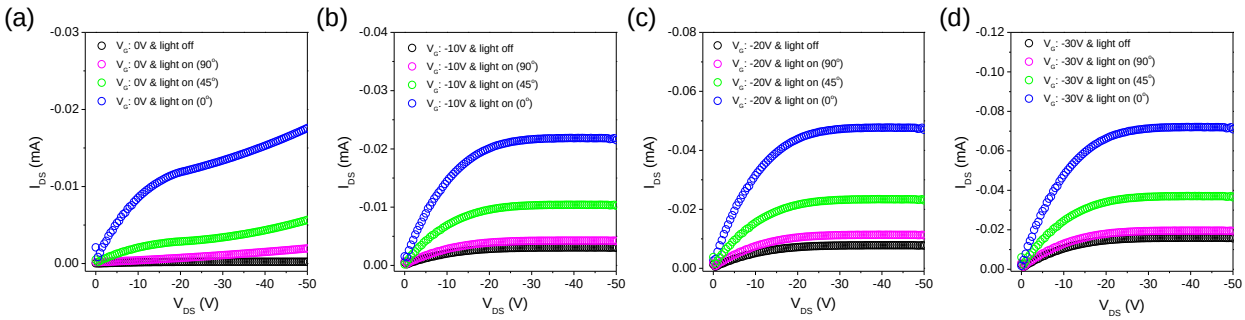

Figure 2.8 Drain current-drain voltage (I_{DS}-V_{DS}) curves of an aligned CP1 OTFT device at a gate voltage (V_G) of (a) 0 V, (b) -10 V, (c) -20 V, and (d) -30 V, respectively. The angle in the figure legend (0º, 45º, 90º) is the angle between the polarized incident light and the CP alignment direction.

2.3 Experimental Section

2.3.1 Materials and Synthesis

All the chemicals and solvents for the synthesis were purchased from commercial suppliers (TCI, Acros, Sigma-Aldrich, and Fisher Sci.). The synthesis of monomers were conducted following the previously described synthetic routes.[42,57-65]

2.3.1.1 Synthesis of 1,3-Dibromo-5,5-bis(((2-ethylhexyl)oxy)methyl)-5,6-dihydro-4*H*-cyclopenta[*c*]thiophene (2)

Compound 1 is prepared as the previously described manner.[42] Compound 1 (2 g, 4.89 mmol) was added to dry chloroform (25 mL). Under Ar condition, the mixture was cooled down to 0 ^{o}C, and *N*-bromosuccinimide (2.18 g, 12.23 mmol) was added. After stirring 4 hrs at room temperature, the reaction mixture was poured into water and extracted with methylene chloride. The organic phase was dried over $MgSO_4$, and the solvent was evaporated in *vacuo*. Column chromatography using the mixed solvent (methylene chloride : n-hexane = 1 : 1) as an eluent gave the product (2.397 g, 87% yield) as a colorless liquid (Figure 2.9). ^{1}H NMR (500 MHz, $CDCl_3$, δ): 3.32 (s, 4 H), 3.28 (d, *J*=6.0 Hz, 4H), 2.53 (s, 4H), 1.50 – 1.45 (m, 2H), 1.42 – 1.26 (m, 16H), 0.91 – 0.84 (m, 12H). MS m/z (APCI+, relative intensity): 567 (M^++1, 100), 409 (5), 279 (10), 205 (5), 149 (29), 113 (19). HRMS (APCI+) calcd. for $C_{25}H_{42}Br_2O_2S$ (M^++1) 565.1345, found 565.1340.

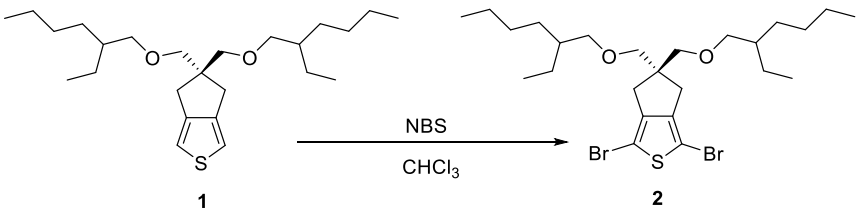

Figure 2.9 Synthesis of compound 2 for NCP4, NCP5, and NCP7.

2.3.1.2 Synthesis of 4,4-Bis(5-methylhexyl)-4*H*-cyclopenta[2,1-*b*:3,4-*b*']dithiophene (3)

4*H*-cyclopenta[2,1-*b*:3,4-*b*']dithiophene (0.2 g, 1.12 mmol), 1-bromo-5-metyl hexane (0.442 g, 2.47 mmol), potassium iodide (0.013 g, 0.076 mmol) were added to dimethyl sulfoxide (20 mL). The solution was cooled down to 0 ºC followed by the addition of potassium hydroxide (0.201 g, 3.59 mmol) in small portions. After stirring overnight at room temperature, the reaction mixture was poured into water and extracted with methylene chloride. The organic phase was dried over $MgSO_4$, and the solvent was evaporated in *vacuo*. Column chromatography using n-hexane as an eluent gave the product (0.301 g, 72% yield) as a yellowish liquid (Figure 2.10). ^{1}H NMR (400 MHz, $CDCl_3$, δ): 7.15 (d, *J*=4.9 Hz, 2H), 6.94 (d, *J*=4.9 Hz, 2H), 1.85 – 1.81 (m, 4H), 1.44 – 1.36 (m, 2H) 1.15 – 1.06 (m, 4H) 1.05 – 0.99 (m, 4H), 0.95 – 0.88 (m, 4H), 0.79 (d, *J*=6.7 Hz, 12H). MS m/z (EI+, relative intensity): 374 (M^+, 100), 289 (25), 275 (25), 203 (23), 191 (32), 179 (33), 57 (23), 43 (27). HRMS (EI+) calcd. for $C_{23}H_{34}S_2$ (M^+) 374.2102, found 374.2106.

2.3.1.3 Synthesis of 2,6-Dibromo-4,4-bis(5-methylhexyl)-4*H*-cyclopenta[2,1-*b*:3,4-*b*']dithiophene (4)

Compound 3 (0.2 g, 0.534 mmol) was added to dry tetrahydrofuran (15 mL). Under Ar condition, the mixture was cooled down to 0 ºC, and *N*-bromosuccinimide (0.209 g, 1.17 mmol) was added. After stirring overnight at room temperature, the reaction mixture was poured into water and extracted with methylene chloride. The organic phase was dried over $MgSO_4$, and the solvent was evaporated in *vacuo*. Column chromatography using n-hexane as an eluent gave the product (0.245 g, 86% yield) as a yellowish liquid (Figure 2.10). ^{1}H NMR (400 MHz, $CDCl_3$, δ): 6.93 (s, 2H), 1.80–1.74 (m, 4H), 1.45–1.38 (m, 2H) 1.16–1.08 (m, 4H) 1.08–0.99 (m, 4H), 0.95 – 0.86 (m, 4H), 0.81 (d, J=6.6 Hz, 12H). MS m/z (EI+, relative intensity): 532 (M^+, 100),

453 (11), 354 (15), 283 (18), 270 (14), 84 (35), 57 (54), 43 (76). HRMS (EI+) calcd. for $C_{23}H_{32}Br_2S_2$ (M^+) 530.0312, found 530.0310.

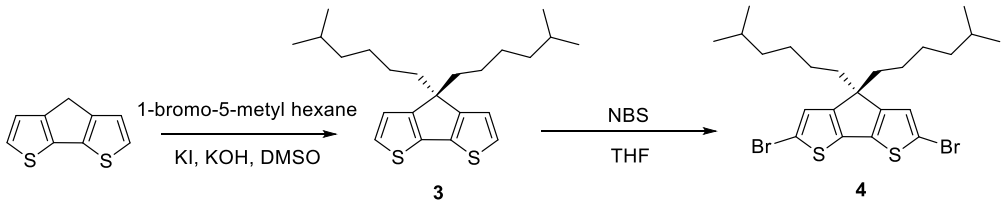

Figure 2.10 Synthetic routes of compounds 3 and 4.

2.3.1.4 Synthesis of ((2,5-Dimethoxy-1,4-phenylene)bis(thiophene-5,2-diyl))bis(trimethylstannane) (6)

Compound 5 is prepared as previously described manner.[59] Under Ar condition, compound 5 (0.5 g, 1.65 mmol) was added to dry tetrahydrofuran. At 0 ºC, *n*-butyllithium (2.5 M in hexanes, 1.52 mL) was added into the solution dropwise. The reaction mixture was stirred for 30 min at room temperature, and trimethyltin chloride (1 M in tetrahydrofuran, 4.13 mL) was added. The mixture was further stirred overnight at room temperature. Then, it was poured into water and extracted with chloroform. The organic phase was dried over $MgSO_4$, and the solvent was evaporated in *vacuo*. The product (0.54 g, 52% yield) was purified by recrystallization, which was conducted in ethanol (Figure 2.11). ^{1}H NMR (500 MHz, $CDCl_3$, δ): 7.63 (d, *J*=3.5 Hz, 2H), 7.23 (s, 2H), 7.19 (d, J=3.5 Hz, 2H), 3.932 (s, 6H), 0.39 (s, 18H). MS m/z (EI+, relative intensity): 628 (M^+, 100), 466 (14), 299 (32), 165 (16), 84 (17), 49 (25). HRMS (APCI+) calcd. for $C_{22}H_{30}O_2S_2Sn_2$ (M^++1) 630.9731, found 630.9781.

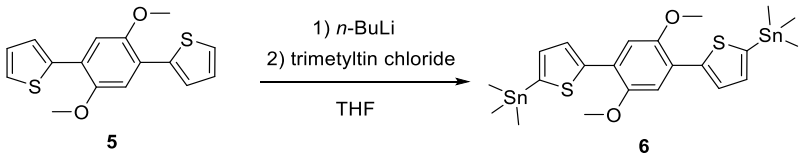

Figure 2.11 Synthesis of compound 6 for NCP7.

2.3.1.5 Synthesis of 3,4-Difluoro-2,5-bis(trimethylstannyl)thiophene (8)

A stirred solution of 2,5-dibromo-3,4-difluorothiophene (2.78 g, 10.0 mmol) in anhydrous THF (100 mL) was cooled down to -78 °C. *n*-butyllithium (24 mmol, 9.6 mL, 2.5 M in hexanes) was added dropwise to the mixture. After stirring at -78 °C for 1 hr, a freshly prepared 1 M trimethyltin chloride stock solution in THF (28.0 mL; corresponding to 5.58 g, 28.0 mmol) was added slowly and the mixture was stirred for an additional 30 min before it was allowed to warm up to room temperature. The mixture was quenched with water, extracted with ether (3×50 mL). The organic layer was then washed with brine (1×100 mL) and dried over anhydrous MgSO4. The solvents were removed under reduced pressure, affording a light yellow solid. The yellow solid was recrystallized three times from n-hexane to yield 2.49 g (55% yield) of a white crystalline solid (Figure 2.12).1H NMR (600 MHz, $CDCl_3$, δ): 0.39 (s, 18H); ^{13}C NMR (125 MHz, $CDCl_3$, δ): -8.56 (9×CH_3) 119.9 (d, J = 35.7 Hz, 2×C-S), 151.8 (dd, J = 231.4, 25.5 Hz, 2×C-F); 19F NMR (470 MHz $CDCl_3$, δ): -132.40 (2F).

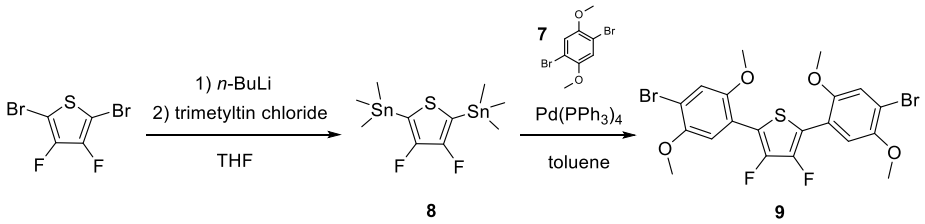

Figure 2.12 Synthetic routes of compounds 8 and 9 for NCP8.

2.3.1.6 Synthesis of 2,5-Bis(4-bromo-2,5-dimethoxyphenyl)-3,4-difluorothiophene (9)

Compound 7 is prepared as the previously described manner.[63] An oven-dried round-bottom flask was charged with starting materials: compound 7 (1.33 g, 4.48 mmol) and compound 8 (250 mg, 0.56 mmol) and 5 mol%, $Pd(PPh_3)_4$ catalyst (32 mg). Anhydrous toluene (5 mL) was added and the reaction mixture was stirred at 100 ºC for 18 hrs to form a dark orange, fluorescent solution. Cooled down crude reaction mixture was dried with a small amount of silica gel and purified by chromatography: 10-20% $CHCl_3$/n-hexane to removal excess of compound 7, 30-50% $CHCl_3$/n-hexane to wash out the product. The solvent was evaporated, and the product (158 mg, 51% yield) was obtained as a bright yellow solid (Figure 2.12). ^{1}H NMR (400 MHz, $CDCl_3$, δ): 3.89 (s, 6H), 3.90 (s, 6H), 7.19 (s, 2H), 7.30 (s, 2H), ^{13}C NMR (125 MHz, $CDCl_3$, δ): 56.5 (2×CH_3), 56.8 (2×CH_3), 111.5 (2×C-Br), 112.8 (t, J = 4.4 Hz, C), 114.8 (t, J = 5.5 Hz, C), 117.2 (2×CH), 119.2 (2×CH), 142.0 (dd, J = 264.0, 21.9 Hz, 2×C-F), 150.2 (2×C-O), 150.3(2xC-O); ^{19}F NMR (376 MHz, $CDCl_3$, δ): -134.64(2F).

2.3.1.7 General Procedure of Stille Type Polymerization

Under Ar conditions, the prepared monomers, compound 4 and 6 for NCP7 for example, were added (1:1 in equivalent) into an anhydrous toluene and *N*,*N*-dimethylformamide mixed solvent (5:1 in volume). After adding 5 mol% of tetrakis(triphenylphosphine)palladium (0), the reaction mixture was heated up to 120 ºC and stirred for 12 hrs. End-capping was further conducted by adding 2-tributylstannyl thiophene and stirring for 6 hrs, followed by adding 2-bromothiophene and stirring for another 6 hrs. The final CPs were collected via reprecipitation of the reaction mixture into methanol. The precipitated polymers were collected through a nylon filter, and further washed with n-hexane, methanol, and acetone in a Soxhlet apparatus to remove

the small molecular weight portion and catalyst residue. Only the part of CPs soluble to chloroform and toluene was obtained. For the alignment test, CPs were further purified through column chromatography using Cellite and Florisil as packing materials. The molecular weights of the synthesized polymers were measured by mean of gel permeation chromatography (GPC): NCP1 (M_n: 6800, M_w: 8800, polydispersity index (PDI): 1.3), NCP2 (M_n: 7300, M_w: 9700, PDI: 1.3), NCP3 (M_n: 2500, M_w: 4200, PDI: 1.7), NCP4 (M_n: 8100, M_w: 16700, PDI: 2.1), NCP5 (M_n: 8200, M_w: 10500, PDI: 1.3), NCP6 (M_n: 7000, M_w: 10400, PDI: 1.5), NCP7 (M_n: 20200, M_w: 38100, PDI: 1.89)

2.3.1.8 Synthesis of NCP8 via Suzuki Polymerization

A solution containing 2,2'-(5,5-bis(((2-ethylhexyl)oxy)methyl)-5,6-dihydro-4*H*-cyclopenta[*c*]thiophene-1,3-diyl)bis(4,4,5,5-tetramethyl-1,3,2-dioxaborolane)[42] (83 mg, 0.15 mmol) and compound 9 (100 mg, 0.15 mmol) in toluene was degassed. Under Ar conditions, 5 mol% of tetrakis(triphenylphospine)palladium (0) and tetraethyl ammonium hydroxide (20% solution) were added to the solution. Under Ar conditions, the reaction mixture was vigorously stirred at 95 ^{o}C for 12 hrs. Bromobenzene and boronic acid were added respectively to the mixture after polymerization. The reaction mixture was cooled down to room temperature and the product was precipitated in methanol. The precipitated solid was subjected to Soxhlet extraction with methanol, n-hexane, acetone, and chloroform. The chloroform soluble fraction was precipitated into methanol and filtered to afford NCP8. The weight-average molecular weight (M_w) was 3100 g/mol (PDI: 1.2).

2.3.2 Spectroscopic Characterization

^{1}H-NMR spectrum was characterized by a Varian, Inova 500 (500 MHz) and Varian, MR400 (400 MHz) in $CDCl_3$ solution. ^{19}F-NMR and ^{13}C-NMR spectra were acquired on a Bruker Ascend 600 and Ultrashield 400Mhz spectrometers. Chemical shift values were recorded as parts per million relative to tetramethylsilane as an internal standard. Coupling constants were recorded in Hertz. Mass spectra were recorded on an Agilent Q-TOF 6520 system using electron impact ionization and atmospheric-pressure chemical ionization in positive ion detection mode. UV-visible absorption spectra were measured on a Varian Cary50 UV/Vis spectrophotometer. Photoluminescence (PL) of contact coated CP films were measured to verify dichroic ratio by mean of the ratio of polarized PL intensity, using PTI QuantaMasterTM spectrofluorometers equipped with a linear polarizer.

2.3.3 GIXRD Characterization

GIXRD was performed on beamline 3C (incident angle: 0.16º) at the Pohang Accelerator Laboratory (PAL). The samples were mounted on a hexapod goniometer, and monochromatized X-rays (λ = 0.123 nm) under vacuum was used. The scattered beam intensity was recorded with a Rayonix 2D MAR165 CCD detector (2048×2018 pixels, pixel size 0.079 um). The diffraction intensity plots of the 2D GIXRD patterns were obtained using SAXS_FIT2D software provided by the European Synchrotron Radiation Facility.

2.3.4 Computational Details

To investigate the conformational preference of polymers, the DFT calculations were performed with the Gaussian 09 software. Molecular geometries of compounds were optimized using the B3LYP functional and 6-31G (d) basis set.

2.3.5 Contact Coating of CP Solution

The CP solutions were prepared in a concentration of 2.5 mg mL^{-1} in *o*-dichlorobenzene, containing 5 vol% of 1,8-octanedithiol. Substrates were cleaned by sonication in a sequence of water, acetone, and isopropanol for 15 min each, followed by UV/O_3 treatment for 10 min (UV/Ozone ProCleaner, BioForce Nanosciences). The cleaned substrate was placed on a hot stage, and the gap between the substrate and contact coating blade was controlled as 50 μm with standard polyimide film including micro-gauge. The CP solution was spread onto the substrate and coated by moving blade (speed: 25 μm sec^{-1}) at 140 ºC.

2.3.6 OTFT Device Fabrication

OTFT devices were fabricated in a top-contact/bottom-gate configuration. The n-type Si/SiO_2 wafers (thermally grown SiO_2, 260 nm) were cleaned by sonication in a sequence of water, acetone, and isopropanol for 15 min each, followed by Piranha solution treatment. Phenyltrichlorosilane (PTS) layer was formed on the cleaned wafers by means of spin coating. Then, CP1 film (80 nm) was fabricated onto PTS treated Si/SiO_2 wafer by means of contact coating. Source and drain electrode deposition (Au, 100 nm) was subsequently performed onto the CP1 film through shadow mask (channel width: 200 μm, channel length:100 μm). The device performance was evaluated utilizing the Keithley 4200-SCS semiconductor analyzer.

2.4 Conclusions

In summary, the molecular design parameters to realize directed CP alignment are systematically investigated and expanded with eight newly designed polymers, especially for the structural parameters critically affecting CP alignment characteristics: out-of-plane side chain linker, main chain planarity, branching point of bulky side chains, induced chain planarization unit, and surface energy of CPs. The previously identified molecular design rules were validated by NCP1 that is designed to satisfy the three requirements: (1) concentration-induced planarization unit, and (2) bulky side chains linked to (3) an out-of-plane carbon linker. A detailed study regarding the backbone planarization has been conducted using NCP3, NCP4, and NCP5. The rather large dihedral angle of NCP3 results in a significantly lower dichroic ratio compared to that of NCP1. NCP4 and NCP5, which have an intrinsically planar conformation even in the dilute solution, are not free from π-π aggregation and thereby no alignment can be achieved due to premature CP aggregation in the solution. The side chain form factor to prevent massive aggregation is critically important (NCP6). Only if the branch junction of side chains is near the conjugated backbone so that the side chains provide effective enough steric hindrance, π-π stacking between CP main chains can be efficiently prevented. We have further investigated the role of fluorine atoms in CP analogue beyond the concentration-induced planarization function through S-F interaction (NCP7 and NCP8). It is confirmed that lowering the surface energy of CPs is an imperative role of fluorine to control the arrangement of CP chains on a substrate (edge-on or face-on), which critically affects directed alignment of CPs upon applied shear field. In this contribution, multimodal switching is also demonstrated with OTFT devices having an aligned CP film. The device exhibits significantly different photocurrent gains depending on the relative orientation of the polarized light illumination direction to the CP

alignment and an excellent on-to-off switching ratio of 7.2×10^4. Our results provide insightful molecular design strategies for directed self-assembly and alignment of CPs to fully realize their anisotropic optoelectronic properties in various device applications.

2.5 Author Contributions

Kyeongwoon Chung,* Da Seul Yang,* Woo-Hwan Sul, Bong-Gi Kim, Jongho Kim, Geunseok Jang, Min Sang Kwon, Maciej Barłóg, Taek Seung Lee, Soo-Young Park, Mohammed Al-Hashimi, Jinsang Kim Molecular Design Approach for Directed Alignment of Conjugated Polymers *Macromolecules*, **2019**, *52*, 6485–6494. (*equal contribution)

J.K., B.-G.K., and K.C. conceived the work. K.C., D.S.Y., B.-G.K. synthesized polymers with the help of J.K., G.J., M.S.K., M.B, and T.S.L. K.C., D.S.Y., and B.-G.K. designed the experiments. K.C. and D.S.Y. measured and analyzed emission spectra, absorption spectra, and LC properties under crossed polarizers with the help of B.-G.K. D.S.Y. performed DFT calculations. W.-H.S. and S.-Y.P. performed the X-ray measurements and analyzed the data. B.-G.K. fabricated and analyzed the OTFT devices. M.A.-H., S.-Y.P., and J.K. supervised the project. K.C., D.S.Y., and J.K. wrote the manuscript through contributions of all authors.

2.6 References

1. Lee, J.; Jun, H.; Kim, J. Polydiacetylene-Liposome Microarrays for Selective and Sensitive Mercury(II) Detection. *Adv. Mater.* **2009**, *21*, 3674–3677.

2. Kim, J.; McQuade, D. T.; McHugh, S. K.; Swager, T. M. Ion-Specific Aggregation in Conjugated Polymers: Highly Sensitive and Selective Fluorescent Ion Chemosensors. *Angew. Chem.* **2000**, *112*, 4026–4030.

3. Lee, K.; Povlich, L. K.; Kim, J. Recent Advances in Fluorescent and Colorimetric Conjugated Polymer-Based Biosensors. *Analyst* **2010**, *135*, 2179–2189.

4. Lee, J.; Seo, S.; Kim, J. Colorimetric Detection of Warfare Gases by Polydiacetylenes Toward Equipment-Free Detection. *Adv. Funct. Mater.* **2012**, *22*, 1632–1638.

5. Ho, H.-A.; Boissinot, M.; Bergeron, M. G.; Corbeil, G.; Doré, K.; Boudreau, D.; Leclerc, M. Colorimetric and Fluorometric Detection of Nucleic Acids Using Cationic Polythiophene Derivatives. *Angew. Chem. Int. Ed.* **2002**, *41*, 1548–1551.

6. Yoon, B.; Lee, J.; Park, I. S.; Jeon, S.; Lee, J.; Kim, J.-M. Recent Functional Material Based Approaches to Prevent and Detect Counterfeiting. *J. Mater. Chem. C* **2013**, *1*, 2388–2403.

7. Yoon, B.; Ham, D.-Y.; Yarimaga, O.; An, H.; Lee, C. W.; Kim, J.-M. Inkjet Printing of Conjugated Polymer Precursors on Paper Substrates for Colorimetric Sensing and Flexible Electrothermochromic Display. *Adv. Mater.* **2011**, *23*, 5492–5497.

8. Yoon, B.; Shin, H.; Yarimaga, O.; Ham, D.-Y.; Kim, J.; Park, I. S.; Kim, J.-M. An Inkjet-Printable Microemulsion System for Colorimetric Polydiacetylene Supramolecules on Paper Substrates. *J. Mater. Chem.* **2012**, *22*, 8680–8686.

9. Chung, K.; McAllister, A.; Bilby, D.; Kim, B.-G.; Kwon, M. S.; Kioupakis, E.; Kim, J. Designing Interchain and Intrachain Properties of Conjugated Polymers for Latent Optical Information Encoding. *Chem. Sci.* **2015**, 6, 6980–6985.

10. Tsao, H. N.; Müllen, K. Improving Polymer Transistor Performance via Morphology Control. *Chem. Soc. Rev.* **2010**, *39*, 2372–2386.

11. Gross, M.; Müller, D. C.; Nothofer, H.-G.; Scherf, U.; Neher, D.; Braüchle, C.; Meerholz, K. Improving the Performance of Doped π-Conjugated Polymers for Use in Organic Light-Emitting Diodes. *Nature* **2000**, *405*, 661–665.

12. Günes, S.; Neugebauer, H.; Sariciftci, N. S. Conjugated Polymer-Based Organic Solar Cells. *Chem. Rev.* **2007**, *107*, 1324–1338.

13. Cimrová, V.; Remmers, M.; Neher, D.; Wegner, G. Polarized Light Emission from LEDs Prepared by the Langmuir-Blodgett Technique. *Adv. Mater.* **1996**, *8*, 146–149.

14. Kim, J.; McHugh, S. K.; Swager, T. M. Nanoscale Fibrils and Grids: Aggregated Structures from Rigid-Rod Conjugated Polymers. *Macromolecules* **1999**, *32*, 1500–1507.

15. Kanetake, T.; Ishikawa, K.; Koda, T.; Tokura, Y.; Takeda, K. Highly Oriented Polydiacetylene Films by Vacuum Deposition. *Appl. Phys. Lett.* **1987**, *51*, 1957–1959.

16. Heil, H.; Finnberg, T.; von Malm, N.; Schmechel, R.; von Seggern, H. The Influence of Mechanical Rubbing on the Field-Effect Mobility in Polyhexylthiophene. *J. Appl. Phys.* **2003**, *93*, 1636–1641.

17. Biniek, L.; Pouget, S.; Djurado, D.; Gonthier, E.; Tremel, K.; Kayunkid, N.; Zaborova, E.; Crespo-Monteiro, N.; Boyron, O.; Leclerc, N.; Ludwigs, S.; Brinkmann, M. High-

Temperature Rubbing: A Versatile Method to Align π-Conjugated Polymers without Alignment Substrate. *Macromolecules* **2014**, *47*, 3871–3879.

18. Zheng, Z.; Yim, K.-H.; Saifullah, M. S. M.; Welland, M. E.; Friend, R. H.; Kim, J.-S.; Huck, W. T. S. Uniaxial Alignment of Liquid-Crystalline Conjugated Polymers by Nanoconfinement. *Nano Lett.* **2007**, *7*, 987–992.

19. Aryal, M.; Trivedi, K.; Hu, W. Nano-Confinement Induced Chain Alignment in Ordered P3HT Nanostructures Defined by Nanoimprint Lithography. *ACS Nano* **2009**, *3*, 3085–3090.

20. Ding, G.; Wu, Y.; Weng, Y.; Zhang, W.; Hu, Z. Solvent-Assistant Room Temperature Nanoimprinting-Induced Molecular Orientation in Poly(3-hexylthiophene) Nanopillars. *Macromolecules* **2013**, *46*, 8638–8643.

21. De Rosa, C.; Park, C.; Thomas, E.L.; Lotz, B. Microdomain Patterns from Directional Eutectic Solidification and Epitaxy. *Nature* **2000**, *405*, 433–437.

22. Brinkmann, M.; Wittmann, J.-C. Orientation of Regioregular Poly(3-hexylthiophene) by Directional Solidification: A Simple Method to Reveal the Semicrystalline Structure of a Conjugated Polymer. *Adv. Mater.* **2006**, *18*, 860–863.

23. Müller, C.; Aghamohammadi, M.; Himmelberger, S.; Sonar, P.; Garriga, M.; Salleo, A.; Campoy-Quiles, M. One-Step Macroscopic Alignment of Conjugated Polymer Systems by Epitaxial Crystallization during Spin-Coating. *Adv. Funct. Mater.* **2013**, *23*, 2368–2377.

24. Dörling, B.; Vohra, V.; Dao, T. T.; Garriga, M.; Murata, H.; Campoy-Quiles, M. Uniaxial Macroscopic Alignment of Conjugated Polymer Systems by Directional Crystallization during Blade Coating. *J. Mater. Chem. C* **2014**, *2*, 3303–3310.

25. Kuo, C.-C.; Wang, C.-T.; Chen, W.-C. Highly-Aligned Electrospun Luminescent Nanofibers Prepared from Polyfluorene/PMMA Blends: Fabrication, Morphology, Photophysical Properties and Sensory Applications. *Macromol. Mater. Eng.* **2008**, *293*, 999–1008.

26. Campoy-Quiles, M.; Ishii, Y.; Sakai, H.; Murata, H. Highly Polarized Luminescence from Aligned Conjugated Polymer Electrospun Nanofibers. *Appl. Phys. Lett.* **2008**, *92*, 213305.

27. Yin, K.; Zhang, L.; Lai, C.; Zhong, L.; Smith, S.; Fong, H.; Zhu, Z. Photoluminescence Anisotropy of Uni-Axially Aligned Electrospun Conjugated Polymer Nanofibers of MEH-PPV and P3HT. *J. Mater. Chem.* **2011**, *21*, 444–448.

28. Sirringhaus, H.; Wilson, R. J.; Friend, R. H.; Inbasekaran, M.; Wu, W.; Woo, E. P.; Grell, M.; Bradley, D. D. C. Mobility Enhancement in Conjugated Polymer Field-Effect Transistors through Chain Alignment in a Liquid-Crystalline Phase. *Appl. Phys. Lett.* **2000**, *77*, 406–408.

29. Tseng, H.-R.; Ying, L.; Hsu, B. B. Y.; Perez, L. A.; Takacs, C. J.; Bazan, G. C.; Heeger, A. J. High Mobility Field Effect Transistors Based on Macroscopically Oriented Regioregular Copolymers. *Nano Lett.* **2012**, *12*, 6353–6357.

30. Tseng, H.-R.; Phan, H.; Luo, C.; Wang, M.; Perez, L. A.; Patel, S. N.; Ying, L.; Kramer, E. J.; Nguyen, T.-Q.; Bazan, G. C.; Heeger, A. J. High-Mobility Field-Effect Transistors

Fabricated with Macroscopic Aligned Semiconducting Polymers. *Adv. Mater.* **2014**, *26*, 2993–2998.

31. Luo, C.; Kyaw, A. K. K.; Perez, L. A.; Patel, S.; Wang, M.; Grimm, B.; Bazan, G. C.; Kramer, E. J.; Heeger, A. J. General Strategy for Self-Assembly of Highly Oriented Nanocrystalline Semiconducting Polymers with High Mobility. *Nano Lett.* **2014**, *14*, 2764–2771.

32. Wu, J.; Gross, A. F.; Tolbert, S. H. Host−Guest Chemistry Using an Oriented Mesoporous Host: Alignment and Isolation of a Semiconducting Polymer in the Nanopores of an Ordered Silica Matrix. *J. Phys. Chem. B* **1999**, *103*, 2374–2384.

33. Molenkamp, W. C.; Watanabe, M.; Miyata, H.; Tolbert, S. H. Highly Polarized Luminescence from Optical Quality Films of a Semiconducting Polymer Aligned within Oriented Mesoporous Silica. *J. Am. Chem. Soc.* **2004**, *126*, 4476–4477.

34. Martini, I. B.; Craig, I. M.; Molenkamp, W. C.; Miyata, H.; Tolbert, S. H.; Schwartz, B. J. Controlling Optical Gain in Semiconducting Polymers with Nanoscale Chain Positioning and Alignment. *Nat. Nanotechnol.* **2007**, *2*, 647–652.

35. Iacopino, D.; Lovera, P.; O'Riordan, A.; Redmond, G. Highly Polarized Luminescence from β-Phase-Rich Poly(9,9-dioctylfluorene) Nanofibers. *J. Phys. Chem. A* **2014**, *118*, 5437–5442.

36. Hagler, T. W.; Pakbaz, K.; Voss, K. F.; Heeger, A. J. Enhanced Order and Electronic Delocalization in Conjugated Polymers Oriented by Gel Processing in Polyethylene. *Phys. Rev. B* **1991**, *44*, 8652–8666.

37. Weder, C.; Sarwa, C.; Bastiaansen, C.; Smith, P. Highly Polarized Luminescence from Oriented Conjugated Polymer/polyethylene Blend Films. *Adv. Mater.* **1997**, *9*, 1035–1039.

38. Zhu, Z.; Swager, T. M. Conjugated Polymer Liquid Crystal Solutions: Control of Conformation and Alignment. *J. Am. Chem. Soc.* **2002**, *124*, 9670–9671.

39. Chung, K.; Yu, Y.; Kwon, M. S.; Swets, J.; Kim, J.; Youk, J. H. Assembly and Alignment of Conjugated Polymers: Materials Design, Processing, and Applications. *MRS Commun.* **2015**, *5*, 169–189.

40. Bridges, C. R.; Ford, M. J.; Bazan, G. C.; Segalman, R. A. Molecular Considerations for Mesophase Interaction and Alignment of Lyotropic Liquid Crystalline Semiconducting Polymers. *ACS Macro Lett.* **2017**, *6*, 619–624.

41. Giri, G.; Verploegen, E.; Mannsfeld, S. C. B.; Atahan-Evrenk, S.; Kim, D. H.; Lee, S. Y.; Becerril, H. A.; Aspuru-Guzik, A.; Toney, M. F.; Bao, Z. Tuning Charge Transport in Solution-Sheared Organic Semiconductors Using Lattice Strain. *Nature* **2011**, *480*, 504–508.

42. Kim, B.-G.; Jeong, E. J.; Chung, J. W.; Seo, S.; Koo, B.; Kim, J. A Molecular Design Principle of Lyotropic Liquid-Crystalline Conjugated Polymers with Directed Alignment Capability for Plastic Electronics. *Nat. Mater.* **2013**, *12*, 659–664.

43. Kim, H. G.; Kang, B.; Ko, H.; Lee, J.; Shin, J.; Cho, K. Synthetic Tailoring of Solid-State Order in Diketopyrrolopyrrole-Based Copolymers via Intramolecular Noncovalent Interactions. *Chem. Mater.* **2015**, *27*, 829–838.

44. Barłóg, M.; Kulai, I.; Ji, X.; Bhuvanesh, N.; Dey, S.; Sliwinski, E. P.; Bazzi, H. S.; Fang, L.; Al-Hashimi, M. Synthesis, Chracterzation and Crystal Structures of Novel Fluorinated Di(thiazolyl)benzene Derivatives. *Org. Chem. Front.* **2019**, *6*, 780–790.

45. Irvin, J. A.; Schwendeman, I.; Lee, Y.; Abboud, K. A.; Reynolds, J. R. Low-Oxidation-Potential Conducting Polymers Derived from 3,4-Ethylenedioxythiophene and Dialkoxybenzenes. *J. Polym. Sci. Part A Polym. Chem.* **2001**, *39*, 2164–2178.

46. Huang, H.; Chen, Z.; Ortiz, R. P.; Newman, C.; Usta, H.; Lou, S.; Youn, J.; Noh, Y.-Y.; Baeg, K.-J.; Chen, L. X.; Facchetti, A.; Marks, T. Combining Electron-Neutral Building Blocks with Intramolecular "Conformational Locks" Affords Stable, High-Mobility P- and N-Channel Polymer Semiconductors. *J. Am. Chem. Soc.* **2012**, *134*, 10966–10973.

47. Guo, X.; Quinn, J.; Chen, Z.; Usta, H.; Zheng, Y.; Xia, Y.; Hennek, J. W.; Ortiz, R. P.; Marks, T. J.; Facchetti, A. Dialkoxybithiazole: A New Building Block for Head-to-Head Polymer Semiconductors. *J. Am. Chem. Soc.* **2013**, *135*, 1986–1996.

48. Panzer, F.; Bässler, H.; Köhler, A. Temperature Induced Order–Disorder Transition in Solutions of Conjugated Polymers Probed by Optical Spectroscopy. *J. Phys. Chem. Lett.* **2017**, *8*, 114–125.

49. Casey, A.; Han, Y.; Fei, Z.; White, A. J. P.; Anthopoulos, T. D.; Heeney, M. Cyano Substituted Benzothiadiazole: A Novel Acceptor Inducing N-Type Behaviour in Conjugated Polymers. *J. Mater. Chem. C* **2015**, *3*, 265–275.

50. Shao, B.; Vanden Bout, D. A. Probing the Molecular Weight Dependent Intramolecular Interactions in Single Molecules of PCDTBT. *J. Mater. Chem. C* **2017**, *5*, 9786–9791.

51. Kim, N.-K.; Jang, S.-Y.; Pace, G.; Caironi, M.; Park, W.-T.; Khim, D.; Kim, J.; Kim, D.-Y.; Noh, Y.-Y. High-Performance Organic Field-Effect Transistors with Directionally Aligned Conjugated Polymer Film Deposited from Pre-Aggregated Solution. *Chem. Mater.* **2015**, *27*, 8345–8353.

52. Koynov, K.; Bahtiar, A.; Ahn, T.; Bubeck, C.; Hörhold, H.-H. Molecular Weight Dependence of Birefringence of Thin Films of the Conjugated Polymer Poly[2-methoxy-5-(2'-ethyl-hexyloxy)-1, 4-phenylenevinylene]. *Appl. Phys. Lett* **2004**, *84,* 3792–3794.

53. Kim, J.; Swager, T. M. Control of Conformational and Interpolymer Effects in Conjugated Polymers. *Nature* **2001**, *411*, 1030–1034.

54. Bouffard, J.; Swager, T. M. Self-Assembly of Amphiphilic Poly(phenylene ethynylene)s in Water–potassium Dodecanoate–decanol Lyotropic Liquid Crystals. *Chem. Commun.* **2008**, 5387–5389.

55. Jackson, N. E.; Savoie, B. M.; Kohlstedt, K. L.; de la Cruz, M. O.; Schatz, G. C.; Chen, L. X.; Ratner, M. A. Controlling Conformations of Conjugated Polymers and Small Molecules: The Role of Nonbonding Interactions. *J. Am. Chem. Soc.*, **2013**, *135*, 10475–10483.

56. Liu, X.; He, B.; Garzón-Ruiz, A.; Navarro, A.; Chen, T. L.; Kolaczkowski, M. A.; Feng, S.; Zhang, L.; Anderson, C. A.; Chen, J. Unraveling the Main Chain and Side Chain Effects on Thin Film Morphology and Charge Transport in Quinoidal Conjugated Polymers. *Adv. Funct. Mater.* **2018**, *28*, 1801874.

57. Bijleveld, J. C.; Shahid, M.; Gilot, J.; Wienk, M. M.; Janssen, R. A. J. Copolymers of Cyclopentadithiophene and Electron-Deficient Aromatic Units Designed for Photovoltaic Applications. *Adv. Funct. Mater*. **2009**, *19*, 3262–3270.

58. Grisorio, R.; Piliego, C.; Striccoli, M.; Cosma, P.; Fini, P.; Gigli, G.; Mastrorilli, P.; Suranna, G. P.; Nobile, C. F. Influence of Keto Groups on the Optical, Electronic, and Electroluminescent Properties of Random Fluorenone-Containing Poly(fluorenylene-vinylene)s. *J. Phys. Chem. C* **2008**, *112*, 20076–20087.

59. Hermet, P.; Lois-Sierra, S.; Bantignies, J.-L.; Rols, S.; Sauvajol, J.-L.; Serein-Spirau, F.; Lère-Porte, J.-P.; Moreau, J. J. E. Lattice Dynamics of Oligo(phenylenethienylene)s: A Far-Infrared and Inelastic Neutron Scattering Study. *J. Phys. Chem. B* **2009**, *113*, 4197–4202.

60. Cho, C.-H.; Kang, H.; Kang, T. E.; Cho, H.-H.; Yoon, S. C.; Jeon, M.-K.; Kim, B. J. Controlling Side-Chain Density of Electron Donating Polymers for Improving Their Packing Structure and Photovoltaic Performance. *Chem. Commun.* **2011**, *47*, 3577–3579.

61. Zhou, E.; Nakamura, M.; Nishizawa, T.; Zhang, Y.; Wei, Q.; Tajima, K.; Yang, C.; Hashimoto, K. Synthesis and Photovoltaic Properties of a Novel Low Band Gap Polymer Based on N-Substituted Dithieno[3,2-*b*:2′,3′-*d*]pyrrole. *Macromolecules* **2008**, *41*, 8302–8305.

62. Mueller, C. J.; Gann, E.; McNeill, C. R.; Thelakkat, M. Influence of Fluorination in π-Extended Backbone Polydiketopyrrolopyrroles on Charge Carrier Mobility and Depth-Dependent Molecular Alignment. *J. Mater. Chem. C* **2015**, *3*, 8916–8925.

63. Zhang, W.-Y.; Sun, C.; Hunt, D.; He, M.; Deng, Y.; Zhu, Z.; Chen, C.-L.; Katz, C. E.; Niu, J.; Hogan, P. C.; Xiao, X.-Y.; Dunwoody, N.; Ronn, M.; Process Development and Scale-up of Fully Synthetic Tetracycline TP-2758: A Potent Antibacterial Agent with Excellent Oral Bioavailability. *Org. Process Res. Dev.* **2016**, *20*, 284–296.

64. Mueller, C. J.; Singh, C. R.; Fried, M.; Huettner, S.; Thelakkat, M. High Bulk Electron Mobility Diketopyrrolopyrrole Copolymers with Perfluorothiophene. *Adv. Funct. Mater.* **2015**, *25*, 2725–2736.

65. Liu, S.; Kan, Z.; Thomas, S.; Cruciani, F.; Brédas, J.-L.; Beaujuge, P. M. Thieno[3,4-c]pyrrole-4,6-dione-3,4-difluorothiophene Polymer Acceptors for Efficient All-Polymer Bulk Heterojunction Solar Cells. *Angew. Chemie Int. Ed*. **2016**, *55*, 12996–13000.

Chapter 3

Alignment of Lyotropic Liquid Crystalline Conjugated Polymers in Floating Films

ACS Omega **2018**, *3*, 14807–14813; published by American Chemical Society

3.1 Introduction

Liquid crystalline (LC) conjugated polymers (CPs) combine benefits from both LC and CP properties. In other words, they not only possess the unique LC features of self-assembly and molecular alignment by external treatments, but also show flexibility, solution processability, and structure tunability from the molecular design of CPs. A combination of these properties offers significant advantages for the development of highly aligned polymer films promoting efficient charge transport characteristics in organic electronics.[1–4] Sirringhaus et al. reported that enhanced mobilities were achieved in poly-9,9-dioctyl-fluorene-*co*-bithiophene (F8T2) by aligning polymer chains parallel to the charge transport direction.[5] Another LC polyfluorene copolymer, 9,9-dioctylfluorene-*co*-benzothiadiazole (F8BT), showed mobility anisotropies of 10-15 and 5-7 for hole and electron transport, respectively, when the conjugated backbones were aligned along the direction of nanolines formed by a nanoimprinting process.[6] We also reported LC CP design rules and demonstrated a hole mobility of 0.86 cm^2 V^{-1} s^{-1} along the polymer alignment direction that is 1600 times faster than that perpendicular to the polymer alignment.[7] Recently, Bridge and coworkers presented that different intermolecular interactions of lyotropic cyclopentadithiophene-based polymers contributed to the formation of macroscopically aligned polymer films by varying flexible side chains.[8]

Although many previous studies elaborated distinct advantages of LC that lead to a charge transport anisotropy in polymer films,[5,6,9] the structural diversity remains a challenge because of the lack of systematic analysis on correlations between the molecular structure and LC behavior of CPs. In this work, a newly designed LC CP, poly(bis(5-(dodecyloxy)-2-nitrobenzyl)-1-(5-(2,5-difluoro-4-(thiophen-2-yl)phenyl)thiophen-2-yl)-4*H*-cyclopenta[*c*]thiophene-5,5(6*H*)-dicarboxylate) (CP1-P), is being synthesized. Specifically, this polymer has *o*-nitrobenzyl ester (ONB) side chain, which is one of the most commonly used photocleavable moieties,[10–12] but has not been widely applied for lyotropic LC CPs. We confirmed that the polymer forms typical schlieren-like texture at a highly concentrated LC phase. This proves comparability of the photocleavable side chains with our previously reported design rule for LC CPs.[7] Because of its LC character, the polymer showed a unique intermolecular interaction leading to a uniaxial alignment during the film formation process by the floating film transfer method (FTM).[13–15] This method was first reported with poly(3-hexylthiophene) (P3HT) by Morita et al.[16] It is similar to Langmuir-Schaefer technique except that controlling a surface-pressure to make a compact film is not required. To be specific, a small drop of hydrophobic polymer solution is put on the surface of subphase hydrophilic liquid. The solution then spreads out rapidly over the liquid followed by a thin and uniform film formation. Several factors, such as temperature and viscosity of the hydrophilic liquid, solvent, and backbone structure, affecting this film formation process have been investigated.[17–19] Very recently, a modified FTM with a customized slider to provide a directional force has been also introduced using poly(3,3‴-didodecyl-quaterthiophene) (PQT-12), which is one of the widely studied polymers as the charge transporting layer in organic field effect transistors (OFETs).[15]

We found an interesting new phenomenon in the solvent composition for FTM. Although it has been shown that using a high boiling point (BP) solvent induces strong self-assembly and large crystalline grains of polymer chains,[20,21] the complete replacement of a low BP solvent with a high BP solvent resulted in negative impact on the polymer chain alignment in FTM.[18] Instead, we systematically controlled the solvent composition by using a high BP solvent as an additive to provide adequate time for polymer chains to self-assemble while maintaining a low BP solvent as the primary solvent for CPs to undergo lyotropic LC phase transition. The precisely controlled amount of high BP solvent brings about a slow evaporation and uniform morphology without losing the alignment feature. This produces remarkably enhanced optical anisotropy and charge-carrier mobility compared to the case of polymer solutions without containing any high BP solvent. Moreover, the polymer chain alignment was essentially maintained after cleavage of ONB side chains, yielding solvent-resistance, which can be useful for a solution-based multilayer processing in organic electronics.

3.2 Results and Discussion

Our group reported previously a molecular design principle of lyotropic LC CPs which states the following three points: (1) the interaction between sulfur and fluorine atoms, which is weak enough not to induce interpolymer aggregation but will make chain planarization in a highly concentrated regime only; (2) introducing two bulky side chains to prevent interdigitation of the side chains between lamellar layers; (3) the tetrahedral carbon to minimize undesired massive interpolymer aggregation.[7] As one approach to expand the previously established design principle, we have been interested in modification on side chains without sacrificing LC properties. Even if incorporating side chains to CPs is a common strategy to make the polymers

solution processable for OFETs, the side chains do not contribute to charge transport properties because they are electrically insulating. For this reason, we assumed that removing side chains after a film formation might be beneficial for more efficient charge transport. We chose ONB esters as photocleavable side chains not only because of their photo responsivity but also because of their bulkiness to provide sufficient solubility before the cleavage. The detailed synthetic process for the polymer is described in the Experimental Section.

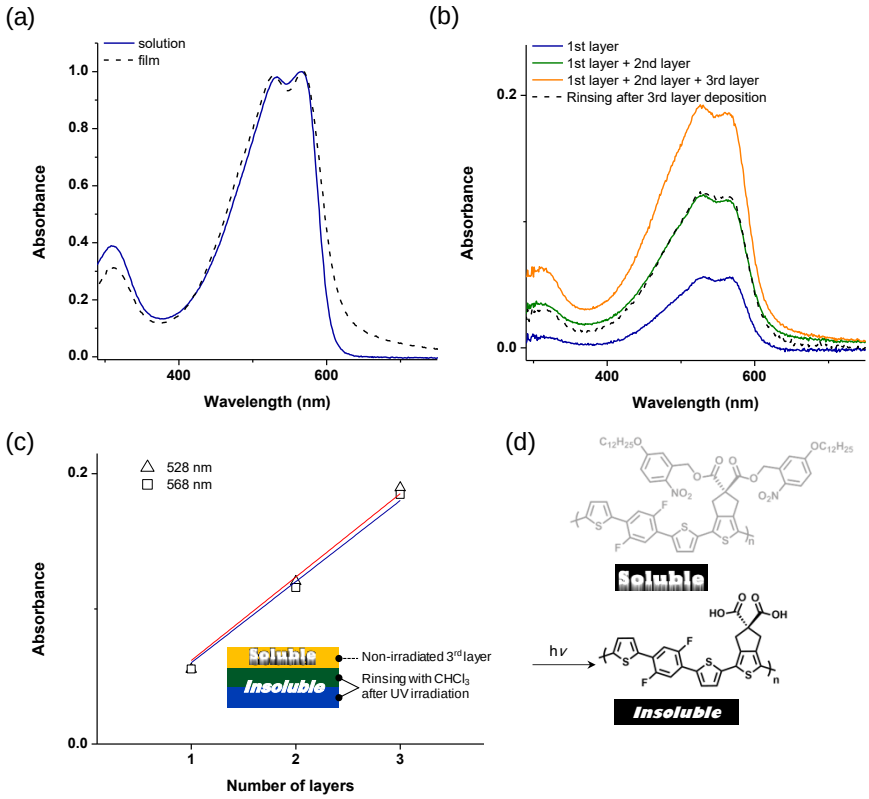

Figure 3.1 (a) The normalized absorbance spectra of CP1-P in chloroform (blue solid line) and solid state (grey dashed line), respectively. (b) UV-vis absorption spectra of CP1-P films at various layers. (c) The linear relationship between the absorbance of $\lambda_{abs}{}^{max}$ and the number of layers. The 1st and 2nd layers were irradiated with 365 nm light, and then rinsed with chloroform. The inset shows a schematic illustration of the multilayer film. (d) Chemical structures of before and after the side chain cleavage.

The absorption profiles of CP1-P in solution and the solid state were almost identical, indicating that the polymer has a similar structural order in solution as in the film state (Figure 3.1a). To remove the photo-labile ONB side chains, the spin-casted films on glass substrates were irradiated with UV light (365 nm). UV irradiation resulted in the side chain cleavage and after CF rinsing the absorbance intensity and absorption maxima of the CP film remained intact because of the removal of the solubilizing side chains. The nonirradiated third layer having ONB side chains was completely removed by the same CF rinsing as shown in Figure 3.1b. The cleavage of side chains clearly displayed that it makes the polymers insoluble, enabling the deposition of consecutive layers from the same solvent without disrupting the bottom layers (Figure 3.1c,d). Continuously, optical anisotropy of films prepared by another film formation method, FTM, was investigated (Figure 3.2). A uniaxial alignment of polymer chains perpendicular to the radial direction in a spreading polymer droplet on subphase liquid is induced by this method. The dichroic ratio (DR), defined as $DR=A_{parallel}/A_{perpendicular}$, where $A_{parallel}$ is the maximum absorbance of polarized light parallel to the alignment direction, and $A_{perpendicular}$ is the maximum absorbance of polarized light perpendicular to the alignment direction, was calculated at 573 nm. The calculated DR of 4.8 under optimum conditions gives clear evidence of the uniaxially aligned polymer chains. In addition to the DR value reflecting the absorbance intensity difference depending on the polarized light, it is worth mentioning that the absorption maximum is red-shifted by 5 nm for CP1-P, when films are prepared by FTM compared to that of the film by spin-casting (Figures 3.1a and 3.2a). The absorption of longer wavelength together with much stronger main peak (565-575 nm) intensity compared to the second peak (520-530 nm) can be attributed to enhanced intermolecular packing because of the alignment.[19,22]

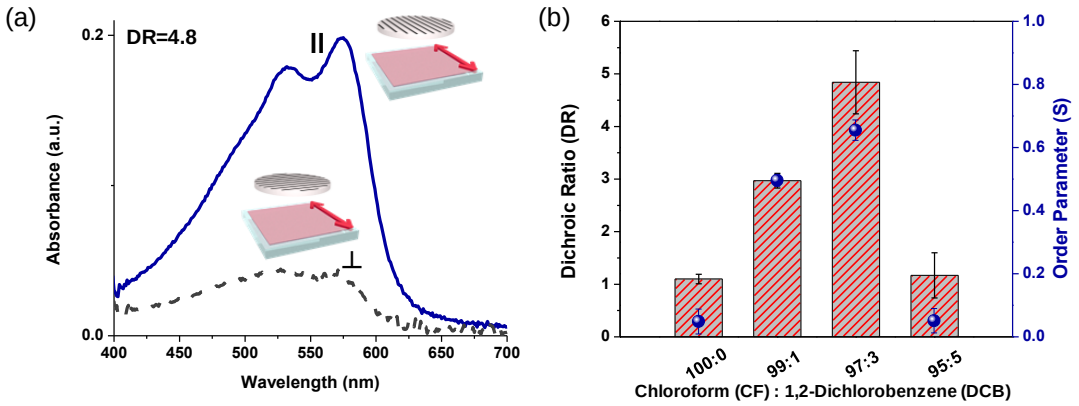

Figure 3.2 (a) Polarized UV-Vis absorption spectra of CP1-P film from the solution in CF with 3 vol% DCB. The inset represents the directions of linear polarizer (black lines) and polymer chain alignment (red arrow), respectively. (b) Dichroic ratio (DR, the bar graph) and order parameter (S, the blue solid sphere) as a function of CF-DCB blend ratios. The error bars represent the standard deviation. All films were formed by FTM on the subphase liquid of ethylene glycol-glycerol blend (1:1 v/v).

The effect of solvent composition for the polymer solution and hydrophilic subphase liquid (ethylene glycol-glycerol blends) on the DR values are presented in Figures 3.2b and 3.3. Also, the order parameters (S), defined as S = (DR-1)/(DR+1), where DR is the dichroic ratio, were calculated for each solvent composition.[23,24] Complete alignment should exhibit S=1 and no preferential orientation corresponds to S=0. The optimum blending ratio of hydrophilic liquid was found to be 1:1 (ethylene glycol: glycerol v/v). When the amount of glycerol is smaller than ethylene glycol, the spreading speed of the polymer droplet was too fast so that the resulted film tended to be torn apart before it solidified into a uniformly aligned thin film. On the other hand, when the mixture contained more glycerol than ethylene glycol, the solution dried even before the polymer droplet formed a thin film. This is because the high viscosity of glycerol hampers the mobility of the polymer on it. In case of solvent composition to prepare polymer solutions, we compared four different conditions; CF only and CF containing small amounts of the high BP

solvent (DCB) with different volume ratios (CF/DCB 99:1, 97:3, and 95:5). The use of a high BP solvent is one common approach to improve device performance by providing enough time for self-assembly of CPs. However, it has been described that the FTM polymer films from a high BP solvent tend to have a random macromolecular arrangement unlike the films from a low BP solvent, because the choice of solvent affects the balance between the solvent evaporation and the spreading speeds in the process.[18] Instead, we used only a small volume of the high BP solvent as an additive not as the primary solvent so that we can take advantage of relatively slower evaporation and uniform morphology without sacrificing the alignment feature of FTM.[20] When we added 1 vol% of DCB, a slight improvement in terms of alignment was noticed, whereas when 5 vol% was added, we observed no significant alignment, which is similar to the CF-only case. A schematic illustration of the differences in the alignment during the film formation process is shown in Figure 3.4a. We speculated that if we had too much DCB, the polymer solution would spread out all over the surface without forming a highly concentrated region because of its high BP so that we could not induce an efficient lyotropic LC property of CP1-P. We experienced when we used 3 vol% of DCB, the solvent composition provided enough time for close packing and self-assembly of polymer chains. By having this optimum blending ratio of DCB and CF, the remaining 97 vol% of CF still allows relatively fast drying to form a highly concentrated region, resulting in lyotropic LC phase transition. Thus, the alignment can be the most efficient. The degree of alignment quantified by DR was improved by almost three times as we added the high BP solvent through the formation of a more ordered structural alignment.

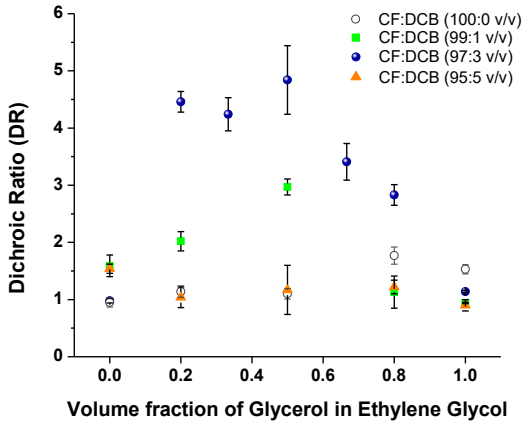

Figure 3.3 DR as a function of the volume fraction of glycerol in ethylene glycol. The error bars represent the standard deviation.

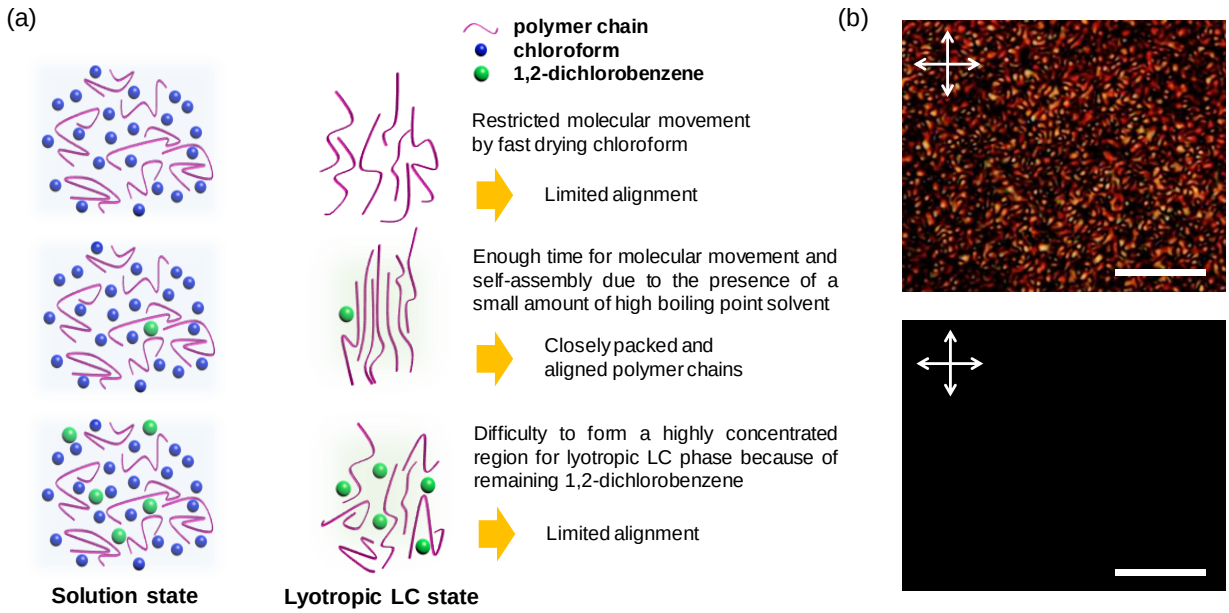

Figure 3.4 (a) Schematic illustration of the FTM film formation mechanism by CP1-P solution in CF (top) and CF/DCB mixtures (middle and bottom). (b) Optical microscopy images of a highly concentrated (top) and a dilute (bottom) CP1-P solution under crossed polarizers. The white scale bars represent 10 μm.

The lyotropic LC properties of the polymer were identified by a cross-polarized optical microscope. As shown in Figure 3.4b, the polymer displayed the schlieren texture, which is commonly observed in LC mesophases, only at a highly concentrated regime.[25] This lyotropic LC behavior is an important characteristic leading to alignment properties with potentially high charge-carrier transport.[7] To investigate the effect of the polymer chain alignment from the lyotropic LC CPs, we fabricated OFETs in the bottom-gate and top-contact configuration. The aligned polymer films were transferred from the hydrophilic liquid surface (ethylene glycol-glycerol 1:1 blend) to the OTS-treated substrate by stamping. The samples were then rinsed with isopropyl alcohol to remove the remaining liquid. The best charge transport performance was observed from the devices postannealed at 200 ^{o}C. The thermal gravimetric analysis shows that CP1-P is thermally stable up to 250 ^{o}C (Figure 3.5). In order to explore charge transport anisotropy, the source-drain electrodes were deposited in two different directions (channel angles of 0^{o} and 90^{o} relative to the alignment direction of polymer chains). As a control, spin-cast films were also prepared in the same device geometry (Figure 3.6). In comparison to the device when source-drain electrodes are deposited perpendicularly ($\perp$), the device with parallel direction (//) is responsible for its higher hole mobilities by more than an order of magnitude from 8.73×10^{-4} cm^2 V^{-1} s^{-1} ($\mu_{\perp}$) to 1.21×10^{-2} cm^2 V^{-1} s^{-1} ($\mu_{//}$) (Figure 3.7). The primary reason for this mobility anisotropy is due to a substantial difference in charge transport pathways, which are determined by the orientation of the polymer chain alignment relative to the source-drain electrode direction. In other words, in a parallel device, a charge-carrier can travel mainly along the polymer chains, whereas it should move by hopping through π-π stacks in a perpendicular device.[26] As anticipated, the devices prepared by spin-coating, which have no anisotropic orientation, showed their hole mobility values (μ_{iso}) between $\mu_{\perp}$ and $\mu_{//}$ of the device with aligned CP1-P.

Additionally, the effect of side chain removal followed by solvent rinsing on the device performance was investigated. Although a ~1.3-fold decrease in mobility was observed upon the side chain cleavage and rinsing process, the device still exhibited superior hole transporting property over randomly oriented devices. This suggests that the alignment feature has been only slightly disturbed after exposure to UV and organic solvent (CF). The maximum mobility values for each condition with an average mobility, on/off ratio, and threshold voltage are summarized in Table 3.1. Even though the overall trend matches well with the result predicted by an anisotropic orientation, the difference between the spin-coated film and the aligned film was relatively small compared to our previous data.[7] A plausible explanation for this result is that bulky aromatic rings in the side chains are likely to hinder more efficient alignment and close packing during the film formation process.[27] As discussed above in the optical property analysis, when the polarized light is perpendicular to the alignment direction, the absorbance is not zero, indicating less effective polymer alignment.

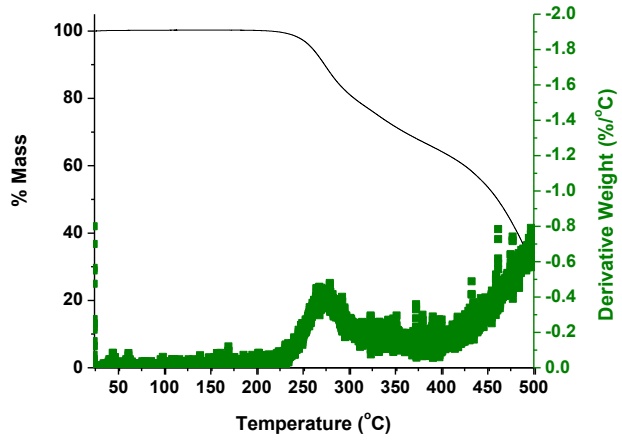

Figure 3.5 Thermogravimetric data for CP1-P in the temperature range of 25–500 °C. Heating rate: 10 °C min^{-1}.

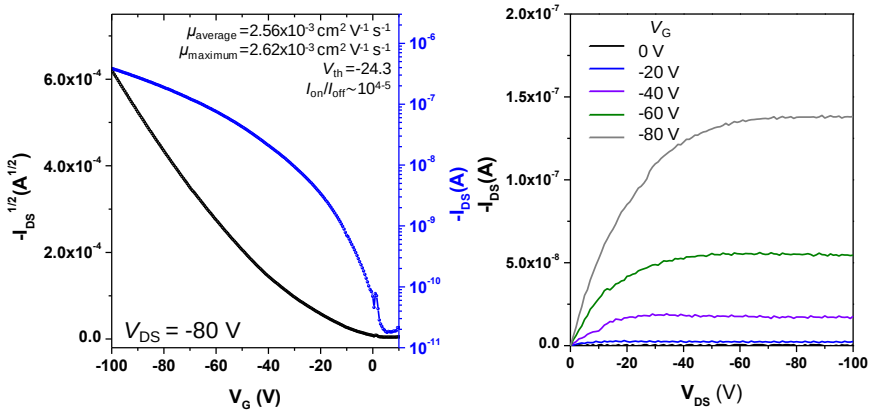

Figure 3.6 Transfer (left) and output (right) curves of CP1-P prepared by spin-coating.

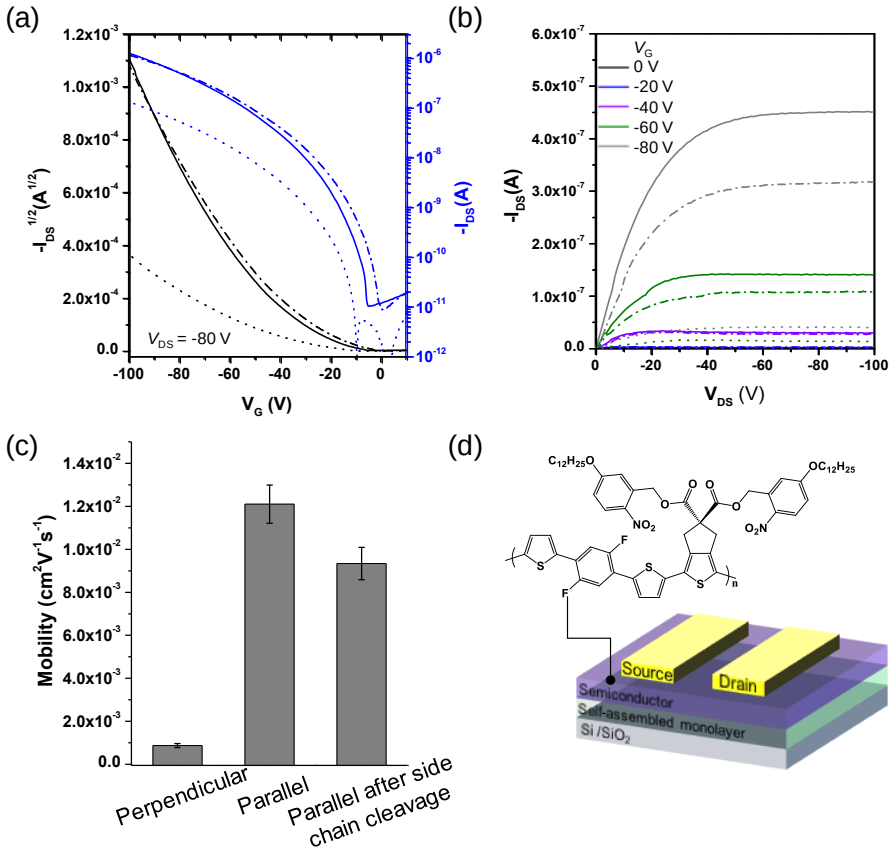

Figure 3.7 (a) Transfer and (b) output curves of CP1-P prepared by FTM. Perpendicular (dotted line), and parallel before (solid line) and after (dash-dotted line) the side chain cleavage. (c) Average mobilities of CP1-P with different conditions. (d) Schematic diagram of a bottom-gate top-contact OFET structure.

Table 3.1 OFET performance of CP1-P[a]

	Side chains	μ^c (cm^2 V^{-1} s^{-1})	V_{th} (V)	I_{on}/I_{off}
Spin-coated (annealed at 200 °C)	before cleavage	2.56×10^{-3} [2.62×10^{-3}]	-24.3	10^{4-5}
FTM-perpendicular[b] (annealed at 200 °C)	before cleavage	8.73×10^{-4} [9.58×10^{-4}]	-31.7	10^{4-5}
FTM-parallel[b] (annealed at 200 °C)	before cleavage	1.21×10^{-2} [1.36×10^{-2}]	-30.5	10^{5}
FTM-parallel[b] (annealed at 200 °C)	after cleavage	9.34×10^{-3} [1.01×10^{-2}]	-30.6	10^{5}

[a]μ is the carrier mobility, V_{th} is the threshold voltage, and I_{on}/I_{off} is the on/off current ratio. [b]All active layer processing by FTM was done in air. [c]Mobility values were measured under a nitrogen atmosphere. The maximum values are listed in parentheses.

The surface morphology of the films formed by spin-coating, and FTM before and after the removal of side chains was investigated by tapping-mode atomic force microscopy (Figure 3.8). The root-mean-square (RMS) roughness values for the spin-coated film was 1.11 nm and that for the FTM films before and after the cleavage were 1.59 nm, 1.47 nm, respectively. It should be noted that the film morphology after the side chain cleavage is comparable with the one before the cleavage reaction. This substantiates that the side chain removal process involving the treatment of organic solvent does not disrupt the morphology of the polymer films because of the excellent solvent resistance. Inappreciable polymer alignments from the atomic force microscopy (AFM) images can be understood considering that AFM is used to analyze the surface topography of samples rather than the chain alignment in bulk.[28]

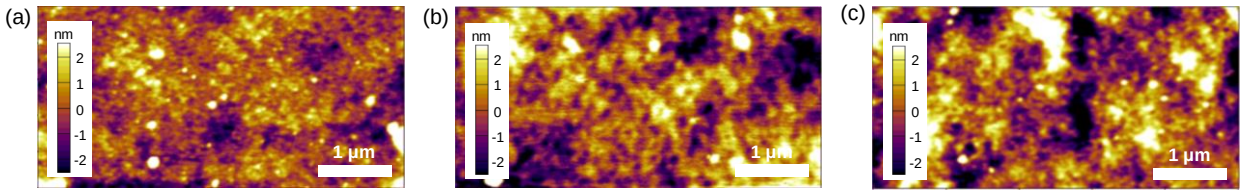

Figure 3.8 AFM height images (5×2.5 μm^2) of polymer films prepared by (a) spin-casting, and FTM (b) before and (c) after the removal of side chains on OTS-treated SiO_2/Si substrates.

XRD measurement was conducted to analyze preferential orientation (i.e. edge-on or face-on) and crystallinity of the FTM films before and after the side chain cleavage (Figure 3.9 and Table 3.2). The absence of (010) peak corresponding to the interchain π-π stacking and the discernable (100) peak representing lamellar packing of the FTM films in the out-of-plane direction suggest dominant edge-on orientation of the polymer chains. The peak positions for both parallel and perpendicular directions were observed at 2θ = 3.98^o (d = 22.2 Å), indicating no anisotropic orientation in the out-of-plane direction. Unexpectedly, the lamellar packing distance showed almost no change after removing the bulky side chains. This observation could be explained by insufficient mobility of the rigid polymer chains in the solid state. While the location of the lamellar peak was almost identical, it is also worthy of note that the lamellar packing peak became broader (full-width at half-maximum (FWHM) = 0.56) than that of the film before cleavage (FWHM = 0.40) because of the slightly disturbed packing. The XRD results are consistent with the slightly decreased transistor performance.

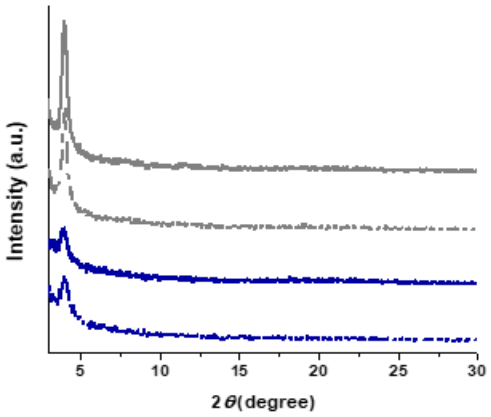

Figure 3.9 Out-of-plane XRD patterns of CP1-P films before (gray line) and after (blue line) the side chain cleavage with the incident X-ray perpendicular (dotted line) and parallel (solid line) to the chain alignment direction.

Table 3.2 X-ray diffraction parameters of CP1-P

The incident X-ray beam relative to the chain alignment direction	**Side chains**	**(hkl)**	**2θ (degree)**	**d (Å)**
parallel[a]	before cleavage	(100)	3.98	22.2
perpendicular[a]	before cleavage		3.98	22.2
parallel[a]	after cleavage		4.00	22.1
perpendicular[a]	after cleavage		4.00	22.1

[a]All active layer processing by FTM was done in air followed by annealing at 200 °C.

3.3 Experimental Section

3.3.1 Materials and Synthesis

All reagents were acquired from commercial suppliers (Aldrich or Tokyo Chemical Industry Co., Ltd. (TCI)) and used without any further purification. ((2,5-difluoro-1,4-phenylene)bis(thiophene-5,2-diyl))bis(trimethylstannane) was prepared according to the reported procedures.[7] The synthetic procedures used to prepare the monomer with cleavable side chains are shown in Figures 3.10 and 3.11, and the details are presented below.

3.3.1.1 Synthesis of Diethylthiophene-3,4-dicarboxylate

Thiophene-3,4-dicarboxylic acid (4 g, 23.2 mmol) was dissolved in ethanol (40 mL) and conc. sulphuric acid was added (1 mL). The reaction mixture was heated to reflux for 2 hrs. It was then cooled down, and K_2CO_3 was added (2 g). After removing solvent under vacuum, the crude product was dissolved in EtOAc (50 mL), filtrated to remove insoluble part, and then concentrated to yield, a yellow, dense oil (5.25 g, quant.). The product was confirmed as analytically pure by ^{1}H NMR analysis and used in the next step without any purification.

3.3.1.2 Synthesis of Thiophene-3,4-diyldimethanol

Diethyl thiophene-3,4-dicarboxylate (2.9 g, 12.7 mmol) was dissolved in anhydrous THF (40 mL) and cooled down to 0 ^{o}C. $LiAlH_4$ in THF (1 M, 36.2 mL, 36.2 mmol) was added dropwise changing the solution color to bright yellow. The reaction mixture was stirred at 0 ^{o}C for 1 hr and warmed up to room temperature. After stirring for 2 hrs, the mixture was cooled down to 0 ^{o}C again and then cold isopropyl alcohol was added slowly until no further reaction occurred. The crude reaction mixture was poured into water (300 mL) and neutralized. The

product was extracted with EtOAc (3×100 mL), dried over Na_2SO_4, and evaporated in vacuo to produce a yellow oil solidifying on standing (1.49 g, 82%). ^{1}H NMR (400 MHz, $CDCl_3$): δ 3.68 (s, 2H), 4.55 (s, 4H), 7.17 (s, 2H). ^{13}C NMR (100 MHz, $CDCl_3$): δ 59.2 (2×CH_2), 124.8 (2×CH), 140.4 (2×C).

3.3.1.3 Synthesis of 3,4-Bis(bromomethyl)thiophene (4)

Compound 4 was prepared using a modified procedure from that described in the literature.[22] Thiophene-3,4-diyldimethanol (300 mg, 2.08 mmol) was dissolved in dry $CHCl_3$ (95 mL). Tribromophosphine (0.6 mL, 5.67 mmol) was added dropwise slowly at room temperature. The reaction mixture was stirred at room temperature for 1 hr followed by quenching with water (50 mL). The product was extracted with CH_2Cl_2 (3×30 mL), washed with sat. $NaHCO_3$ solution (50 mL), dried with $MgSO_4$ and concentrated in vacuo to yield the desired product as a yellow oil crystalizing on standing (443 mg, 79%) (Figure 3.10). ^{1}H NMR (400 MHz, $CDCl_3$): δ 4.63 (s, 4H), 7.35 (s, 2H). ^{13}C NMR (100 MHz, $CDCl_3$): δ 25.5 (2×CH_2), 127.1 (2×CH), 136.4 (2×C).

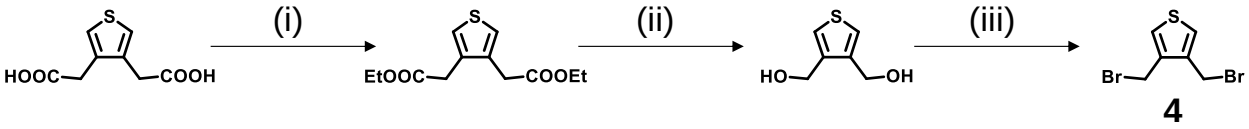

Figure 3.10 Synthesis of compound 4. (i) EtOH, H_2SO_4 cat. 100 °C; (ii) $LiAlH_4$, THF, 0 °C; (iii) PBr_3, $CHCl_3$, rt.

3.3.1.4 Synthesis of (5-(Dodecyloxy)-2-nitrophenyl)methanol (1)

A flame dried round-bottom-flask was charged with 3-(hydroxymethyl)-4-nitrophenol (3.15 g, 18.62 mmol) and anhydrous K_2CO_3 (5.23 g, 37.84 mmol). Dry *N,N*-dimethylformamide (DMF) (15 mL) was added followed by dodecyl bromide (7.08 g, 28.4 mmol) under inert gas. The reaction mixture was stirred at room temperature for 96 hrs. After consuming all the starting material, the reaction mixture was quenched with deionized water (100 mL) followed by adding a mixture of EtOAc: n-hexane (1:1, 100 mL). The organic phase was further washed with water (2×100 mL), dried over Na_2SO_4, and concentrated under vacuum to form a yellow oil. The product was recrystallized from boiling hexane to give pale yellow crystals (5.93 g, 94%). ^{1}H NMR (400 MHz, $CDCl_3$): δ 0.88 (t, *J* = 6.8 Hz, 3H), 1.19-1.53 (m, 18H), 1.78-1.85 (m, 2H), 2.59 (br, s, 1H), 4.06 (t, *J* = 6.5 Hz, 2H), 4.98 (s, 2H), 6.84 (dd, *J* = 9.1, 2.7 Hz, 1H), 7.19 (d, 2.7 Hz, 1H), 8.17 (d, *J* = 9.1 Hz, 1H).

3.3.1.5 Synthesis of 3-(5-(Dodecyloxy)-2-nitrobenzyloxy)-3-oxopropanoic Acid (2)

Compound 2 was prepared according to a modified literature procedure.[23] Compound 1 (1 g, 2.95 mmol) and Meldrum's acid (430 mg, 2.95 mmol) were placed in a sealed vial connected to a bubbler. Dry toluene (3 mL) was added and the reaction mixture was stirred at 120 ºC for 3 hrs. The solvent was evaporated and ^{1}H NMR of the crude mixture confirmed completion (Shift of the benzylic protons from 5.0 ppm for alcohol to 5.7 ppm for ester). The crude product was used in the next step without purification.

3.3.1.6 Synthesis of Bis(5-(dodecyloxy)-2-nitrobenzyl)malonate (3)

Compound 3 was synthesized by a modified procedure reported in the literature.[24] To a crude mixture of compound 2 dissolved in dry CH_2Cl_2 (15 mL), compound 1 was added (1.2 g, 3.54 mmol) followed by 4-dimethylaminopyridine (80 mg, 0.65 mmol). The reaction mixture was cooled down to 0 ºC and *N,N'*-dicyclohexylcarbodiimide (730 mg, 3.54 mmol) was added to the mixture in portions over 20 minutes. The mixture was stirred at 0 ºC, then warmed up to room temperature and left to stir overnight. The resulting solution was filtered, washed with CH_2Cl_2, and concentrated. The crude mixture was purified with column chromatography with a slow gradient of 0-7% EtOAc in n-hexane to obtain the desired product as a white solid: 1.67 g (78% over two steps). ^{1}H NMR (600 MHz, $CDCl_3$): δ 0.88 (t, *J* = 7.1 Hz, 6H), 1.26-1.43 (m, 36H), 1.73-1.76 (m, 4H), 3.67 (s, 2H), 3.99 (t, *J* = 6.5 Hz, 4H), 5.66 (s, 4H), 6.86 (dd, *J* = 9.1, 2.2 Hz, 2H), 7.07 (s, 2H), 8.18 (d, *J* = 9.1 Hz, 2H). ^{13}C NMR (150 MHz, $CDCl_3$): δ 14.1 (2×CH_3), 22.7-31.9 (multiple CH_2), 41.5 (CH_2), 64.3 (2×CH_2), 69.0 (2×CH_2), 113.6 (2×CH), 113.7 (2×CH), 128.0 (2×CH), 134. 8 (2×C), 139.7 (2×C), 163.7 (2×C), 165.5 (2×C).

3.3.1.7 Synthesis of Bis(5-(dodecyloxy)-2-nitrobenzyl)-4*H*-cyclopenta[*c*]thiophene-5,5(6*H*)-dicarboxylate (5)

Compound 5 was synthesized by a modified literature procedure.[25] Compound 3 (1.27 g, 1.71 mmol) was dissolved in dry butanone with suspended anhydrous K_2CO_3 (720 mg, 5.13 mmol) followed by compound 4 (462 mg, 1.71 mmol). The reaction mixture was stirred at 60 ºC for 10 hrs until the consumption of malonate was observed. After, the mixture was cooled down, filtrated, and washed with EtOAc (2×20 mL). The combined organic phase was concentrated under reduced pressure and purified with column chromatography, with a slow gradient of 0-5%

EtOAc in n-hexane. The product was obtained as a dense yellow oil: 1.12 g (76%). ^{1}H NMR (600 MHz, $CDCl_3$): δ (0.88, t, *J* = 7.1 Hz, 6H), 1.27-1.45 (m, 36H), 1.74-1.78 (m, 4H), 3.50 (s, 4H), 3.95 (t, *J* = 6.5 Hz, 4H), 5.63 (s, 4H), 6.82 (dd, *J* = 9.1, 2.2 Hz, 2H), 6.87 (s, 2H), 6.89 (br, s, 2H), 8.14 (dd, *J* = 9.1 Hz, 2H). ^{13}C NMR (150 MHz, $CDCl_3$) δ 14.1 (2×CH_3), 22.6-35.3 (multiple CH_2), 64.6 (2×CH_2), 66.6(C), 69.0 (2×CH_2), 113.3 (2×CH), 113.7 (2×CH), 115.7 (2×CH), 127.9 (2×CH), 134.7 (2×C), 139.6 (2×C), 143.4 (2×C), 163.6 (2×C), 170.3 (2×C).

3.3.1.8 Synthesis of Bis(5-(dodecyloxy)-2-nitrobenzyl)1,3-dibromo-4*H*-cyclopenta[*c*]thiophene-5,5(6*H*)-dicarboxylate (6)

Compound 6 was prepared using a modified synthetic procedure.[26] Compound 5 (760 mg, 0.89 mmol) was dissolved in DMF (8 mL). *N*-bromosuccinimide (500 mg, 2.8 mmol) was added and the reaction mixture was stirred at room temperature for 2 hrs. The mixture was quenched with water (50 mL) and the product was extracted with n-hexane (2×30 mL). The hexane solution was dried over Na_2SO_4 and evaporated in vacuo . Then, the crude product was passed through flash chromatography (0-5% EtOAc/n-hexane) to yield the desired product as a yellow oil, solidifying on standing. 816 mg (91%). ^{1}H NMR (600 MHz, $CDCl_3$): δ 0.87 (t, *J* = 9.1 Hz, 6H), 1.26-1.45 (m, 36H), 1.74-1.79 (m, 4H), 3.42 (s, 4H), 3.96 (t, *J* = 6.5 Hz, 4H), 5.64 (s, 4H), 6.83 (dd, *J* = 9.1, 2.4 Hz, 2H), 6.89 (br, s, 2H), 8.14 (d, 9.1 Hz, 2H). ^{13}C NMR (150 MHz, $CDCl_3$): δ 14.0 (2×CH_3), 22.6-36.3 (multiple CH_2), 64.8 (2×CH_2), 65.0 (C), 69.0 (2×CH_2), 102.4 (2×CH), 113.4 (2×CH), 113.8 (2×CH), 127.9 (2×CH), 134.4 (2×C), 139.6 (2×C), 143.9 (2×C), 163.6 (2×C), 169.5 (2×C).

3.3.1.9 Polymer Synthesis

To a 100 mL round-bottom flask, compound 6 (0.13 g, 0.22 mmol) and compound 7 (0.22 g, 0.22 mmol), P(*o*-tolyl)$_3$ (5.4 mg, 0.018 mmol), and $Pd_2(dba)_3$ (8.1 mg, 0.0088 mmol) were added. The flask was degassed by three repeated cycles of evacuation and refilling with Ar. Then, 15 mL of anhydrous toluene and 3 mL of DMF were added. The mixture was left to stir for 8 hrs at 110 ºC under Ar atmosphere. To complete the reaction, 2-tributylstannyl thiophene (35 µL) and 2-bromothiophene (11 µL) were added with an interval time of 12 hrs. After cooling down to room temperature, the reaction mixture was precipitated in methanol followed by filtration. The solid was further purified by Soxhlet extraction with acetone, methanol, and n-hexane to remove impurities and low molecular weight fractions. Finally, the CF fraction was concentrated under reduced pressure and reprecipitated in methanol to afford the final product CP1-P (0.1293 g, 52%). Gel permeation chromatography (GPC) in CF: M_n=14900 g/mol, M_w=18300 g/mol, Polydispersity index (PDI)=1.23.

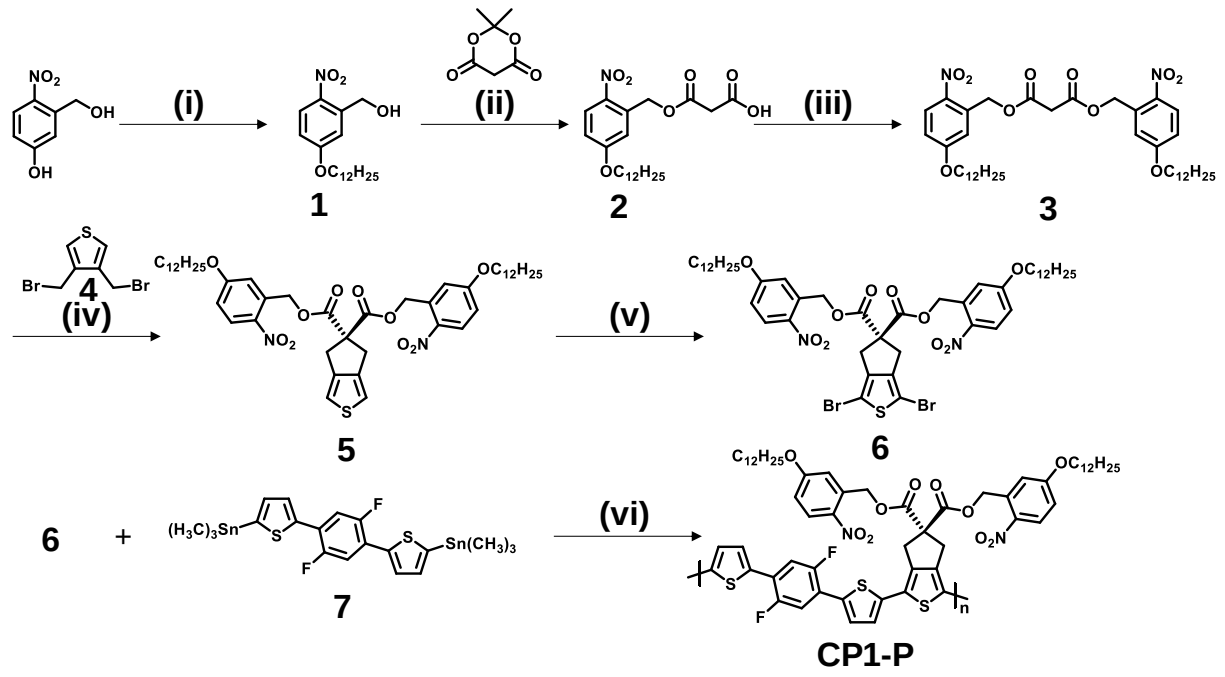

Figure 3.11 Synthesis of CP1-P. (i) $C_{12}H_{25}Br$, K_2CO_3, *N,N*-dimethylformamide (DMF), rt; (ii) Toluene, 120 °C; (iii) Compound 1, 4-dimethylaminopyridine, *N,N'*-dicyclohexylcarbodiimide, dichloromethane, rt; (iv) K_2CO_3, butanone, 60 °C; (v) *N*-bromosuccinimide, DMF, rt; (vi) $Pd_2(dba)_3$, P(*o*-tolyl)$_3$, toluene, DMF, 110 °C.

3.3.2 Instrumentation

Molecular weights were determined by GPC in CF against polystyrene standards using a Waters 515 High Performance Liquid Chromatography (HPLC) Pump equipped with a Waters 2410 refractive index detector and three Waters styragel columns (flow rate: 1.0 mL min^{-1}). NMR spectra were recorded using a Bruker Ultrashield 400 MHz or Bruker Avance 600 MHz spectrometers in $CDCl_3$ at 298 K. Absorption spectra were measured using a Cary 50 Bio UV/Vis spectrophotometer (Varian). UV light irradiation was performed using a 365 nm Light-emitting diode (LED) lamp with a power density of 25 mW cm^{-2}. AFM images were recorded on an Asylum Research MFP-3D stand-alone AFM in tapping mode with a CT300-25 Aspire probe (spring constant 40 N/m and radius of curvature of 8 nm). Out-of-plane X-ray diffraction (XRD)

patterns were collected using a Rigaku Ultima III diffractometer system with graphite monochromatized Cu-Kα radiation (λ = 1.5406 Å) at 48 kV and 40 mA.

3.3.3 Multilayer Film Formation

Multilayer films were prepared with repetitive spin-casting, followed by UV-irradiation and rinsing with CF, for each of the first two layers. The photocleavage of side chains gave good solvent resistance to the resulting film. The subsequent spin-casting on top of the insoluble first (second) layer produced the second (third) layer.

3.3.4 Device Fabrication and Characterization

Top-contact, bottom-gate OTFTs were fabricated on heavily n-doped silicon wafers with a 300 nm thick thermally grown SiO_2 as the gate dielectric (capacitance 10 nF cm^{-2}). The substrates were cleaned by sonication in detergent and deionized water, acetone, and isopropyl alcohol, followed by a UV-ozone treatment for 20 min. The surface of the cleaned silicon substrates was treated with 0.1 M octadecyltrichlorosilane (OTS) in toluene at 60 ºC for 30 min followed by rinsing with toluene and isopropyl alcohol. The polymer film was prepared either by spin-casting at 1000 rpm under a nitrogen environment or by FTM under ambient conditions, from 0.4 wt.% solution in CF and 0.3 wt.% solution in CF containing 0-5 vol% 1,2-dichlorobenzene (DCB), respectively. Subsequently, the devices made by FTM were annealed at 80 ºC for 3 min to remove any residual solvent. Au source/drain electrodes were deposited by thermal evaporation through a shadow mask (L=100 μm, W=500 μm). Electrical characterization was carried out under nitrogen atmosphere using an Agilent 4156C precision semiconductor parameter analyzer. The mobilities were extracted according to the equation of $I_{DS} = \mu C_i (W/2L)$

$(V_G - V_{th})^2$, where I_{DS} is the drain current, μ is the mobility in saturation regime, C_i is the gate dielectric capacitance per unite area, W and L are the channel width and length, respectively, V_G is the gate voltage, and V_{th} is the threshold voltage.

3.4 Conclusions

We report a lyotropic LC CP with photocleavable side chains and their uniaxial alignment via FTM. The lyotropic LC behavior leads to the uniaxial orientation of polymer chains and the photolabile side chains render solvent resistance of the polymer and multilayer fabrication capability. The optical and electrical anisotropies achieved by FTM have been explored through optical spectra and OFET devices. The effect of solvent composition and subphase liquid composition on the polymer alignment was systematically investigated. The small amount of high BP solvent as an additive, which was added into the polymer solution prior to the film formation process, largely enhances the polymer alignment by providing ample time for close packing and self-assembly of the polymer. The average charge-carrier mobility anisotropy ($\mu_{//}/\mu_{\perp}$) in the optimized condition was found to be 13.86, emphasizing the importance of controlling solvent composition to maximize the degree of alignment. The hole mobility of CP1-P after the side chain cleavage decreased from 1.21×10^{-2} cm^2 V^{-1} s^{-1} to 9.34×10^{-3} cm^2 V^{-1} s^{-1}, but was still significantly larger than the devices having perpendicular (8.73×10^{-4} cm^2 V^{-1} s^{-1}) or spin-cast random orientation (2.56×10^{-3} cm^2 V^{-1} s^{-1}) before the cleavage. This indicates that the alignment has been preserved during the process of rinsing with CF, which is a good solvent for CP1-P. Our results demonstrate that rodlike LC CPs having photocleavable side chains are promising for various flexible organic electronics as highly aligned and solvent-resistant semiconducting materials. Rational functionalization on the carboxylic acid, which was obtained

as the result of side chain cleavage, will enable wider range of applications for organic electronics such as potentiometric sensors.

3.5 Author Contributions

Da Seul Yang, Maciej Barłóg, Jongsik Park, Kyeongwoon Chung, Apoorv Shanker, Jonathan Sun, Joonkoo Kang, Kwangyeol Lee, Mohammed Al-Hashimi, Jinsang Kim Alignment of Lyotropic Liquid Crystalline Conjugated Polymers in Floating Films *ACS Omega* **2018**, *3*, 14807–14813 (https://pubs.acs.org/doi/abs/10.1021/acsomega.8b02205).

D.S.Y. planned the study and designed the experiments with the help of K.C. and J.K. D.S.Y. and M.B. prepared monomers with the help of M.A-H. D.S.Y. synthesized the polymer and developed the film fabrication procedure. D.S.Y. prepared and characterized the polymer films with the help of J.P. and A.S. D.S.Y. and J.P. measured and analyzed XRD data with the help of K.L. J. S. and J. Kang assisted in the side chain removal process of the polymer films. D.S.Y. carried out all the device fabrication and analysis. J.K. supervised the research. D.S.Y. wrote the manuscript and J.K. revised the manuscript through contributions of all authors.

3.6 References

1. McCulloch, I.; Heeney, M.; Bailey, C.; Genevicius, K.; MacDonald, I.; Shkunov, M.; Sparrowe, D.; Tierney, S.; Wagner, R.; Zhang, W.; Chabinyc, M. L.; Kline, J.; McGehee, M. D.; Toney, M. F. Liquid-Crystalline Semiconducting Polymers with High Charge-Carrier Mobility. *Nat. Mater.* **2006**, *5*, 328–333.

2. Wang, L.; Cho, H.; Lee, S.-H.; Lee, C.; Jeong, K.-U.; Lee, M.-H. Liquid Crystalline Mesophases Based on Symmetric Tetrathiafulvalene Derivatives. *J. Mater. Chem.* **2011**, *21*, 60–64.

3. Suzuki, A.; Zushi, M.; Suzuki, H.; Ogahara, S.; Akiyama, T.; Oku, T. Photovoltaic Properties and Morphology of Organic Solar Cells Based on Liquid-Crystal Semiconducting Polymer with Additive. *AIP Conf. Proc.* **2014**, *1585,* 164–170.

4. Zhao, B.; Li, C.-Z.; Liu, S.-Q.; Richards, J. J.; Chueh, C.-C.; Ding, F.; Pozzo, L. D.; Li, X.; Jen, A. K.-Y. A Conductive Liquid Crystal via Facile Doping of an N-Type Benzodifurandione Derivative. *J. Mater. Chem. A* **2015**, *3*, 6929–6934.

5. Sirringhaus, H.; Wilson, R. J.; Friend, R. H.; Inbasekaran, M.; Wu, W.; Woo, E. P.; Grell, M.; Bradley, D. D. C. Mobility Enhancement in Conjugated Polymer Field-Effect Transistors through Chain Alignment in a Liquid-Crystalline Phase. *Appl. Phys. Lett.* **2000**, *77*, 406–408.

6. Zheng, Z.; Yim, K.-H.; Saifullah, M. S. M.; Welland, M. E.; Friend, R. H.; Kim, J.-S.; Huck, W. T. S. Uniaxial Alignment of Liquid-Crystalline Conjugated Polymers by Nanoconfinement. *Nano Lett.* **2007**, *7*, 987–992.

7. Kim, B.-G.; Jeong, E. J.; Chung, J. W.; Seo, S.; Koo, B.; Kim, J. A Molecular Design Principle of Lyotropic Liquid-Crystalline Conjugated Polymers with Directed Alignment Capability for Plastic Electronics. *Nat. Mater.* **2013**, *12*, 659–664.

8. Bridges, C. R.; Ford, M. J.; Bazan, G. C.; Segalman, R. A. Molecular Considerations for Mesophase Interaction and Alignment of Lyotropic Liquid Crystalline Semiconducting Polymers. *ACS Macro Lett.* **2017**, *6*, 619–624.

9. Khim, D.; Luzio, A.; Bonacchini, G. E.; Pace, G.; Lee, M.-J.; Noh, Y.-Y.; Caironi, M. Uniaxial Alignment of Conjugated Polymer Films for High-Performance Organic Field-Effect Transistors. *Adv. Mater.* **2018**, *30*, 1705463.

10. Klán, P.; Šolomek, T.; Bochet, C. G.; Blanc, A.; Givens, R.; Rubina, M.; Popik, V.; Kostikov, A.; Wirz, J. Photoremovable Protecting Groups in Chemistry and Biology : Reaction Mechanisms and Efiicacy. *Chem. Rev.* **2013**, *113*, 119–191.

11. Smith, Z. C.; Meyer, D. M.; Simon, M. G.; Staii, C.; Shukla, D.; Thomas, S. W. Thiophene-Based Conjugated Polymers with Photolabile Solubilizing Side Chains. *Macromolecules* **2015**, *48*, 959–966.

12. Smith, Z. C.; Pawle, R. H.; Thomas, S. W. Photoinduced Aggregation of Polythiophenes. *ACS Macro Lett.* **2012**, *1*, 825–829.

13. Pandey, M.; Nagamatsu, S.; Pandey, S. S.; Hayase, S.; Takashima, W. Enhancement of Carrier Mobility along with Anisotropic Transport in Non-Regiocontrolled Poly(3-hexylthiophene) Films Processed by Floating Film Transfer Method. *Org. Electron.* **2016**, *38*, 115–120.

14. Pandey, M.; Gowda, A.; Nagamatsu, S.; Kumar, S.; Takashima, W.; Hayase, S.; Pandey, S. S. Rapid Formation and Macroscopic Self-Assembly of Liquid-Crystalline, High-Mobility, Semiconducting Thienothiophene. *Adv. Mater. Interfaces* **2018**, *5*, 1700875.

15. Tripathi, A. S. M.; Pandey, M.; Sadakata, S.; Nagamatsu, S.; Takashima, W.; Hayase, S.; Pandey, S. S. Anisotropic Charge Transport in Highly Oriented Films of Semiconducting Polymer Prepared by Ribbon-Shaped Floating Film. *Appl. Phys. Lett.* **2018**, *112*, 123301.

16. Morita, T.; Singh, V.; Nagamatsu, S.; Oku, S.; Takashima, W.; Kaneto, K. Enhancement of Transport Characteristics in Poly(3-hexylthiophene) Films Deposited with Floating Film Transfer Method. *Appl. Phys. Express* **2009**, *2*, 111502.

17. Pandey, M.; Nagamatsu, S.; Pandey, S. S.; Hayase, S.; Takashima, W. Orientation Characteristics of Non-Regiocontrolled Poly(3-hexyl-thiophene) Film by FTM on Various Liquid Substrates. *J. Phys. Conf. Ser.* **2016**, *704*, 012005.

18. Pandey, M.; Pandey, S. S.; Nagamatsu, S.; Hayase, S.; Takashima, W. Solvent Driven Performance in Thin Floating-Films of PBTTT for Organic Field Effect Transistor: Role of Macroscopic Orientation. *Org. Electron.* **2017**, *43*, 240–246.

19. Pandey, M.; Pandey, S. S.; Nagamatsu, S.; Hayase, S.; Takashima, W. Influence of Backbone Structure on Orientation of Conjugated Polymers in the Dynamic Casting of Thin Floating-Films. *Thin Solid Films* **2016**, *619*, 125–130.

20. Na, J. Y.; Kim, M.; Park, Y. D. Solution Processing with a Good Solvent Additive for Highly Reliable Organic Thin-Film Transistors. *J. Phys. Chem. C* **2017**, *121*, 13930–13937.

21. Chang, J.; Lin, Z.; Li, J.; Lim, S. L.; Wang, F.; Li, G.; Zhang, J.; Wu, J. Enhanced Polymer Thin Film Transistor Performance by Carefully Controlling the Solution Self-Assembly and Film Alignment with Slot Die Coating. *Adv. Electron. Mater.* **2015**, *1*, 1500036.

22. Gibson, G. L.; Gao, D.; Jahnke, A. A.; Sun, J.; Tilley, A. J.; Seferos, D. S. Molecular Weight and End Capping Effects on the Optoelectronic Properties of Structurally Related "Heavy Atom" Donor–Acceptor Polymers. *J. Mater. Chem. A* **2014**, *2*, 14468–14480.

23. O'Connor, B.; Kline, R. J.; Conrad, B. R.; Richter, L. J.; Gundlach, D.; Toney, M. F.; DeLongchamp, D. M. Anisotropic Structure and Charge Transport in Highly Strain-Aligned Regioregular Poly(3-hexylthiophene). *Adv. Funct. Mater.* **2011**, *21*, 3697– 3705.

24. O'Connor, B. T.; Reid, O. G.; Zhang, X.; Kline, R. J.; Richter, L. J.; Gundlach, D. J.; DeLongchamp, D. M.; Toney, M. F.; Kopidakis, N.; Rumbles, G. Morphological Origin of Charge Transport Anisotropy in Aligned Polythiophene Thin Films. *Adv. Funct. Mater.* **2014**, *24*, 3422–3431.

25. Yang, S.-H.; Hsu, C.-S. Liquid Crystalline Conjugated Polymers and Their Applications in Organic Electronics. *J. Polym. Sci. Part A: Polym. Chem.* **2009**, *47*, 2713–2733.

26. Jimison, L. H.; Toney, M. F.; McCulloch, I.; Heeney, M.; Salleo, A. Charge-Transport Anisotropy Due to Grain Boundaries in Directionally Crystallized Thin Films of Regioregular Poly(3-hexylthiophene). *Adv. Mater.* **2009**, *21*, 1568–1572.

27. Chang, S.; Han, C. D. Effect of Bulky Pendent Side Groups on the Structure of Mesophase in a Thermotropic Main-Chain Liquid-Crystalline Polymer. *Macromolecules* **1996**, *29*, 2103–2112.

28. Molina-Lopez, F.; Wu, H.-C.; Wang, G.-J. N.; Yan, H.; Shaw, L.; Xu, J.; Toney, M. F.; Bao, Z. Enhancing Molecular Alignment and Charge Transport of Solution-Sheared Semiconducting Polymer Films by the Electrical-Blade Effect. *Adv. Electron. Mater.* **2018**, *4*, 1800110.

29. Takahashi, T.; Musha, K.; Sakamaki, K.; Shoji, Y. Functional Thin Film. U.S. Patent 2005/0240061 A1, October 27, 2005.

30. Kim, K. N.; Choi, C. S.; Kay, K.-Y. A Novel Phthalocyanine with Two Axial Fullerene Substituents. *Tetrahedron Lett.* **2005**, *46*, 6791–6795.

31. Padwa, A.; Straub, C. S. Synthesis of Furo[2,4-*c*]furans Using a Rhodium(II)-Catalyzed Cyclization/Diels-Alder Cycloaddition Sequence. *J. Org. Chem.* **2003**, *68*, 227–239.

32. Müller, P.; Miao, Z. Synthesis of Functionalized Cycloprop[*f*]indenes *via* the Carbene Addition Route. *Helv. Chim. Acta* **1994**, *77*, 2051–2059.

33. Kiya, Y.; Henderson, J. C.; Hutchison, G. R.; Abruña, H. D. Synthesis, Computational and Electrochemical Chracterization of a Family of Functionalized Dimercaptothiophenes for Potential Use as High-Energy Cathod Materials for Lithium/Lithium-Ion Batteries. *J. Mater. Chem.* **2007**, *17*, 4366–4376.

Chapter 4

Controlled Alignment of Polymer Chains near the Semiconductor-Dielectric Interface

Organic Electronics **2020**, *76*, 105484; published by Elsevier B.V.

4.1 Introduction

Organic field effect transistors (OFETs) have drawn considerable attention as cost-effective, large-area, light weight and flexible electronic devices with the use of a wide variety of organic materials.[1–6] In OFETs, the gate dielectric layer is located in between the gate electrode and an organic semiconductor so as to prevent them from direct contact with each other. When a voltage is applied to the gate electrode, mainly the charge carriers accumulated at the semiconductor/gate dielectric interface determine the charge transport properties.[7,8] It has been demonstrated that the effective accumulation layer, which critically contributes to the charge transport, is only the first few semiconducting layers adjacent to the gate dielectric interface.[9–14] Moreover, the in situ measurements of the source-drain current as a function of the molecular monolayer coverage showed that the hole mobility of α,ω-dihexylsexithiophene was saturated even at the monolayer-thickness of the two-dimensional layers.[15] However, the active layer thickness dependent charge transport properties have also been observed and discussed on several occasions in the literature.[16–20] For example, the experimental results of the mobility dependence on the pentacene thickness matched well with the simulations only when a low-mobility layer next to the pentacene-dielectric interface and a trap filled region above a certain thickness are introduced to reflect the structural inhomogeneities.[18] Also, a notable thickness

dependence of the electron mobility was described by Ribierre et al.[19] The authors suggested that this dependency can be explained by altered depth and shape of grain boundaries affecting electron trapping or a high vertical bulk resistance of electrons in thick films. Janasz and coworkers reported the transition from two-dimensional to three-dimensional charge transport as the film thickness of poly(3-hexylthiophene) (P3HT) increased.[20] They claimed that the transition along with the larger grain size in the upper layers enables the charge transport to bypass the trapping sites at the P3HT/SiO_2 interface, which leads to an increase in charge transport properties.

As discussed above, the contribution of the semiconducting layer near the interface to the charge transport property is critically important yet difficult to be discretely investigated because of the experimental challenges: controlling thickness affects not only the thickness, but also charge transport path and homogeneity (e.g. grain size) in films. Unlike other methods having these experimental limitations, the unique nature of the floating film transfer method (FTM) limits the vertical variation within a very thin layer so that the film uniformity can be maintained for layers from bottom to top. In our previous work, we successfully optimized the FTM conditions to achieve chain alignment of poly(bis(5-(dodecyloxy)-2-nitrobenzyl) 1-(5-(2,5-difluoro-4-(thiophen-2-yl)phenyl)thiophen-2-yl)-4*H*-cyclopenta[*c*]thiophene-5,5(6*H*)-dicarboxylate (CP1-P) for efficient charge transport.[21] The experimental result indicated that the bulk side chains of CP1-P do not hinder the molecular alignment. In this study, we utilized the potential feature of FTM enabling the formation of a multilayer film composed of each layer having a different polymer chain orientation direction. This experimental design allowed us to study the effects of polymer chain arrangement of CP1-P films, particularly right next to the dielectric interface, on the OFET performance. Furthermore, because of a constant thickness of

the polymer films obtained by FTM, we could rule out possible problems originated from the film thickness variation. Interestingly, we discovered that the direction of uniaxially oriented polymer chains near the interface results in noticeable differences in carrier mobilities. A similar finding has been reported for a diketopyrrolopyrrole (DPP)-based polymer.[22] Despite the overall minor alignment in the bulk of the polymer film, the highly aligned polymer chains at the top interface resulted in a charge transport anisotropy of 5.4, which was elucidated through the carefully studied mechanism of the meniscus-guided film preparation technique. However, the chain orientations of the top and bottom parts of the DPP polymer film could not be independently controllable and the morphology of the bottom part was not comparable to that of the top surface. Another approach for the independent polymer chain alignment control of the top surface and the bottom polymer film-substrate interface has been reported via the combination of the blade coating and nanostructured substrates.[23] Although the polymer chain orientations of the top and bottom parts were controlled independently, it is difficult to predict the chain alignment direction of the middle part since it will be affected by both the directions of the blade coating and the nanogrooves on substrates. Therefore, the independently addressable polymer chain orientation of each layer in a multilayer film with uniform film characteristics through the whole semiconducting layer can be considered a unique way for accurate analysis of the contribution of the top and bottom portions of the film to the device performance. We further investigated the device performance with varying the bottom half layer orientations while retaining the same orientations in the top half layer of the polymer films and vice versa. To the best of our knowledge, this is the first study systematically analyzing the essential role of molecular alignment in a well-defined multilayer CP film in order to understand the OFET device performance. Our results highlight that the polymer chain alignment close to the

semiconductor/dielectric interface in OFET devices is vital for dictating the charge transport properties.

4.2 Results and Discussion

FTM has been used as a simple and straightforward technique to induce the molecular alignment yielding high optical and electrical anisotropies from the lyotropic liquid crystalline (LC) phase of CPs.[24–28] By applying this technique, our group recently found an interesting strategy to promote the self-assembly and alignment behavior of a lyotropic LC CP, CP1-P.[21] To be specific, a small amount of a high boiling point solvent was introduced into a primary solvent having a relatively lower boiling point when preparing the polymer solution. The prolonged solvent evaporation rate because of the presence of the high boiling point solvent offers adequate time for utilizing the LC behavior in the film formation process.

Based on our previous finding, we further extended the alignment and thickness control capability of FTM to build a fundamental understanding in OFETs. Especially, we focused on achieving directed molecular alignments for each layer during multilayer formations by FTM. The detailed descriptions of FTM are shown in Figure 4.1a. A small drop (~10 μL) of CP1-P polymer solution on a hydrophilic liquid subphase (ethylene glycol/glycerol, 1/1 v/v) spreads out at room temperature and forms a thin aligned CP1-P film owing to its lyotropic LC phase. The film is then transferred to an octadecyltrichlorosilane (OTS)-treated silicon wafer by stamping (Figure 4.1b) followed by rinsing with isopropyl alcohol and drying at 80 ºC. As a result, a uniformly aligned polymer film is achieved on the substrate. The maximum absorbance of aligned CP1-P films was observed when the propagation direction of the polymer solution is

perpendicular to the direction of the liner polarizer, confirming that the polymer chains are aligned perpendicular to the solution spreading direction (Figure 4.1c).[21,24–26,29,30]

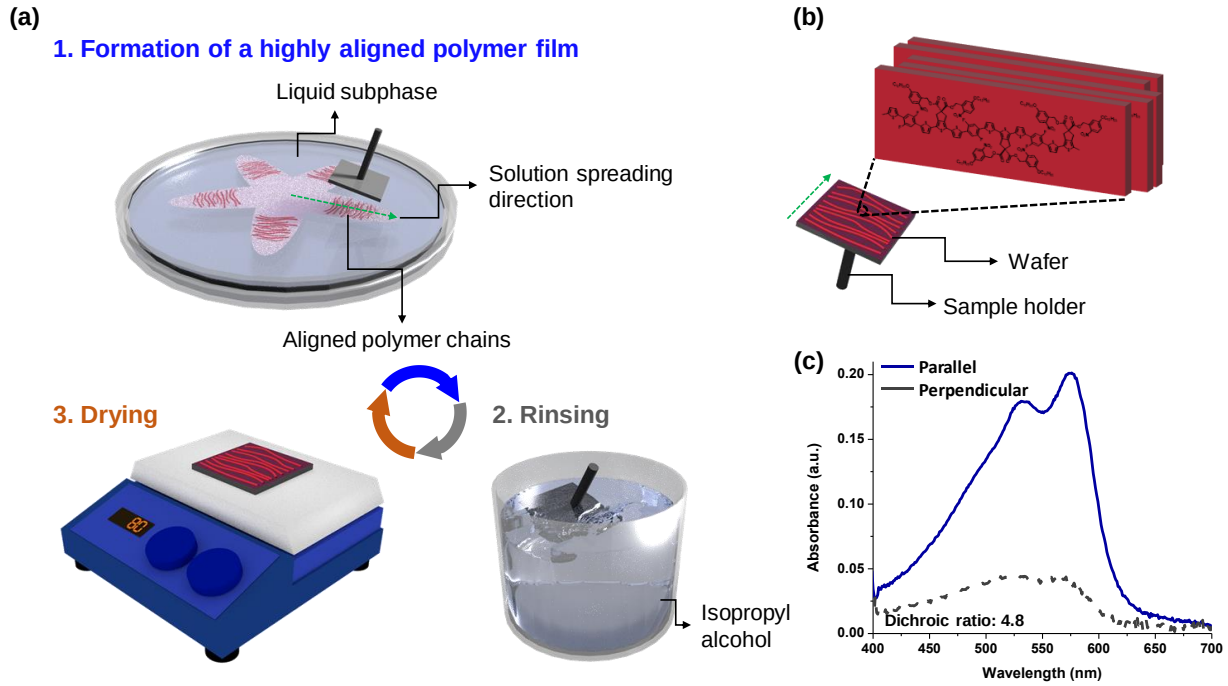

Figure 4.1 Schematic illustrations of (a) the multilayer deposition process by FTM and (b) a polymer film stamped on a wafer. The green dashed arrow represents the polymer solution spreading direction. (c) Polarized UV-vis absorption spectra of the CP1-P film for the incident light polarized parallel (blue solid line) and perpendicular (grey dashed line) to the polymer alignment direction.

FTM requires us simply to repeat the whole cycle to fabricate a multilayer film,[24,29–31] rather than making a thicker film by changing other conditions (e.g. solution concentration, processing temperature or film formation speed) which may induce large variations in grain size, degree of alignment, and film morphology.[32–36] Also, the multilayer deposition by FTM makes it possible to avoid microstructural variations at the interface, which can be largely affected by the roughness of the surface.[37] The reason is that the same liquid subphase always serves as a surface

in the film forming step. According to the procedure, we fabricated the multilayer films in various thicknesses. The thickness of the multilayer films calculated from three samples for each data point is proportional to the number of the coating processes (Figure 4.2a). It is indicative of reproducibility and uniformity in the multilayer deposition. On the other hand, the obtained hole mobilities, varying from 9.67×10^{-4} cm^2 V^{-1} s^{-1} to 1.21×10^{-2} cm^2 V^{-1} s^{-1}, show the absence of explicit correlation to the thickness (Figure 4.2b). A higher density of charge traps, which are likely because of poor coverage, may be attributed to the notably lower mobilities for the single deposition sample. However, a more detailed investigation needs to be carried out for clarity. In order to minimize the film thickness effect, all of the comparisons in this study were made using four layers (~28 nm) of CP1-P films and all of the layers contribute to the charge transport in the semiconducting polymer films. Since the film formation conditions remain unchanged throughout the entire process, the root-mean-square (RMS) surface roughness (1.27 nm) and the

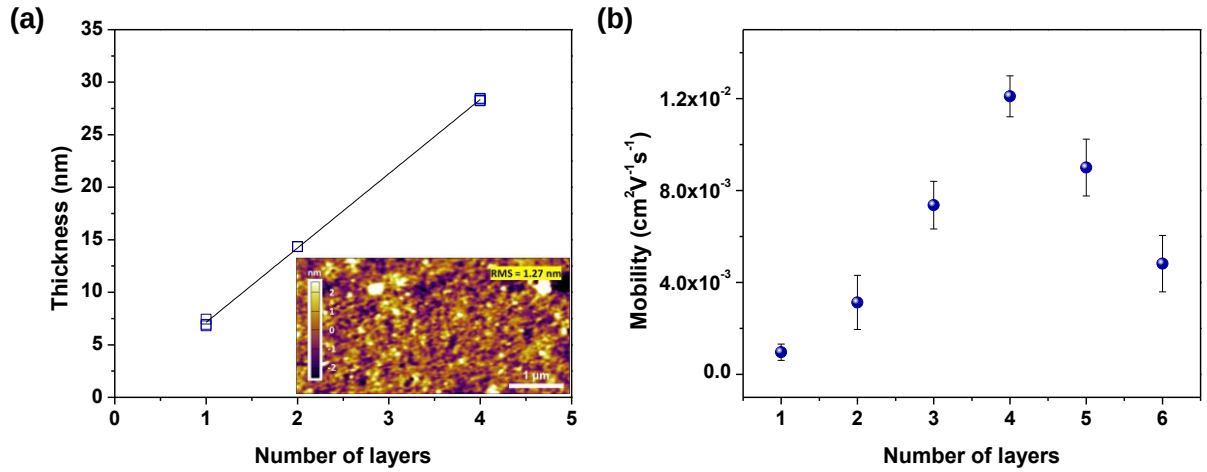

Figure 4.2 (a) Film thickness as a function of the number of layers. The solid line shows a linear fit to the experimental data. The inset shows an atomic force microscopy (AFM) height image of a bilayer film. The root-mean-square (RMS) roughness value is 1.27 nm. (b) Variation of mobility with the number of layers when polymer chains are aligned along the source-drain electrode direction in each layer. The error bars represent the standard deviation.

morphology of the bilayer film were similar to those of the previously reported thicker films (Figure 4.2a).[21] In other words, not only the effect of the active layer thickness, but also the morphological difference between the top and bottom parts of the multilayer films can be mostly ignored.

OFET devices of the bottom-gate top-contact configuration were fabricated on OTS-treated Si/SiO_2 substrates (Si wafers with 300 nm thick SiO_2 as a gate dielectric layer). Figure 4.3 provides schematic illustrations of the devices and the molecular structure of CP1-P. The polymer films comprise of two parts (a thickness of ~14 nm for each part, total thickness of ~28 nm): the top layer, which is in contact with the source and drain electrodes; and the bottom layer, which is in contact with the dielectric layer. In the polymer films, the overall bulk polymer chain alignment, which reflects the combination of the chain orientations from both the top and the bottom layers, kept constant (the bottom and top layer chain orientations are perpendicular to one another) with varying polymer chain orientations of the bottom and top layers relative to the source-drain direction (Figure 4.3b-d). We speculated that the hole mobility is primarily determined by the bottom layer orientation of the CP backbones because charges can be accumulated only at the first few monolayers close to the gate dielectric.[9–14] Accordingly, it was expected to achieve the best device performance when the chain alignment direction of the bottom layer is parallel to the source-drain electrode direction among the three different combinations of bottom/top layer polymer chain orientations.

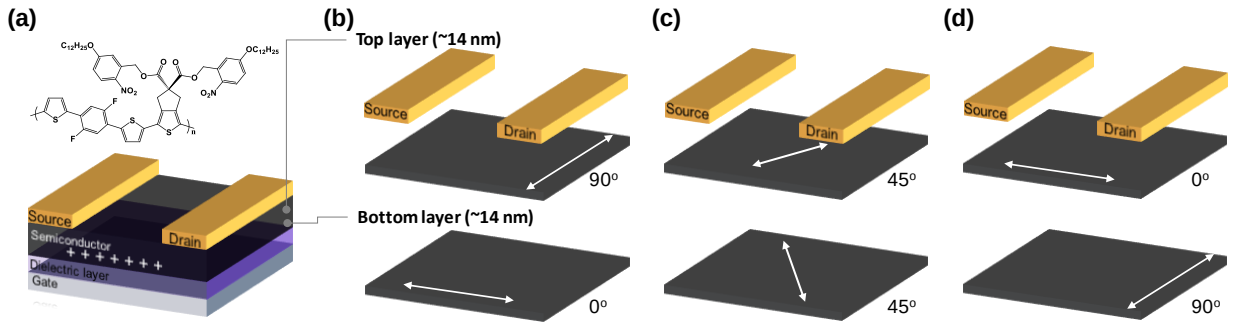

Figure 4.3 Schematic illustrations of (a) the device configuration and chemical structure of CP1-P and (b-d) combinations of the polymer chain orientation for top and bottom layers. The angles between the polymer chain alignment direction and the source-drain electrode direction of each layer were varied: (b) 90° (perpendicular) and 0° (parallel), (c) 45° and 45°, (d) 0° (parallel) and 90° (perpendicular), for the top and bottom layers, respectively. The double-sided white arrows represent the polymer chain alignment directions.

Figure 4.4a,b exhibits the transfer and output characteristics of the CP1-P devices prepared by FTM. The bulk alignment of the CP1-P backbone in films was quantified by the optical dichroic ratio (DR). The DR values, defined as the ratio between the maximum absorbance of polarized light parallel and perpendicular to the polymer chain alignment direction, were almost the same for all three conditions. However, it is clear that the device characteristics could be remarkably different even with nearly identical DR values (~1.1, Figures 4.4c and 4.5). As anticipated, when the polymer chains were oriented along the direction of the source-drain electrode in the bottom layer (0°) and arranged perpendicularly (90°) to the source-drain electrode direction in the top layer (Figure 4.3b configuration), the average hole mobility (μ = 6.14×10^{-3} cm^2 V^{-1} s^{-1}, Figure 4.4a, red line) was three times higher than the corresponding value of the opposite case (μ = 1.86×10^{-3} cm^2 V^{-1} s^{-1}, Figure 4.4a, black line) in which the polymer chains in the bottom and top layers were perpendicular (90°) and parallel (0°) to the source-drain direction, respectively (Figure 4.3d configuration). The difference is presumably

from the FET operation principle that charges move along the semiconducting layer/gate dielectric interface. Thus, the molecular alignment along the source-drain direction at the interface is beneficial. When the source-drain electrodes were placed in a diagonal direction (45°) to the polymer chains for both layers, the hole mobility value was found in between the other two cases. It is also worth pointing out that the mobility from this 45° oriented film (μ = 3.00×10^{-3} cm^2 V^{-1} s^{-1}, Figure 4.4a, blue line), which is intuitively most similar to the spin-cast random orientation of polymer backbones, is in a similar range of that obtained from the spin-cast film (μ = 2.56×10^{-3} cm^2 V^{-1} s^{-1}).[21] Therefore, the measured hole mobilities correlated well with the bottom layer polymer chain orientations for efficient charge transport: 0° (the most favorable), 45° (moderate), and 90° (the least favorable).

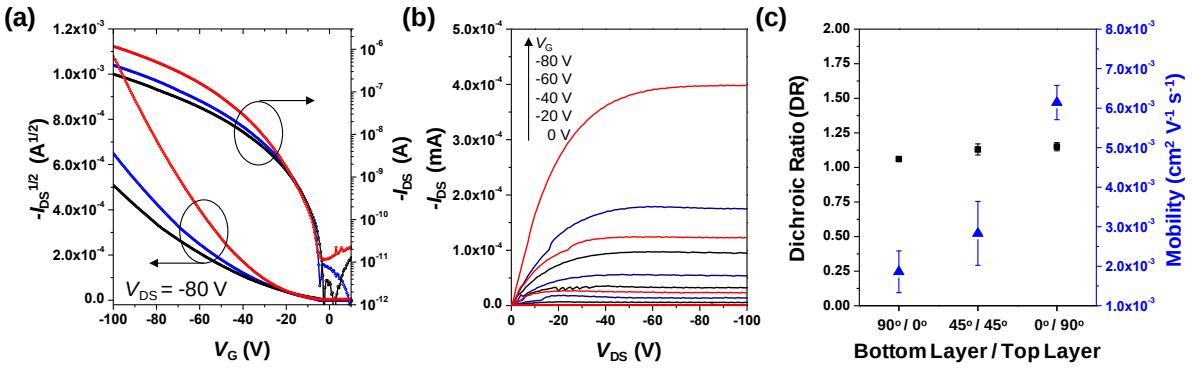

Figure 4.4 (a) Transfer (gate voltage, V_G, vs. source-drain current, I_{DS}) and (b) output (source-drain voltage, V_{DS}, vs. source-drain current, I_{DS}) curves of CP1-P prepared by FTM in three different polymer chain orientation directions of the top and bottom layers: 0° and 90° (black), 45° for both layers (blue) and 90° and 0° (red) , respectively, relative to the source-drain direction. All three transfer curves were collected under constant V_{DS} of -80 V with variation in V_G. (c) Dichroic ratios (black squares) and average mobilities (blue triangles) at different conditions. The error bars represent the standard deviation.

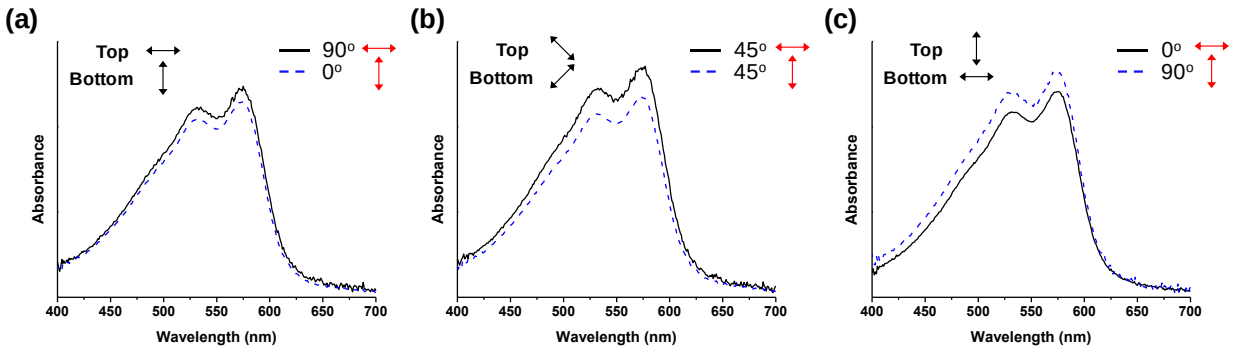

Figure 4.5 Polarized UV-vis absorption spectra of CP1-P having orthogonal polymer chain alignment directions of the top and bottom layers. The spectra were recorded at different angles of polarized incidence light relative to the bottom layer orientation: (a) 90° and 0°, (b) 45° for both lines, and (c) 0° and 90°, for the black solid line and blue dashed line, respectively. The double-sided black and red arrows represent the polymer chain alignment direction and the direction of the polarized incident light, respectively. All the three films displayed almost identical absorption intensity regardless of the orientation angle, verifying that the top layer has orthogonal orientation relative to the bottom layer orientation.

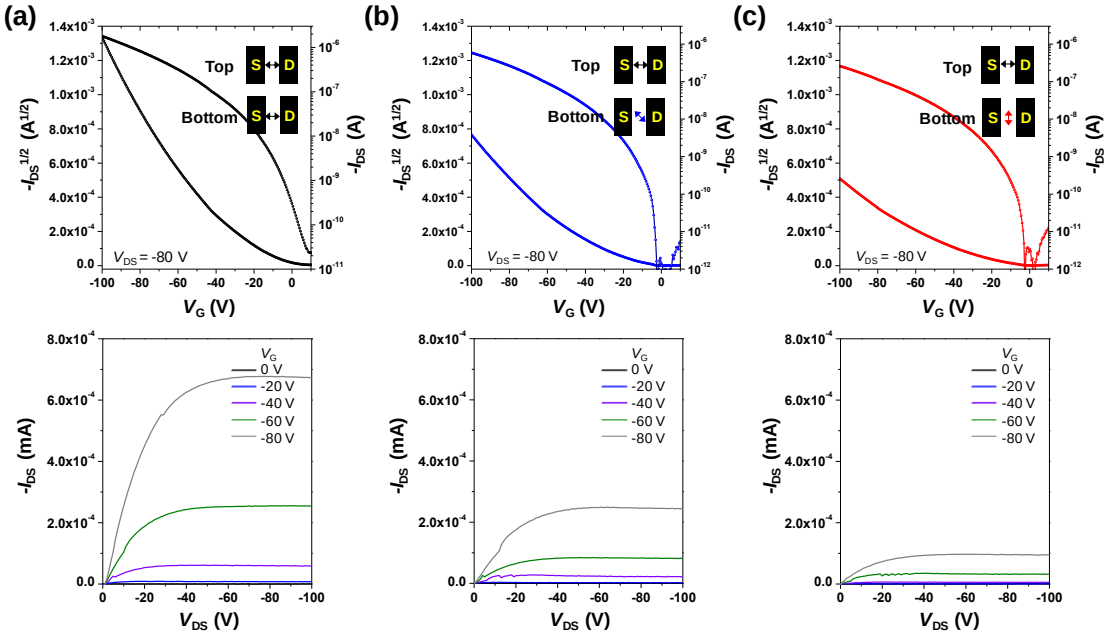

Figure 4.6 Transfer (top) and output (bottom) curves of CP1-P prepared by FTM in three different polymer chain orientation directions of the bottom layers: (a) 0°, (b) 45°, and (c) 90°, respectively, relative to the source-drain direction with the constant chain orientations of the top layers (parallel to the source-drain electrode direction, 0°). The insets in the transfer curves show the polymer chain orientation directions in the devices.

In order to gain further insight into the role of the bottom layer chain orientation on the device performance, the polymer chain orientation direction in the bottom (top) layer was held constant and the top (bottom) layer chain orientations were modulated (i.e. polymer chains are aligned 0^o, 45^o, and 90^o relative to the source-drain direction) (Figures 4.6 and 4.7). Interestingly, the mobility difference was smaller when the bottom layer chain orientation remained unchanged with the three different top layer chain orientations compared to the opposite case. Particularly, once the bottom layer chain orientations are parallel to the source-drain direction (blue bars in Figure 4.8), the device performances are greater than any other combinations with the other two bottom layer chain orientations of 45^o and 90^o (the green and orange bars in Figure 4.8, respectively), regardless of the top layer chain orientations. This result indicates that the favorable polymer chain orientation adjacent to the dielectric layer has a major impact on the efficient charge transport in OFET devices. Additionally, two more combinations of 45^o and 90^o, one for the bottom layer and the other for the top layer, were investigated. In all cases, typical p-type FET characteristics with high on/off current ratios in the range of $10^{5\text{-}6}$ were observed as summarized in Table 4.1.

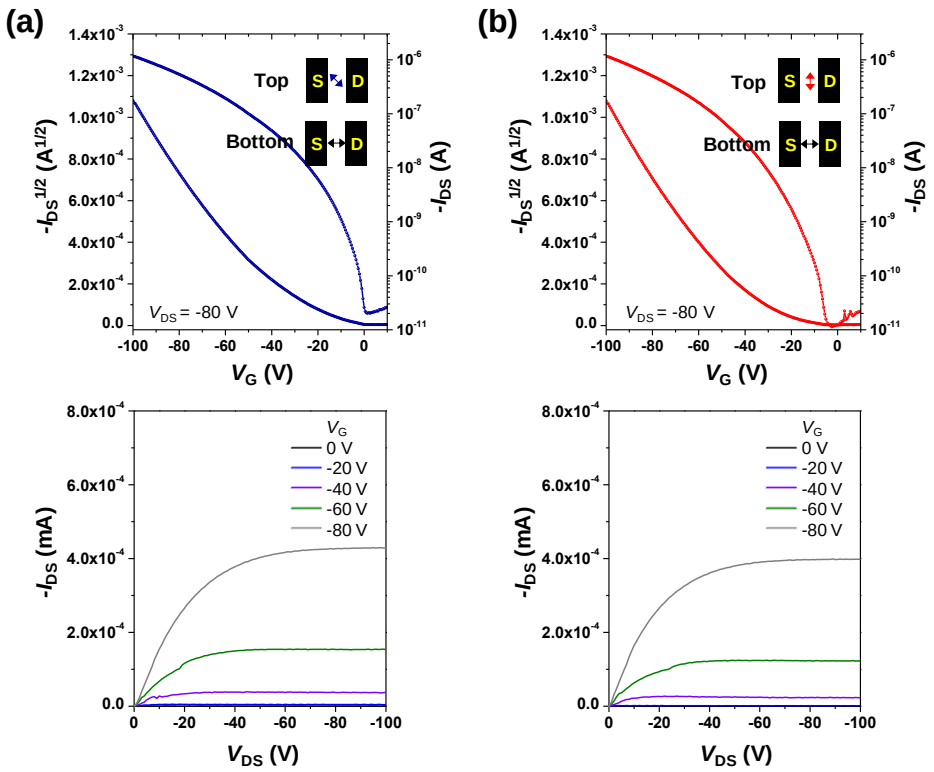

Figure 4.7 Transfer (top) and output (bottom) curves of CP1-P prepared by FTM in two different polymer chain orientation directions of the top layers: (a) 45°, and (b) 90°, respectively, relative to the source-drain direction with the constant chain orientations of the bottom layers (0°). The insets in the transfer curves show the polymer chain orientation directions in the devices.

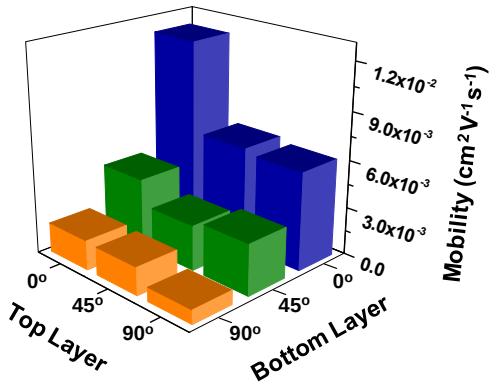

Figure 4.8 Mobility of CP1-P prepared by FTM through various combinations of the top and bottom layer polymer chain orientations. The angles between the polymer chain alignment direction and the source-drain electrode direction of each layer were varied from 0° (parallel), 45°, to 90° (perpendicular).

Table 4.1 OFET device performance of CP1-P at varying top and bottom layers orientations[a]

Bottom layer chain orientation[b]	Top layer chain orientation[b]	μ (cm^2 V^{-1} s^{-1})	V_{th} (V)	I_{on}/I_{off}
0°	0°	1.21×10^{-2}	-30.5	10^5
	45°	6.42×10^{-3}	-28.0	10^5
	90°	6.14×10^{-3}	-31.5	10^5
45°	0°	4.39×10^{-3}	-27.9	10^{5-6}
	45°	3.00×10^{-3}	-29.8	10^{5-6}
	90°	3.21×10^{-3}	-29.6	10^5
90°	0°	1.86×10^{-3}	-27.1	10^{5-6}
	45°	1.76×10^{-3}	-28.2	10^5
	90°	8.73×10^{-4}	-31.7	10^{4-5}

[a]μ is the average hole mobility, V_{th} is the threshold voltage, I_{on}/I_{off} is the on/off current ratio. [b]The angles between the polymer chain alignment direction and the source-drain direction are given. All parallel (0°, the first row of the table) and all perpendicular (90°, the last row of the table) device data were reported previously, see ref 21.

4.3 Experimental Section

4.3.1 Materials and Instrumentation

All reagents and solvents were purchased from commercial suppliers (Aldrich or Tokyo Chemical Industry Co., Ltd. (TCI)) and used without any further purification. The synthetic procedure of CP1-P has been reported previously.[21] UV-Vis data were obtained from a Varian Cary 50 Bio UV/Vis spectrophotometer. AFM images were acquired using an Asylum Research MFP-3D stand-alone AFM in tapping mode with a CT300-25 Aspire probe (spring constant 40 N m^{-1} and radius of curvature of 8 nm). The thickness of polymer films was measured by a spectroscopic ellipsometer (M-2000, J. A. Woollam Co.).

4.3.2 Device Fabrication and Characterization

The heavily n-doped silicon wafers with a 300 nm thick thermally grown SiO_2 as the gate dielectric (capacitance 10 nF cm^{-2}) were cleaned in an ultrasonic bath using detergent and deionized water, acetone, and isopropyl alcohol, followed by a UV-ozone treatment for 20 min. The substrates were then treated with 0.1 M OTS in toluene at 60 ºC for 30 min. After rinsing by ultrasonication in toluene and isopropyl alcohol for 5 min each, the polymer films were prepared by FTM under ambient conditions, from 0.3 wt.% solution in chloroform containing 3 vol% 1,2-dichlorobenzene. All polymer films were additionally annealed at 200 ºC for 15 min prior to metal depositions. Source/drain electrodes (100 nm gold) were evaporated through a shadow mask (L=80-100 μm, W=450-500 μm). OFET devices were measured using an Agilent 4156C precision semiconductor parameter analyzer in a nitrogen-filled glove box. The mobilities were calculated using the equation of $I_{DS} = \mu\ C_i\ (W/2L)\ (V_G - V_{th})^2$, where I_{DS} is the source-drain current, μ is the mobility in saturation regime, C_i is the gate dielectric capacitance per unit area, W is the channel width, L is the channel length, V_G is the gate voltage, and V_{th} is the threshold voltage.

4.4 Conclusions

Motivated by the absence of a systematic investigation on the effect of the molecular alignment at the semiconductor-dielectric interface on OFET performance, we developed a new empirical approach by exploiting the unique feature of FTM. This method enabled exploration of the influence of the polymer chain orientation on the charge transport with regard to the proximity of the gate dielectric interface to aligned polymer layers. In particular, FTM allowed us to discretely control the polymer chain alignment of top and bottom layers of a lyotropic LC

CP while keeping the total thickness of the multilayer films to avoid other effects accompanied by the thickness variation. Under the constant active layer thickness, the differences in charge transport characteristics based on the polymer chain alignment directions were analyzed through the bottom-gate top-contact device architecture. The results unambiguously exhibited that carrier mobilities can be varied greatly (over a three-fold difference) by the polymer chain alignment direction at the interface relative to the source-drain direction. More specifically, the chain orientation of the bottom layer, which is close to the interface, was found to be primarily responsible for the overall device performance with a much weaker contribution from the top layer chain orientation. Our study provides solid experimental evidence for the significance of polymer chain orientations specifically at the gate dielectric-semiconductor interface. This approach for precise regulation of the molecular alignment within a CP thin layer is expected to have a broad impact on the fundamental understanding and applications of organic electronics.

4.5 Author Contributions

Da Seul Yang, Kyeongwoon Chung, Jinsang Kim Controlled Alignment of Polymer Chains near the Semiconductor-Dielectric Interface. *Organic Electronics* **2020**, *76***,** 105484.

D.S.Y. planned the study, performed the experiments, and analyzed the data. K.C. and J.K. assisted in material design and participated in discussion. D.S.Y. and J.K. wrote the manuscript. J.K. supervised the research.

4.6 References

1. Sirringhaus, H. 25th Anniversary Article: Organic Field-Effect Transistors: The Path Beyond Amorphous Silicon. *Adv. Mater*. **2014**, *26*, 1319–1335.
2. Sirringhaus, H. Device Physics of Solution-Processed Organic Field-Effect Transistors. *Adv. Mater.* **2005**, *17*, 2411–2425.
3. Forrest, S. R. The Path to Ubiquitous and Low-Cost Organic Electronic Appliances on Plastic. *Nature* **2004**, *428*, 911–918.
4. Dong, H.; Fu, X.; Liu, J.; Wang, Z.; Hu, W. 25th Anniversary Article: Key Points for High-Mobility Organic Field-Effect Transistors. *Adv. Mater*. **2013**, *25*, 6158–6183.
5. Yan, H.; Chen, Z.; Zheng, Y.; Newman, C.; Quinn, J. R.; Dötz, F.; Kastler, M.; Facchetti, A. A High-Mobility Electron-Transporting Polymer for Printed Transistors. *Nature* **2009**, *457*, 679–686.
6. Reese, C.; Roberts, M.; Ling, M.-m.; Bao, Z. Organic Thin Film Transistors. *Mater. Today* **2004**, *7*, 20–27.
7. Salleo, A. Charge Transport in Polymeric Transistors. *Mater. Today* **2007**, *10*, 38–45.
8. Park, D. Y.; Lim, J. A.; Lee, H. S.; Cho, K. Interface Engineering in Organic Transistors. *Mater. Today* **2007**, *10*, 46–54.
9. Dimitrakopoulos, C. D.; Malenfant, P. R. L. Organic Thin Film Transistors for Large Area Electronics. *Adv. Mater.* **2002**, *14*, 99–117.
10. Dinelli, F.; Murgia, M.; Levy, P.; Cavallini, M.; Biscarini, F.; de Leeuw, D. M. Spatially Correlated Charge Transport in Organic Thin Film Transistors. *Phys. Rev. Lett.* **2004**, *92*, 116802.

11. Joshi, S.; Grigorian, S.; Pietsch, U.; Pingel, P.; Zen, A.; Neher, D.; Scherf, U. Thickness Dependence of the Crystalline Structure and Hole Mobility in Thin Films of Low Molecular Weight Poly(3-hexylthiophene). *Macromolecules* **2008**, *41*, 6800–6808.

12. Liu, S.-W.; Lee, C.-C.; Tai, H.-L.; Wen, J.-M.; Lee, J.-H.; Chen, C.-T. In Situ Electrical Characterization of the Thickness Dependence of Organic Field-Effect Transistors with 1−20 Molecular Monolayer of Pentacene. *ACS Appl. Mater. Interfaces* **2010**, *2*, 2282–2288.

13. Horowitz, G. Tunneling Current in Polycrystalline Organic Thin-Film Transistors. *Adv. Funct. Mater.* **2003**, *13*, 53–60.

14. Dodabalapur, A.; Torsi, L.; Katz, H. E. Organic Transistors: Two-Dimensional Transport and Improved Electrical Characteristics. *Science.* **1995**, *268*, 270–271.

15. Mannebach, E. M.; Spalenka, J. W.; Johnson, P. S.; Cai, Z.; Himpsel, F. J.; Evans, P. G. High Hole Mobility and Thickness-Dependent Crystal Structure in α,ω-Dihexylsexithiophene Single-Monolayer Field-Effect Transistors. *Adv. Funct. Mater.* **2013**, *23*, 554–564.

16. Reséndiz, L.; Estrada, M.; Cerdeira, A.; Iñiguez, B.; Deen, M. J. Effect of Active Layer Thickness on the Electrical Characteristics of Polymer Thin Film Transistors. *Org. Electron.* **2010**, *11*, 1920–1927.

17. Lee, J.; Kim, K.; Kim, J. H.; Im, S.; Jung, D.-Y. Optimum Channel Thickness in Pentacene-Based Thin-Film Transistors. *Appl. Phys. Lett.* **2003**, *82*, 4169–4171.

18. Gupta, D.; Hong, Y. Understanding the Effect of Semiconductor Thickness on Device Characteristics in Organic Thin Film Transistors by Way of Two-Dimensional Simulations. *Org. Electron.* **2010**, *11*, 127–136.

19. Ribierre, J. C.; Watanabe, S.; Matsumoto, M.; Muto, T.; Hashizume, D.; Aoyama, T. Thickness Dependence of the Ambipolar Charge Transport Properties in Organic Field-Effect Transistors Based on a Quinoidal Oligothiophene Derivative. *J. Phys. Chem. C* **2011**, *115*, 20703–20709.

20. Janasz, L.; Gradzka, M.; Chlebosz, D.; Zajaczkowski, W.; Marszalek, T.; Kiersnowski, A.; Ulanski, J.; Pisula, W. Microstructure-Dependent Charge Carrier Transport of Poly(3-hexylthiophene) Ultrathin Films with Different Thicknesses. *Langmuir* **2017**, *33*, 4189–4197.

21. Yang, D. S.; Barłóg, M.; Park, J.; Chung, K.; Shanker, A.; Sun, J.; Kang, J.; Lee, K.; Al-Hashimi, M.; Kim, J. Alignment of Lyotropic Liquid Crystalline Conjugated Polymers in Floating Films. *ACS Omega* **2018**, *3*, 14807–14813.

22. Qu, G.; Zhao, X.; Newbloom, G. M.; Zhang, F.; Mohammadi, E.; Strzalka, J. W.; Pozzo, L. D.; Mei, J.; Diao, Y. Understanding Interfacial Alignment in Solution Coated Conjugated Polymer Thin Films. *ACS Appl. Mater. Interfaces* **2017**, *9*, 27863–27874.

23. Wu, D.; Kaplan, M.; Ro, H. W.; Engmann, S.; Fischer, D. A.; DeLongchamp, D. M.; Richter, L. J.; Gann, E.; Thomsen, L.; McNeil, C. R.; Zhang, X. Blade Coating Aligned, High-Performance, Semiconducting-Polymer Transistors. *Chem. Mater.* **2018**, *30*, 1924-1936.

24. Pandey, M.; Pandey, S. S.; Nagamatsu, S.; Hayase, S.; Takashima, W. Solvent Driven Performance in Thin Floating-Films of PBTTT for Organic Field Effect Transistor: Role of Macroscopic Orientation. *Org. Electron.* **2017**, *43*, 240–246.

25. Pandey, M.; Pandey, S. S.; Nagamatsu, S.; Hayase, S.; Takashima, W. Influence of Backbone Structure on Orientation of Conjugated Polymers in the Dynamic Casting of Thin Floating-Films. *Thin Solid Films* **2016**, *619*, 125–130.

26. Tripathi, A. S. M.; Kumari, N.; Nagamatsu, S.; Hayase, S.; Pandey, S. S. Facile Fabrication of Large Area Oriented Conjugated Polymer Films by Ribbon-Shaped FTM and Its Implication on Anisotropic Charge Transport. *Org. Electron.* **2019**, *65*, 1–7.

27. Pandey, M.; Gowda, A.; Nagamatsu, S.; Kumar, S.; Takashima, W.; Hayase, S.; Pandey, S. S. Rapid Formation and Macroscopic Self-Assembly of Liquid-Crystalline, High-Mobility, Semiconducting Thienothiophene. *Adv. Mater. Interfaces* **2018**, *5*, 1700875.

28. Pandey, M.; Kumari, N.; Nagamatsu, S.; Pandey, S. S. Recent Advances in Orientation of Conjugated Polymers for Organic Field- Effect Transistors. *J. Mat. Chem. C* **2019**, *7*, 13323–13351.

29. Pandey, M.; Nagamatsu, S.; Pandey, S. S.; Hayase, S.; Takashima, W. Orientation Characteristics of Non-Regiocontrolled Poly (3-hexyl-thiophene) Film by FTM on Various Liquid Substrates. *J. Phys.: Conf. Ser.* **2016**, *704*, 012005.

30. Pandey, M.; Nagamatsu, S.; Pandey, S. S.; Hayase, S.; Takashima, W. Enhancement of Carrier Mobility along with Anisotropic Transport in Non-Regiocontrolled Poly(3-hexylthiophene) Films Processed by Floating Film Transfer Method. *Org. Electron.* **2016**, *38*, 115–120.

31. Pandey, M.; Sadakata, S.; Nagamatsu, S.; Pandey, S. S.; Hayase, S.; Takashima, W. Layer-by-Layer Coating of Oriented Conjugated Polymer Films towards Anisotropic Electronics. *Synth. Met.* **2017**, *227*, 29–36.

32. Kim, B.-G.; Jeong, E. J.; Chung, J. W.; Seo, S.; Koo, B.; Kim, J. A Molecular Design Principle of Lyotropic Liquid- Crystalline Conjugated Polymers with Directed Alignment Capability for Plastic Electronics. *Nat. Mater*. **2013**, *12*, 659–664.

33. Chang, J.; Chi, C.; Zhang, J.; Wu, J. Controlled Growth of Large-Area High-Performance Small-Molecule Organic Single-Crystalline Transistors by Slot-Die Coating Using a Mixed Solvent System. *Adv. Mater.* **2013**, *25*, 6442–6447.

34. Rivnay, J.; Mannsfeld, S. C. B.; Miller, C. E.; Salleo, A.; Toney, M. F. Quantitative Determination of Organic Semiconductor Microstructure from the Molecular to Device Scale. *Chem. Rev.* **2012**, *112*, 5488–5519.

35. Wang, S.; Kiersnowski, A.; Pisula, W.; Müllen, K. Microstructure Evolution and Device Performance in Solution-Processed Polymeric Field-Effect Transistors: The Key Role of the First Monolayer. *J. Am. Chem. Soc.* **2012**, *134*, 4015–4018.

36. Chung, K.; Yu, Y.; Kwon, M.S.; Swets, J.; Kim, J. Youk, J.H.; Assembly and Alignment of Conjugated Polymers: Materials Design, Processing, and Applications. *MRS Commun.* **2015**, *5*, 169–189.

37. Li, M.; An, C.; Marszalek, T.; Baumgarten, M.; Müllen, K.; Pisula, W. Impact of Interfacial Microstructure on Charge Carrier Transport in Solution-Processed Conjugated Polymer Field-Effect Transistors. *Adv. Mater*. **2016**, *28*, 2245–2252.

Chapter 5

Work Function Modification via Combined Charge-Based Through-Space Interaction and Surface Interaction

Advanced Materials Interfaces **2018**, *5*, 1800471; published by John Wiley & Sons, Inc.

5.1 Introduction

Work function plays a key role in organic electronics, such as organic field effect transistors, organic solar cells, and organic light emitting diodes, since effective charge carrier injection and collection are largely dependent on the work function of the electrodes.[1–3] In this context, the effective work function modification of various electrodes including zinc oxide (ZnO),[1,4,5] indium tin oxide (ITO),[1,6–15] Au,[1,14,16,17] , or Al[14,18,19] have been widely discussed. For example, He et al. reported that the efficiency of inverted organic solar cells can be raised to 9.2% by effective work function tuning with an alcohol/water-soluble conjugated polymer.[6] Lee et al. showed that high performance organic solar cells with 8.32% efficiency could be fabricated using a combination of poly(3,4-ethylenedioxythiophene):poly(styrenesulfonate) (PEDOT:PSS) and non-conjugated polyelectrolytes as recombination layers that lead to effective work function reduction at the ITO electrode.[15] In other studies, both anionic and cationic polyelectrolyte interlayers have been investigated to achieve a proper energy level alignment for an improved power conversion efficiency by means of reoriented interfacial dipoles in the presence of an externally applied electric field.[19,20]

The work function of electrodes is known to be influenced by organic coatings through changes to the surface electric field; three primary mechanisms that affect the work function are the push back effect, Fermi level pinning and interfacial dipole formation.[21,22] To illustrate, the electron repulsion (push back) between an inactive organic coating and a substrate can result in the formation of a work function reducing dipole.[23,24] Alternately, a reduction (or oxidation) potential of a semiconducting organic material may be lower (or higher) than a Fermi level of an electrode. When these materials are brought into contact, charge transfers between them creating a work function modifying dipole.[21,25] This effect reaches beyond the immediate interface with the substrate, too, for the immediate monolayer can only support a certain charge density.[26,27]

In this chapter, we present a systematic study on the origin of the work function modification using polyelectrolytes coating via various thin film formation methods. It should be noted that the work function modification by the surface interaction through direct contact between a polyelectrolyte layer and its electrode substrate has already been investigated on many occasions.[1,28,29] However, the origin of work function modification is still the focus of great research effort. Specifically, there are experimental results that are not consistent with the well-known direct contact mechanism, such as the thickness dependence of a work function modifying layer in the resulting work function of an electrode.[4,11] In order to provide a more comprehensive understanding of the work function modification process, a representative polyelectrolyte set is carefully selected in this work. With the chosen polyelectrolyte set, we reveal that the surface interaction is not necessary in the modification and at the same time suggest the presence of the charge-based through-space interaction between the polyelectrolyte layer and the electrode. We demonstrate that the work function can be modified through charge-based deposition techniques such as electrophoretic deposition and electrospraying even though

the same materials do not exhibit meaningful work function shifts when their films were formed by spin casting without an external electric field. Our results indicate that a combination of the surface interaction and the charge-based through-space interaction plays a significant role in tuning the work function of electrodes for various electronic device applications.

5.2 Results and Discussion

In order to study the mechanism behind the work function modification, 10 different organic materials were chosen, which are not limited to specific backbones or functional groups (Figure 5.1). To compare the work function shift depending on charge-based properties, we divided the selected materials into four groups: acid-like, base-like, neutral, and ionic polyelectrolytes. When spin-cast samples are prepared from base-like and acid-like materials, the work function of ITO is observed to be decreased or increased, respectively (Table 5.1). To be specific, base-like polyelectrolytes induce negative charges on the ITO surface, forming a dipole pointing outward from the electrode resulting in a decreased work function.[30] On the other hand, acid-like compounds form opposite interfacial dipoles compared to the base-like polymers, which result in an increase in the work function. Although the work function shift has been reported in zwitterionic polymers having an overall charge neutrality,[31] almost no work function shift was observed in nonionic neutral polymer samples since the interfacial dipole is not formed.[14] Similarly, a negligible change in work function is observed with poly(sodium styrene sulfonate) (PSS:Na)[14] and the two other ionic polyelectrolytes. This may be explained by a weak charge-based through-space interaction owing to the counter ions. As shown in Table 5.1, the work function shift of the ITO samples, coated with several different polyelectrolytes, was measured by a custom-build kelvin probe. In order to further validate the values and the trend of

the work function shift, additional measurements were carried out using ultraviolet photoelectron spectroscopy (UPS) and kelvin probe force microscopy (KPFM) (Table 5.1 and Figure 5.2). The experimental results are in agreement with a charged layer model discussed by Schlapak et al.; charged materials create interfacial dipoles and lead to work function modification.[30]

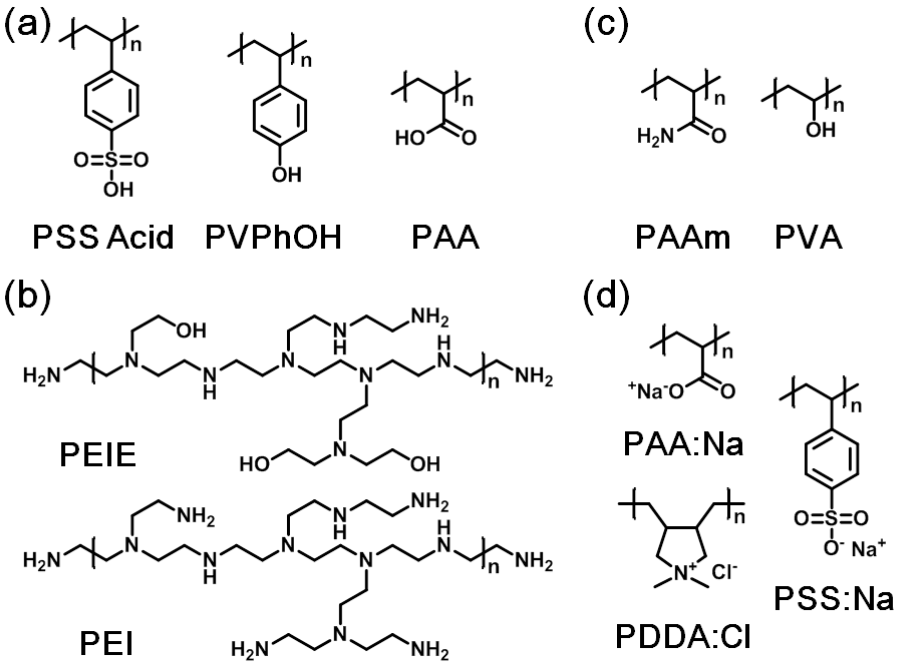

Figure 5.1 The chemical structures of a representative set of (a) acid-like, (b) base-like, (c) neutral, and (d) ionic polyelectrolytes.

Table 5.1 The work function shift of polyelectrolytes, relative to clean ITO, as measured by kelvin probe spectroscopy, kelvin probe force microscopy (KPFM) in air, and ultraviolet photoelectron spectroscopy (UPS)

Polyelectrolytes[a]		Δ Work function relative to ITO		
		Kelvin probe	KPFM	UPS
Base-like	PEI	-0.82 ± 0.01	-	-
	PEIE	-0.72 ± 0.03	-0.51 ± 0.01	-1.26
Acid-like	PAA	0.30 ± 0.02	-	-
	PVPhOH	0.27 ± 0.05	0.13 ± 0.01	0.59
	PSS Acid	0.36 ± 0.01	-	-
Neutral (nonionic)	PVA	0.03 ± 0.04	-	0.00
	PAAm	0.01 ± 0.00	0.00 ± 0.01	-
Ionic	PDDA:Cl	-0.04 ± 0.01	-	-
	PSS:Na	0.02 ± 0.03	0.01 ± 0.01	-0.03
	PAA:Na	0.02 ± 0.04	-	-

[a]PEI is poly(ethylenimine), PEIE is poly(ethylenimine 80% ethoxylated), PAA is poly(acrylic acid), PVPhOH is poly(vinylphenol), PSS Acid is poly(styrenesulfonic acid), PVA is poly(vinyl alcohol) 100% hydrolyzed, PAAm is poly(acrylamide), PDDA:Cl is poly(diallyl dimethylammonium chloride), PSS:Na is poly(sodium styrene sulfonate), and PAA:Na is poly (acrylic acid) sodium salt.

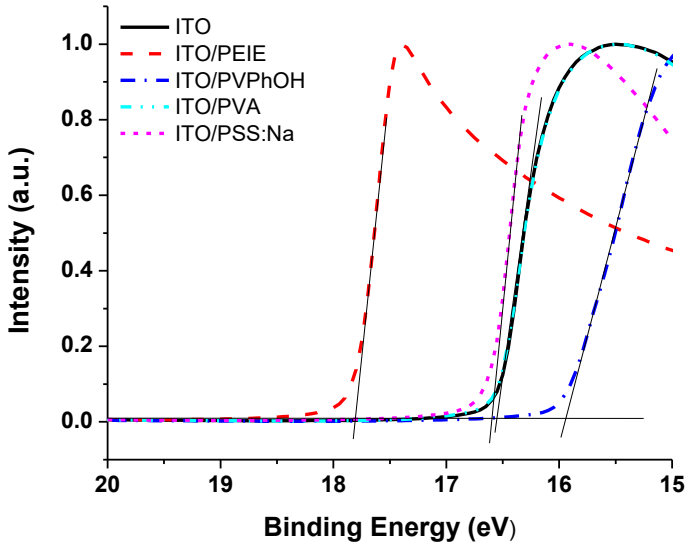

Figure 5.2 UPS spectra (He I) of ITO (black solid line), PEIE (red dashed line), PVPhOH (blue dashdotted line), PVA (cyan short dashed line), PSS:Na (magenta dotted line) showing the onset of the secondary electron cutoff.

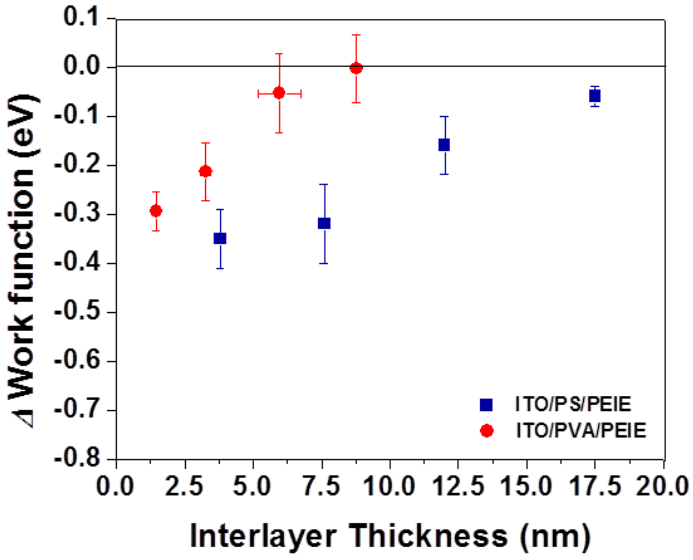

Figure 5.3 Work function shift, relative to bare ITO, of ITO/PEIE when PS (squares) or PVA (circles) is placed as a spacer layer between PEIE and ITO. The dielectric constants of PS and PVA are near 2.8 and 10, respectively.

Based on the aforementioned experimental data and the previous studies cited in this chapter, we questioned whether the work function modification process can occur by the charge-based through-space interaction without direct contact between the polyelectrolyte layer and its electrode. To investigate the effect of the charge-based through-space interaction solely between ITO and the work function modifying layer, thin inactive spacer layers, such as polystyrene (PS) or poly(vinyl alcohol) (PVA), were placed on top of the surface of ITO. Neither PS nor PVA changes the work function of ITO on its own, but the thickness control afforded via spin casting and the difference in dielectric constant near 10 for PVA[32] and near 2.8 for PS[33], will allow for varied attenuation of the expected through-space interaction between poly(ethylenimine 80% ethoxylated) (PEIE) and ITO. Figure 5.3 presents the work function shift of ITO versus the interlayer thickness. PEIE coated substrates having a thin, inactive, surface interaction blocking PS or PVA spacer both displayed a shifted work function of ITO, demonstrating that there is a possibility of the presence of an important factor in modifying the work function. As the thickness of the inactive spacer layer becomes larger, the degree of work function shift decreases in both the PVA and PS cases. This behavior is rationalized by our expectation that the polymer-originated electrical force decreases with increasing inactive spacer layer thickness, which in turn results in a reduction of charge redistribution on the ITO surface, a reduced dipole, and a reduced work function shift. Interestingly, we see that an interlayer with a larger dielectric constant results in a steeper attenuation,[34] consistent with the idea that a through-space electrical force drives the formation of a work function modifying dipole. We further investigated the film morphology by conductive atomic force microscopy (C-AFM) to confirm a full coverage of the ITO surface by the inactive spacer layer. Compared to a clean ITO substrate, significantly lower conductivity at the same applied bias was observed for the PS samples, which indicates that the

observed work function shift is not from direct contact between PEIE and ITO (Figure 5.4). Also, the morphology of the PS and the PVA spacer layers before and after the spin-coating of 2-methoxy ethanol was analyzed using tapping mode AFM to see any surface disruption by the sequential deposition of PEIE solution in 2-methoxy ethanol. AFM topography images of the PS (Figure 5.5) and the PVA (Figure 5.6) layers prepared at two different spin coating speeds do not show any noticeable morphology change.

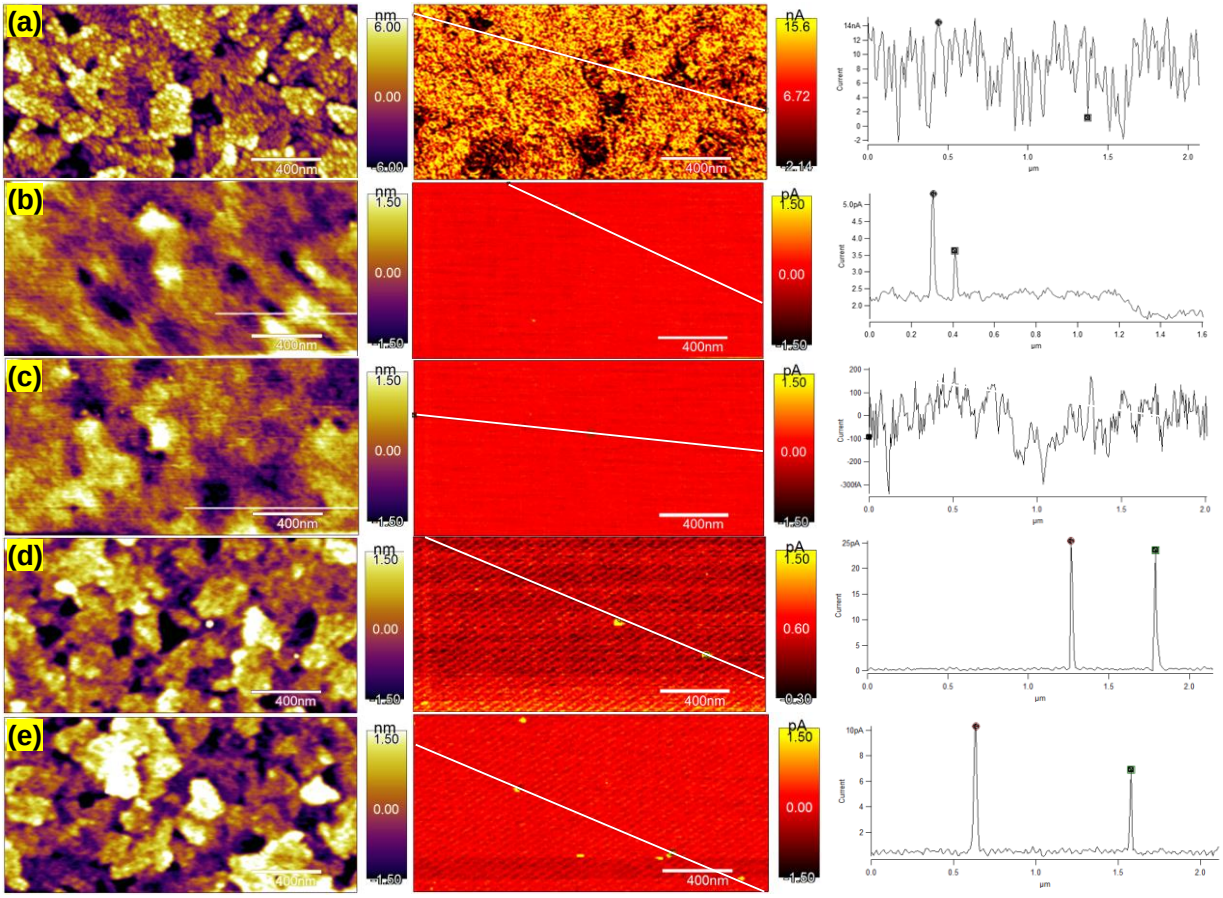

Figure 5.4 C-AFM topography (left column), its corresponding current map (middle column), and line profile of current map along a white solid line shown in each current map (right column) of (a) an ITO substrate and PS thin films deposited on ITO substrates at a spinning speed of (b) 1000 rpm, (c) 2000 rpm, (d) 4000 rpm, and (e) 6000 rpm.

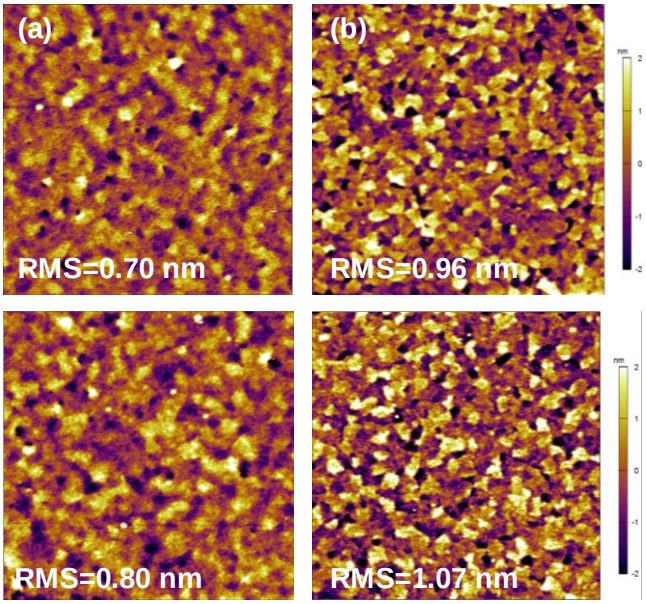

Figure 5.5 AFM topography of PS thin films deposited on ITO substrates at a spinning speed of (a) 1000 rpm and (b) 6000 rpm before (top) and after (bottom) spin cast of 2-methoxy ethanol. The scan area is 5x5 μm^2.

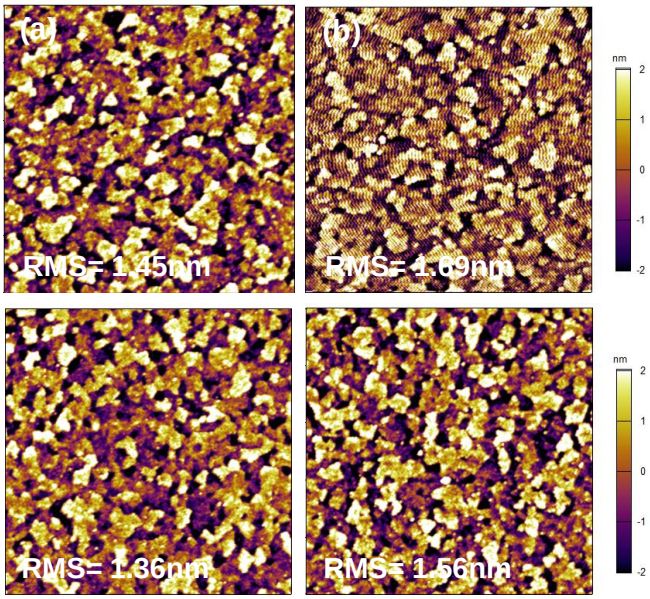

Figure 5.6 AFM topography of PVA thin films deposited on ITO substrates at a spinning speed of (a) 1000 rpm and (b) 6000 rpm before (top) and after (bottom) spin cast of 2-methoxy ethanol. The scan area is 5x5 μm^2.

As mentioned above, ionic polyelectrolytes did not show any meaningful work function shift when they were spin-coated on ITO. According to our proposed mechanism, if we can remove a polyelectrolyte's counter ion from the surface of ITO, the charged-based interaction between PSS^- or poly(diallyl dimethylammonium) ($PDDA^+$) and the ITO will increase and cause a work function shift. To examine this, we deposited PSS:Na, or poly(diallyl dimethylammonium chloride) (PDDA:Cl) on an ITO surface using an electrophoretic deposition method from an aqueous solution. Electrophoretic deposition was performed using a CH instruments CHI600C potentiostat by immersing a clean ITO substrate into a 2 mg mL^{-1} polyelectrolyte solution in water and applying a constant potential for 5 minutes, followed by drying at 100 °C for 10 min. A platinum wire was used as a counter electrode. Electrophoretic deposition consists of two processes.[35] During the first process, the applied electric field allows polyelectrolytes to move electrophoretically to the oppositely charged electrode in the solution (Figure 5.7a). The second process is the deposition of the electrophoretically attracted materials on the electrode, which yields the formation of a polymer film. The amount of material deposited per a given time is dictated by the applied bias.[36] A positive bias was applied to the working electrode for anionic PSS^- and for the deposition of cationic $PDDA^+$, a negative bias was applied.[37] As can be seen in Figure 5.7b, when PSS:Na is deposited under the positive bias and PDDA:Cl deposited under negative bias, they move the work function of ITO, which indicates that the applied bias precludes the presence of counter ions near the substrate by a repulsive interaction and enables us to use ionic polyelectrolytes as work function modifying layers. This is in contrast to the spin cast films of PSS:Na or PDDA:Cl, which are expected to retain their counter ion and only display a negligible work function shift ($\leq \pm 0.04$). The result corresponds to the explanation by the charge-based through-space interaction; when the positively (negatively)

charged ion reaches the ITO surface, it results in the formation of dipoles pointing outward from (toward) the ITO surface. To further clarify the mechanism, control experiments were performed in a NaCl solution without polyelectrolytes and we did not observe any meaningful shift in work function (data not shown).

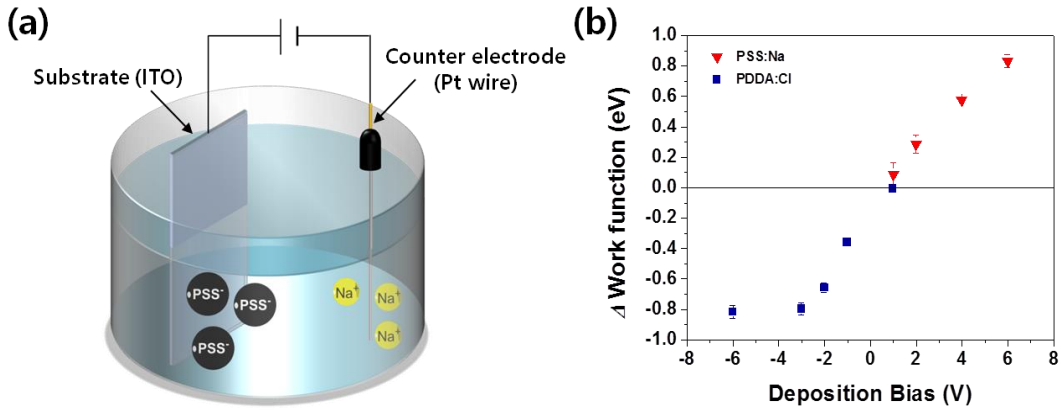

Figure 5.7 (a) Schematic illustration of the electrophoretic deposition of PSS:Na under positive bias. (b) Work function shift, relative to bare ITO, of ITO/PSS:Na (triangles) and ITO/PDDA:Cl (squares), which were prepared using an electrophoretic deposition method.

In order to further investigate the influence of a charge-based through-space interaction, samples deposited with PS using an electrospraying technique were prepared. Electrospraying was performed by injecting polystyrene from a 2 mg mL^{-1} solution in chloroform at a rate of 0.25 mL h^{-1} while applying a bias of 9 kV on the injecting tip relative to a backing plate. The substrate is placed in the injection path (Figure 5.8a). PS does not have any functional group which can easily interact with hydroxyl groups on the ITO surface nor does it have any acidic or basic moiety. The electrospraying technique allows us to achieve deposition of dissolved organic materials onto the desired substrate by forming charged droplets driven by the electric field we applied.[38] As shown in Figure 5.8b, when +9 kV is used during PS deposition, the positively

charged PS droplets which were produced lead to a negative charge on the surface of ITO. Thus, the work function of ITO decreases by 1.5 eV because of the resulting dipole. The degree of work function shift by this electrically induced charge gradually decays for both positive and negative cases since neutral compounds such as PS cannot stabilize either positive or negative charge permanently. Remarkably, the positively charged PS shifts ITO's work function more strongly than a negatively charged (deposited at -9 kV) material, and it remains more stable over time. It is reasonable to postulate that n-type ITO has an excess of relatively free negative charge[39], which enables it to stabilize the positive charge of PS deposited at +9 kV. This result is consistent with our hypothesis that the work function can be modified by the charge-based through-space interaction, even though there is no direct surface interaction with the surface hydroxyl groups on ITO.

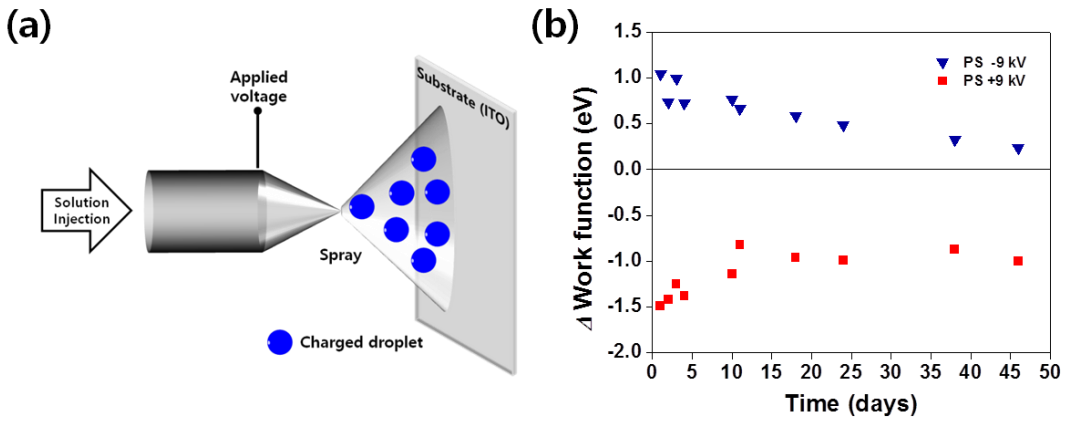

Figure 5.8 (a) Schematic illustration of an electrospraying deposition. (b) Work function shift, relative to bare ITO, of ITO/PS when PS is deposited at –9 kV (triangles) or +9 kV (squares) by the electrospraying technique.

5.3 Experimental Section

5.3.1 Materials and Instrumentation

All polymers and solvents were used as received from Sigma Aldrich. The work function shift of samples, relative to a clean ITO, was measured using a homemade Kelvin probe.[40] C-AFM and KPFM measurements were performed using Asylum Research MFP-3D under ambient conditions. A Pt-Ir5-coated contact-mode AFM probe (Nanosensors, ATEC-CONTPt, spring constant 0.2 N m^{-1}) was used for the top contact of C-AFM, and a PT-coated Si Probe (Nanosensors, stiffness ~0.5-1 N m^{-1}, resonant frequency ~75 kHz) was used for KPFM measurements.[41] UPS spectra were recorded in an ultrahigh vacuum chamber using He I (21.2 eV) photons at a resolution of 0.01 eV.

5.3.2 Film Fabrication

ITO (Delta Technologies CG-50IN-S107) was cleaned prior to use by sonicating in isopropanol and acetone each for 10 min, followed by a 10 min UV-ozone treatment. Polymer solutions were typically cast on ITO at 3000 rpm for 30 s from 2 mg mL^{-1} solvent: PVA, PSS:Na, poly(styrenesulfonic acid) (PSS Acid), poly (acrylic acid) (PAA), poly(acrylamide) (PAAm), poly (acrylic acid) sodium salt (PAA:Na) and PDDA:Cl were cast from water; poly(ethylenimine) (PEI), PEIE (both at 0.4 wt%), and poly(vinylphenol) (PVPhOH) are cast from 2-methoxyethanol; PS, was cast from toluene.

5.4 Conclusions

In conclusion, this study was performed to understand how polyelectrolytes modify the work function of their substrate by focusing on a combination of the surface interaction and the charge-based through-space interaction. We have shown that when acid-like or base-like polyelectrolytes were deposited on ITO substrates, they induce a work function shift by the formation of a surface dipole on ITO. The work function shift is also observed when the direct contact between the ITO substrate and polyelectrolyte is blocked by placing an inactive spacer, although the shift is not as strong as without the spacer. In addition, when an electrophoretic deposition technique was used with ionic polyelectrolytes, which has a negligible effect on the work function shift of ITO when spin cast, ITO samples showed a work function shift. Furthermore, it is interesting to find that the work function of ITO coated with PS, which is neutral, could be modified through the charge-based through-space interaction by employing an electrospraying technique. Taken together, these observations consistently suggest that while the surface interaction is the major factor affecting work function modification processes, the charge-based through-space interaction has also a significant effect on modifying the work function of electrodes. These results motivate the selection and design of materials for work function modification of their electrodes in organic electronic devices.

5.5 Author Contributions

Da Seul Yang,* David Bilby,* Kyeongwoon Chung, Jill K. Wenderott, Jacob Jordahl, Bo Hyun Kim, Joerg Lahann, Peter F. Green, Jinsang Kim Work Function Modification via Combined Charge-Based Through-Space Interaction and Surface Interaction *Advanced Materials Interfaces* **2018**, *5*, 1800471. (*equal contribution)

D.B. conceived the initial ideas of the study with the help of K.C. and J.K. D.B. prepared samples for the home-built kelvin probe measurement and measured the work function shift. J.J and J.L. assisted D.B. in preparing samples by electrospraying. D.S.Y. prepared samples for UPS and KPFM measurements. J.K.W. measured and analyzed KPFM data with the help of P.F.G. B.H.K. measured UPS data. B.H.K. and D.S.Y. analyzed the data with the help of J.K. D.S.Y. carried out AFM and C-AFM measurements and analyzed the data with the help of J.K.W. D.S.Y., D.B., and J.K. wrote the manuscript with contributions from all authors. J.K. supervised the research.

5.6 References

1. Zhou, Y.; Fuentes-Hernandez, C.; Shim, J.; Meyer, J.; Giordano, A. J.; Li, H.; Winget, P.; Papadopoulos, T.; Cheun, H.; Kim, J.; Fenoll, M.; Dindar, A.; Haske, W.; Najafabadi, E.; Khan, T. M.; Sojoudi, H.; Barlow, S. Graham, S.; Brédas, J.-L.; Marder, S. R.; Kahn, A.; Kippelen, B. A Universal Method to Produce Low–Work Function Electrodes for Organic Electronics. *Science.* **2012**, *336*, 327–332.
2. Ratcliff, E. L.; Zacher, B.; Armstrong, N. R. Selective Inter Layers and Contacts in Organic Photovoltaic Cells. *J. Phys. Chem. Lett.* **2011**, *2*, 1337–1350.
3. Po, R.; Carbonera, C.; Bernardi, A.; Camaioni, N. The Role of Buffer Layers in Polymer Solar Cells. *Energy Environ. Sci.* **2011**, *4*, 285.
4. Kim, Y.-H.; Han, T.-H.; Cho, H.; Min, S.-Y.; Lee, C.-L.; Lee, T.-W. Polyethylene Imine as an Ideal Interlayer for Highly Efficient Inverted Polymer Light-Emitting Diodes. *Adv. Funct. Mater.* **2014**, *24*, 3808–3814.
5. Shivanna, R.; Rajaram, S.; Narayan, K. S. Interface Engineering for Efficient Fullerene-

Free Organic Solar Cells. *Appl. Phys. Lett.* **2015**, *106*, 123301.

6. He, Z.; Zhong, C.; Su, S.; Xu, M.; Wu, H.; Cao, Y. Enhanced Power-Conversion Efficiency in Polymer Solar Cells Using an Inverted Device Structure. *Nat. Photonics* **2012**, *6*, 593–597.
7. Li, H.; Paramonov, P.; Brédas, J.-L. Theoretical Study of the Surface Modification of Indium Tin Oxide with Trifluorophenyl Phosphonic Acid Molecules: Impact of Coverage Density and Binding Geometry. *J. Mater. Chem.* **2010**, *20*, 2630–2637.
8. Wang, H.; Gomez, E. D.; Guan, Z.; Jaye, C.; Toney, M. F.; Fischer, D. A.; Kahn, A.; Loo, Y.-L. Tuning Contact Recombination and Open-Circuit Voltage in Polymer Solar Cells via Self-Assembled Monolayer Adsorption at the Organic–Metal Oxide Interface. *J. Phys. Chem. C* **2013**, *117*, 20474–20484.
9. Sharma, A.; Haldi, A.; Potscavage Jr., W. J.; Hotchkiss, P. J.; Marder, S. R.; Kippelen, B. Effects of Surface Modification of Indium Tin Oxide Electrodes on the Performance of Molecular Multilayer Organic Photovoltaic Devices. *J. Mater. Chem.* **2009**, *19*, 5298–5302.
10. Kim, J. S.; Park, J. H.; Lee, J. H.; Jo, J.; Kim, D.-Y.; Cho, K. Control of the Electrode Work Function and Active Layer Morphology via Surface Modification of Indium Tin Oxide for High Efficiency Organic Photovoltaics. *Appl. Phys. Lett.* **2007**, *91*, 112111.
11. Osikowicz, W.; Crispin, X.; Tengstedt, C.; Lindell, L.; Kugler, T.; Salaneck, W. R. Transparent Low-Work-Function Indium Tin Oxide Electrode Obtained by Molecular Scale Interface Engineering. *Appl. Phys. Lett.* **2004**, *85*, 1616–1618.
12. Ganzorig, C.; Kwak, K.-J.; Yagi, K.; Fujihira, M. Fine Tuning Work Function of Indium Tin Oxide by Surface Molecular Design: Enhanced Hole Injection in Organic

Electroluminescent Devices. *Appl. Phys. Lett.* **2001**, *79*, 272–274.

13. Lu, H.-W.; Kao, P.-C.; Juang, Y.-D.; Chu, S.-Y. The Effects of Ultraviolet-Ozone-Treated Ultra-Thin MnO-Doped ZnO Film as Anode Buffer Layer on the Electrical Characteristics of Organic Light-Emitting Diodes. *J. Appl. Phys.* **2015**, *118*, 185501.
14. van Reenen, S.; Kouijzer, S.; Janssen, R. A. J.; Wienk, M. M.; Kemerink, M. Origin of Work Function Modification by Ionic and Amine-Based Interface Layers. *Adv. Mater. Interfaces* **2014**, *1*, 1400189.
15. Lee, J.; Kang, H.; Kong, J.; Lee, K. A Depletion-Free, Ionic, Self-Assembled Recombination Layer for Tandem Polymer Solar Cells. *Adv. Energy Mater.* **2014**, *4*, 1301226.
16. Wu, H.; Huang, F.; Peng, J.; Cao, Y. High-Efficiency Electron Injection Cathode of Au for Polymer Light-Emitting Devices. *Org. Electron.* **2005**, *6*, 118–128.
17. Bröker, B.; Blum, R.-P.; Frisch, J.; Vollmer, A.; Hofmann, O. T.; Rieger, R.; Müllen, K.; Rabe, J. P.; Zojer, E.; Koch, N. Gold Work Function Reduction by 2.2 eV with an Air-Stable Molecular Donor Layer. *Appl. Phys. Lett.* **2008**, *93*, 243303.
18. Lim, K.-G.; Choi, M.-R.; Lee, T.-W. Improvement of Both Efficiency and Stability in Organic Photovoltaics by Using Water-Soluble Anionic Conjugated Polyelectrolyte Interlayer. *Mater. Today Energy* **2017**, *5*, 66–71.
19. Lim, K.-G.; Park, S. M.; Woo, H. Y.; Lee, T.-W. Elucidating the Role of Conjugated Polyelectrolyte Interlayers for High-Efficiency Organic Photovoltaics. *ChemSusChem* **2015**, *8*, 3062–3068.
20. Lim, K.-G.; Ahn, S.; Lee, T.-W. Energy Level Alignment of Dipolar Interface Layer in Organic and Hybrid Perovskite Solar Cells. *J. Mater. Chem. C* **2018**, *6*, 2915–2924.

21. Braun, S.; Salaneck, W. R.; Fahlman, M. Energy-Level Alignment at Organic/Metal and Organic/Organic Interfaces. *Adv. Mater.* **2009**, *21*, 1450–1472.

22. Schwartz, J.; Bruner, E. L.; Koch, N.; Span, A. R.; Bernasek, S. L.; Kahn, A. Controlling the Work Function of Indium Tin Oxide: Differentiating Dipolar from Local Surface Effects. *Synth. Met.* **2003**, *138*, 223–227.

23. Osikowicz, W.; de Jong, M. P.; Braun, S.; Tengstedt, C.; Fahlman, M.; Salaneck, W. R. Energetics at Au Top and Bottom Contacts on Conjugated Polymers. *Appl. Phys. Lett.* **2006**, *88*, 193504.

24. Witte, G.; Lukas, S.; Bagus, P. S.; Wöll, C. Vacuum Level Alignment at Organic/Metal Junctions: "Cushion" Effect and the Interface Dipole. *Appl. Phys. Lett.* **2005**, *87*, 263502.

25. Greiner, M. T.; Helander, M. G.; Tang, W.-M.; Wang, Z.-B.; Qiu, J.; Lu, Z.-H. Universal Energy-Level Alignment of Molecules on Metal Oxides. *Nat. Mater.* **2011**, *11*, 76–81.

26. Niederhausen, J.; Amsalem, P.; Wilke, A.; Schlesinger, R.; Winkler, S.; Vollmer, A.; Rabe, J. P.; Koch, N. Doping of C_{60} (Sub)Monolayers by Fermi-Level Pinning Induced Electron Transfer. *Phys. Rev. B* **2012**, *86*, 081411(R).

27. Oehzelt, M.; Koch, N.; Heimel, G. Organic Semiconductor Density of States Controls the Energy Level Alignment at Electrode Interfaces. *Nat. Commun.* **2014**, *5*, 4174.

28. Kang, H.; Hong, S.; Lee, J.; Lee, K. Electrostatically Self-Assembled Nonconjugated Polyelectrolytes as an Ideal Interfacial Layer for Inverted Polymer Solar Cells. *Adv. Mater.* **2012**, *24*, 3005–3009.

29. Lee, B. H.; Jung, I. H.; Woo, H. Y.; Shim, H.-K.; Kim, G.; Lee, K. Multi-Charged Conjugated Polyelectrolytes as a Versatile Work Function Modifier for Organic Electronic Devices. *Adv. Funct. Mater.* **2014**, *24*, 1100–1108.

30. Schlapak, R.; Armitage, D.; Saucedo-Zeni, N.; Latini, G.; Gruber, H. J.; Mesquida, P.; Samotskaya, Y.; Hohage, M.; Cacialli, F.; Howorka, S. Preparation and Characterization of Dense Films of Poly(amidoamine) Dendrimers on Indium Tin Oxide. *Langmuir* **2007**, 23, 8916–8924.

31. Liu, Y.; Duzhko, V. V.; Page, Z. A.; Emrick, T.; Russell, T. P. Conjugated Polymer Zwitterions: Efficient Interlayer Materials in Organic Electronics. *Acc. Chem. Res.* **2016**, *49*, 2478–2488.

32. Singh, K. P.; Gupta, P. N. Study of Dielectric Relaxation in Polymer Electrolytes. *Eur. Polym. J.* **1998**, *34*, 1023–1029.

33. Yano, O.; Wada, Y. Dynamic Mechanical and Dielectric Relaxations of Polystyrene below the Glass Temperature. *J. Polym. Sci. Part A-2 Polym. Phys.* **1971**, *9*, 669–686.

34. Atkins, P.; de Paula, J. Physical Chemistry 9th ed., W. H. Freeman and Company, NY 2010.

35. Sarkar, P.; Nicholson, P. S. Electrophoretic Deposition (EPD): Mechanisms, Kinetics, and Application to Ceramics. *J. Am. Ceram. Soc.* **1996**, *79*, 1987–2002.

36. Hertkorn, D.; Elsenheimer, H. C.; Bruch, R.; Paul, F.; Müller, C.; Hanemann, T.; Reinecke, H. Thickness Variation of Electrophoretically Deposited Strontium Titanate Films for Photoelectrochemical Energy Conversion. *J. Appl. Phys.* **2013**, *114*, 027020.

37. Cho, C.; Wallace, K. L.; Hagen, D. A.; Stevens, B.; Regev, O.; Grunlan, J. C. Nanobrick Wall Multilayer Thin Films Grown Faster and Stronger Using Electrophoretic Deposition. *Nanotechnology* **2015**, *26*, 185703.

38. Cole, R. B. *Electrospray and MALDI Mass Spectrometry: Fundamentals, Instrumentation, Practicalities, and Biological Applications, 2nd Edition*, John Wiley & Sons, Inc.

Hoboken, NJ, 2010.

39. Keshmiri, S. H.; Rezaee-Roknabadi, M.; Ashok, S. A Novel Technique for Increasing Electron Mobility of Indium-Tin-Oxide Transparent Conducting Films. *Thin Solid Films* **2002**, *413*, 167–170.

40. Bilby, D.; Frieberg, B.; Kramadhati, S.; Green, P.; Kim, J. Design Considerations for Electrode Buffer Layer Materials in Polymer Solar Cells. *ACS Appl. Mater. Interfaces* **2014**, *6* , 14964–14974.

41. Wenderott, J. K.; Dong, B. X.; Green, P. F. Band Bending in Conjugated Polymer Films: Role of Morphology and Implications for Bulk Charge Transport Characteristics. *J. Mater. Chem. C* **2017**, *5*, 7446–7451.

Chapter 6

Conclusions and Future Outlook

6.1 Research Summary

This dissertation first presents a systematic study on molecular design of conjugated polymers to achieve liquid crystalline (LC) phases and consequential control of polymer alignment, as a strategy towards the inherently favorable chain alignment characteristics, suppressing the entanglement and random orientation of the polymer chains. Although conjugated polymers have various advantages over inorganic counterparts, such as readily tunable properties, mechanical flexibility, solution processability, lightweight, and low cost, organic electronic devices constructed from them suffer from low charge transport properties, somewhat limiting their practical applicability. This inferior performance mainly stems from the intrinsic disordered nature of polymers. Their coiled conformation, chain entanglement, and random orientation limit the intrachain charge transport and necessitate slow interchain and sluggish domain-to-domain charge hopping. In order to minimize the interchain and inter-domain hopping and achieve high-performance in organic electronics, effective polymer design parameters for directed alignment of polymer chains have been studied in **Chapter 2**. Specifically, the design efforts in this dissertation are focused on giving LC properties to conjugated polymers so that the LC conjugated polymers can have an intrinsic capability to be aligned along an external shear field. By means of eight newly designed conjugated polymers, we not only validated the universal applicability of the previously identified design parameters[1],

but also expanded and further clarified the design factors as follows: (1) the planarity of polymer chains, (2) intramolecular interaction moieties for chain planarity, (3) the effective bulkiness of side chains, and (4) surface energy of the polymers. **Chapter 3** enlarges the design space by employing cleavable side chains, which enables the synthesis of LC polymers to form solvent-resistant highly aligned films. Chain alignment and solvent resistance of the films prepared by an LC polymer with cleavable side chains are achieved by means of FTM, an LC phase-assisted film fabrication method. The successful LC phase-assisted alignment was achieved in the presence of an optimum amount of high boiling point solvent during the film formation process, which provides ample time for polymer chains to self-assemble and align. The degree of chain alignment was confirmed by high optical (~4.8) and electrical (~14) anisotropies by polarized UV-vis absorption measurements and the fabrication of the organic field effect transistors (OFETs), respectively. The chain alignment was maintained during the side chain cleavage, and thus highly aligned solvent-resistance polymer films were successfully achieved.

The importance of interface engineering for efficient charge transport in organic electronic devices is thoroughly investigated and discussed in **Chapters 4 and 5**. Charge transport in OFETs is known to be mainly determined by a thin charge accumulation layer adjacent to the semiconductor-gate dielectric layer interface.[2–7] In this context, the contribution of the semiconducting polymer films near the interface to the charge transport behavior in the corresponding devices would be critically important. To date, studies of this contribution have emphasized mainly on controlling the thickness of the films.[8–13] However, changes in film thickness often accompany changes in other factors, such as the charge transport path and homogeneity of the film, which can also affect the charge transport properties in the resulting films. To overcome this issue, **Chapter 4** describes a unique experimental design, which enables

a discrete modulation of the polymer chain alignment direction for each layer in multilayered films by FTM. To be specific, we fabricated polymer films by using FTM in such a way that the bottom layer is close to the polymer-dielectric interface and the top layer is in contact with the source-drain electrodes. When the polymer chains in the bottom layer had a parallel orientation and the chains in the top layer were oriented perpendicular to the source-drain direction, a more than three times higher mobility was observed in comparison to the opposite case. More transistor devices were fabricated varying the bottom and top layers polymer chain orientations. The analysis of the device performance evidently revealed that the orientation direction of the bottom layer has a much stronger impact on the overall device performance compared to that of the top layer. Considering that the effective charge accumulation forms at the bottom layer/dielectric interface, these results are in good agreement with the theoretical expectation. They clearly strengthen the fundamental understanding of the role of polymer chain orientation in efficient charge transport and the ideal device architecture, providing a solid foundation for various applications in organic electronics.

The research focus of **Chapter 5** is also on the importance of interface engineering in high performance organic electronics. Organic electronic devices function based on charge injection and charge extraction between electrodes and the organic semiconducting layers. When the work function of a metal (i.e. the minimum energy required to remove an electron from a metal surface) and the energy level of the organic semiconducting layers are close to each other, the charge injection and extraction barrier is small, allowing efficient charge transport. Accordingly, various methods have been devised to modulate the work function of metal electrodes to control the charge transport character at the interface. However, the origin of the change in work function has remained elusive. In order to investigate the origin of this work

function modification, carefully selected polymers and polyelectrolytes (i.e. polymers with several ionizable groups) were coated on ITO by means of a few different film forming methods, such as electrophoretic deposition, electrospraying technique, and spin-coating method. Additionally, a thin insulating spacer layer was placed between the work function modifying polyelectrolytes and ITO to examine the effect of through-space charge buildup. The fabricated films allowed us to study how the work function of electrodes can be modulated with or without a direct surface interaction between the electrode and the polymer layer. The experimental results consistently suggest that while the surface interaction is the major factor affecting the work function of electrodes, the through-space charge interaction has also a significant effect on the work function.

6.2 Future Outlook

The devised conjugated polymer design strategy for directed alignment through the lyotropic LC phase invites an opportunity to achieve efficient charge transport in organic electronic devices. To fully utilize the design rules, described in **Chapters 2 and 3**, it would be desirable to thoroughly investigate and expand feasible moieties in the future. Incorporation of the presented design rules into the reported moieties having intrinsically efficient charge transport properties is expected to result in high performance in the corresponding devices. Moreover, investigating reconfigurable moieties, such as diarylethene,[14,15] in the conjugated polymer design to enhance further charge transport properties by replacing the tetrahedral carbon linkage and bulky side chains, is an interesting future research direction. To be specific, the tetrahedral carbon atom and bulky side chains play a key role in avoiding massive aggregation, but they prevent polymer chains from forming a closely packed structure. The use of

diarylethene units could overcome this problem, because they can undergo a ring-closure reaction triggered by UV irradiation, which induces highly planar and closely packed polymer chains.

In **Chapter 4**, a discrete modulation of polymer chain orientation directions of each layer in a multilayered film by FTM is presented. This precise regulation of the orientation direction in a ~14 nm thick polymer film makes it possible to demonstrate that the orientation direction of semiconducting polymer layer near the polymer/gate dielectric interface is the determining factor in the overall charge transport in OFETs. Future work in exploring ultrathin conjugated polymer films (i.e. thinner than 10 nm) with high surface uniformity and roughness can extend the value of this study because such films possess unique advantages for various applications.[16–18] For example, using rationally designed thin films can provide high sensitivity and fast response rate in potentiometric sensors because of the reduced distance between the surface of the film, where the analyte binding and recognition occur, and the effective charge accumulation layer near the semiconductor/gate dielectric interface. In addition, the ultrathin functionalized films are highly desirable for conformable, lightweight, and flexible health care devices and radiofrequency identification tags.

In **Chapter 5**, the work function modification mechanism is investigated to be disclosed as a combination of the surface interaction and the charge-based through-space interaction. This exploration allows for a wide variety of material selections for modifying work function of electrodes in organic electronics. In order to take full advantage of this finding, further investigation of other commonly used electrode materials such as gold, aluminum, and silver is highly recommended. Moreover, the current understanding of the work function modification

mechanism can be further strengthened by computational studies, for example, the calculation of the distance of the charge-based through-space interaction.

6.3 References

1. Kim, B.-G.; Jeong, E. J.; Chung, J. W.; Seo, S.; Koo, B.; Kim, J. A Molecular Design Principle of Lyotropic Liquid-Crystalline Conjugated Polymers with Directed Alignment Capability for Plastic Electronics. *Nat. Mater*. **2013**, *12*, 659–664.
2. Dimitrakopoulos, C. D.; Malenfant, P. R. L. Organic Thin Film Transistors for Large Area Electronics. *Adv. Mater.* **2002**, *14*, 99–117.
3. Dinelli, F.; Murgia, M.; Levy, P.; Cavallini, M.; Biscarini, F.; de Leeuw, D. M. Spatially Correlated Charge Transport in Organic Thin Film Transistors. *Phys. Rev. Lett.* **2004**, *92*, 116802.
4. Joshi, S.; Grigorian, S.; Pietsch, U.; Pingel, P.; Zen, A.; Neher, D.; Scherf, U. Thickness Dependence of the Crystalline Structure and Hole Mobility in Thin Films of Low Molecular Weight Poly(3-hexylthiophene). *Macromolecules* **2008**, *41*, 6800–6808.
5. Liu, S.-W.; Lee, C.-C.; Tai, H.-L.; Wen, J.-M.; Lee, J.-H.; Chen, C.-T. In situ Electrical Characterization of the Thickness Dependence of Organic Field-Effect Transistors with 1−20 Molecular Monolayer of Pentacene. *ACS Appl. Mater. Interfaces* **2010**, *2*, 2282–2288.
6. Horowitz, G. Tunneling Current in Polycrystalline Organic Thin-Film Transistors. *Adv. Funct. Mater.* **2003**, *13*, 53–60.
7. Dodabalapur, A.; Torsi, L.; Katz, H. E. Organic Transistors: Two-Dimensional Transport and Improved Electrical Characteristics. *Science* **1995**, *268*, 270–271.

8. Reséndiz, L.; Estrada, M.; Cerdeira, A.; Iñiguez, B.; Deen, M. J. Effect of Active Layer Thickness on the Electrical Characteristics of Polymer Thin Film Transistors. *Org. Electron.* **2010**, *11*, 1920–1927.

9. Lee, J.; Kim, K.; Kim, J. H.; Im, S.; Jung, D.-Y. Optimum Channel Thickness in Pentacene-Based Thin-Film Transistors. *Appl. Phys. Lett.* **2003**, *82*, 4169–4171.

10. Gupta, D.; Hong, Y. Understanding the Effect of Semiconductor Thickness on Device Characteristics in Organic Thin Film Transistors by Way of Two-Dimensional Simulations. *Org. Electron.* **2010**, *11*, 127–136.

11. Ribierre, J. C.; Watanabe, S.; Matsumoto, M.; Muto, T.; Hashizume, D.; Aoyama, T. Thickness Dependence of the Ambipolar Charge Transport Properties in Organic Field-Effect Transistors Based on a Quinoidal Oligothiophene Derivative. *J. Phys. Chem. C* **2011**, *115*, 20703–20709.

12. Janasz, L.; Gradzka, M.; Chlebosz, D.; Zajaczkowski, W.; Marszalek, T.; Kiersnowski, A.; Ulanski, J.; Pisula, W. Microstructure-Dependent Charge Carrier Transport of Poly(3-hexylthiophene) Ultrathin Films with Different Thicknesses. *Langmuir* **2017**, *33*, 4189–4197.

13. Mannebach, E. M.; Spalenka, J. W.; Johnson, P. S.; Cai, Z.; Himpsel, F. J.; Evans, P. G. High Hole Mobility and Thickness-Dependent Crystal Structure in *α,ω*-Dihexylsexithiophene Single-Monolayer Field-Effect Transistors. *Adv. Funct. Mater.* **2013**, *23*, 554–564.

14. Gemayel, M. El; Börjesson, K.; Herder, M.; Duong, D. T.; Hutchison, J. A.; Ruzié, C.; Schweicher, G.; Salleo, A.; Geerts, Y.; Hecht, S.; Orgiu, E.; Samorì, P. Optically

Switchable Transistors by Simple Incorporation of Photochromic Systems into Small-Molecule Semiconducting Matrices. *Nat. Commun.* **2015**, *6*, 6330.

15. Tsujioka, T.; Matsui, N. Electrical Characterization of Photochromic Diarylethene Films Consisting of Extraordinarily Large Crystallites. *J. Mater. Chem. C* **2014**, *2*, 3589–3596.
16. Caccami, M. C.; Marrocco, G.; Hogan, M. P.; Alfredsson, M.; Batchelor, J. C. Development of a New Class of On-Skin Radio-Sensors Boosted by Thin Polymer-Based Batteries. In *2017 IEEE MTT-S International Microwave Workshop Series on Advanced Materials and Processes for RF and THz Applications (IMWS-AMP),* Pavia, **2017**, pp 1–3.
17. Takeda, Y.; Hayasaka, K.; Shiwaku, R.; Yokosawa, K.; Shiba, T.; Mamada, M.; Kumaki, D.; Fukuda, K.; Tokito, S. Fabrication of Ultra-Thin Printed Organic TFT CMOS Logic Circuits Optimized for Low-Voltage Wearable Sensor Applications. *Sci. Rep.* **2016**, *6*, 25714.
18. Li, L.; Gao, P.; Baumgarten, M.; Müllen, K.; Lu, N.; Fuchs, H.; Chi, L. High Performance Field-Effect Ammonia Sensors Based on a Structured Ultrathin Organic Semiconductor Film. *Adv. Mater.* **2013**, *25*, 3419–3425.